

Report 1291

Wheeler Laboratories, Inc.

Page 1
of 83+4+12

Report 1291
STUDY OF SMALL OMNIDIRECTIONAL
250-Mc ANTENNA FOR PENETROMETER -
FINAL REPORT ON PHASE I
By Robert E. Puttre
To National Aeronautics
and Space Administration
Contract Number NAS 1-4470
1965 JUL 29 Job 482

FHW
HLB, HAW
REP
jp

Summary

A small rugged omnidirectional antenna is a component of a device called a penetrometer. This device can be employed to investigate certain of the physical characteristics, including hardness, penetrability and load-support capability, of unknown surfaces such as that of our moon. The antenna is to be capable of operating in free space, during impact with a hard surface such as rock, and during immersion into penetrable dielectric media such as sand or dust. The antenna is to be encapsulated in a 4-inch diameter spherical ball of fiberglass-reinforced epoxy resin.

The choice of a small antenna is limited to either electric or magnetic dipoles. For a given size, these two antenna types are theoretically capable of comparable free-space radiation properties. However, the electric-field concentration of the small electric dipole is accompanied by excessive dissipation in the encapsulating material and excessive detuning by proximity to the dielectric surface, especially by immersion therein. Hence, the magnetic-dipole is recommended, in the form of a loop antenna with self-tuning by spaced series capacitors to minimize the external electric field.

The proposed antenna comprises a pair of orthogonal loops fed in quadrature for spherical-pattern radiation coverage. The loops are resonated by the series capacitors and are mounted outside of a shielded spherical core containing a telemetry transmitter, accelerometer, battery, and a directional coupler for power division with quadrature phase.

Calculations indicate that the encapsulated antenna will remain intact during and after impact at 150 feet per second on a hard surface, but dynamic tests are needed for confirmation.

The resulting pattern of the free-space radiated power is nearly isotropic, having an amplitude variation of about 3 db and various polarizations. (A polarization-diversity receiver is required to receive all polarization components.) The free-space pattern is distorted by interface reflection and refraction when the antenna is near or immersed in the landing surface. In addition, antenna detuning occurs both because of proximity to or immersion

in the dielectric surface, and because of deformation of the shape and size of the loop at impact.

For an antenna exactly tuned and operating at 250 Mc, with a loop radius of $1-21/32$ inches, the power radiated into free space is -6 db from the power radiated from a lossless isotropic radiator. If the antenna is immersed in a dielectric medium of $k=3$, or impacted on a hard surface of $k=7$, the least power radiated toward a receiver directly overhead is computed to be -11 db and -10 db, respectively, from an isotrope. Increasing the operating frequency or the size of the antenna increases the efficiency and reduces the sensitivity to environment.

Contents

<u>Section</u>	<u>Page</u>
I. Introduction.	7
II. Definition of Terms and Symbols.	8
III. Specifications.	12
IV. Study of Alternative Antennas.	14
A. Available Types.	14
B. Considerations.	17
C. Alternative Kinds of Dipoles.	18
D. Electric Dipoles.	21
E. Magnetic Dipoles (Loops)	21
F. Recommendation of Crossed Loops.	23
V. Mechanical Problems of Impact.	24
VI. Electromagnetic Problems of Environment.	25
A. Polarization Diversity.	25
B. Radiation Before Impact.	26
C. Radiation at Impact.	34
D. Impedance Variation by Deformation.	39
E. Impedance Variation by Immersion.	40
VII. Study of Design of Crossed-Loop Antenna.	44
A. Self-Tuning.	45
B. Radiation Efficiency.	48
C. Impedance Matching.	54
D. Quadrature Coupling.	57
E. Mechanical Structure.	60
VIII. Description of Proposed Antenna.	68
A. Configuration.	68
B. Anticipated Performance.	71
IX. Antenna Efficiency, Frequency Trade-Off Study.	75
X. Acknowledgements.	81
XI. References.	82
Appendix I. Antenna Efficiency, Core-Size Trade Off.	84
Appendix II. Mechanics of Impact.	88

Contents (continued)

<u>List of Figures</u>	<u>Page</u>
Fig. 1 - Diagrams for explanation of some symbols.	9
Fig. 2 - Small dipoles in a pair crossed for spherical coverage.	16
Fig. 3 - Crossed loop antennas fed in quadrature for spherical coverage.	27
Fig. 4 - Radiation before impact, with reflection from surface.	29
Fig. 5 - Reflection coefficient at dielectric surface.	30
Fig. 6 - Pattern envelope with reflection from surface.	32
Fig. 7 - Polarization patterns of crossed loop antennas.	33
Fig. 8 - Transmission outward through the dielectric interface (ground).	35
Fig. 9 - Variation of transmission efficiency outward through the dielectric interface.	37
Fig. 10 - Decrease of loop inductance for impact deformation.	41
Fig. 11 - Variation of loop impedance from free space to far submerged.	43
Fig. 12 - Inductance of a loop about a metal sphere.	47
Fig. 13 - Methods of coupling to loop antenna.	55
Fig. 14 - Loop antenna and core with magnetic-coupling loop.	56
Fig. 15 - Techniques for quadrature coupling of crossed loops.	58
Fig. 16 - Circuit of antenna and quadrature feed.	59
Fig. 17 - Miniature directional coupler.	61
Fig. 18 - Circuit of the quadrature directional coupler.	62
Fig. 19 - Configuration of crossed antenna loops.	63
Fig. 20 - Capacitor assembly configuration.	65
Fig. 21 - Encapsulating mold.	69
Fig. 22 - Cutaway view of crossed-loop antenna assembly.	72
Fig. 23 - Radiation power factor for a loop antenna.	77
Fig. 24 - Total power factor for a loop antenna.	78
Fig. 25 - Radiation efficiency for a loop antenna.	79
Fig. 26 - Reflection loss for operation 5 mils from resonance.	80

Contents (continued)

<u>List of Figures - Continued</u>	<u>Page</u>
A1.1 - Radiation power factor for a loop about a sphere.	85
A1.2 - Total power factor for a loop about a sphere.	86
A1.3 - Radiation efficiency for a loop about a sphere.	87
A2.1 - Peak impact acceleration of projectile.	91
A2.2 - Total elastic deformation of projectile and target on collision.	92
A2.3 - Total impact time of projectile.	93
A2.4 - Dynamic compressive stress at impact.	95
A2.5 - Diameter of impact contact circle.	96
A2.6 - Depth of penetration into loose sand.	99
Table 1. Specifications.	13
Table 2. Comparison of electric and magnetic dipoles.	20
Table 3. Electrical and mechanical properties of alumina and fused silica.	49
Table 4. Distribution of available antenna-circuit power.	53
Table 5. Antenna-material properties.	66
Table 6. Mixtures of epoxy resin and curing agents.	67
Table 7. Assembly and fabrication procedure for preliminary models.	70
Table 8. Expected transmission losses for loop antenna.	74
Table A2.1 - Projectile and target structural properties.	89

I. Introduction.

Some information regarding the physical properties of lunar or planetary surfaces is required prior to spacecraft landings and post-landing explorations. A research program conducted at the Langley Research Center of the National Aeronautics and Space Administration has shown that impact-measuring instrumented projectiles (penetrometers) can be used to evaluate physical properties such as surface hardness, penetrability and bearing strength.

A measurement technique has been devised by NASA whereby a penetrometer, comprising a piezo-electric acceleration sensor, modulator, FM transmitter, antenna, and battery power supply, impacts the unknown surface at a selected velocity. During the impact process, the transmitter is frequency-modulated by the impact-acceleration sensor. The modulated RF output from the transmitter is then radiated by the antenna to a nearby space probe for retransmission to earth. Analysis of the impact-acceleration time-history signatures is then accomplished by a comparison with the signatures of known terrestrial surfaces, thereby relating the similar physical characteristics.

An omnidirectional antenna mounted in a spherical penetrometer package is required, since attitude stability or elaborate deployment techniques are not feasible, and transmission is required during impact regardless of penetrometer orientation. The antenna must operate reliably during a high-acceleration impact period and in varying proximity with or submersion in the surface material. The size of the penetrometer package and the selection of frequency limit the maximum physical dimension of the antenna to about 1/10 wavelength.

Wheeler Laboratories was selected by NASA to develop, design and fabricate the prototype omnidirectional antenna for the penetrometer. A subcontract from WL to the Hazeltine Electronics Division was awarded to develop the mechanical design of the antenna, and to provide assistance during construction and testing of the experimental model. Phase I of the NASA contract requires: (a) a general study of the possible methods of achieving the development of an antenna system which conforms to the physical, electrical, and

environmental requirements of the penetrometer; (b) construction of physical and electrical mockups; (c) preliminary electrical operational testing; and (d) an investigation of the trade off of antenna efficiency with transmitter operating frequency and antenna size. Plans for Phase II of the contract, as originally proposed, include an intensive investigation of the problem areas discovered in Phase I, and the final design, development, construction, test and delivery of prototype antennas.

This report is the final report on the Phase I study. In this report, the two alternative antenna systems, namely small electric dipoles and small magnetic dipoles, are compared, and the magnetic dipoles in a crossed-loop configuration are recommended. The mechanical problems of impact and the electromagnetic problems of the environment are established. Finally, the report deals with the design of the crossed-loop antenna and its description. The results of the antenna-efficiency, frequency-trade-off study are also presented.

II. Definitions of Terms and Symbols.

In this section, the various symbols used throughout the report are defined. They are generally grouped according to the type of parameter they describe. In addition, there are two main groupings; namely electrical parameters and mechanical parameters. This section is intended as a dictionary and may be passed over until needed. Fig. 1 is an illustration of some of the symbols used and their relation to physical properties of the antenna.

A. Symbols Describing Quantities Associated with Electrical Behavior.

Rationalized MKS units.

- a = radius
- b = strip width, capacitor width
- c = strip thickness
- h = height above ground, measured to center of sphere
- d = magnitude of radial deformation of loop at impact

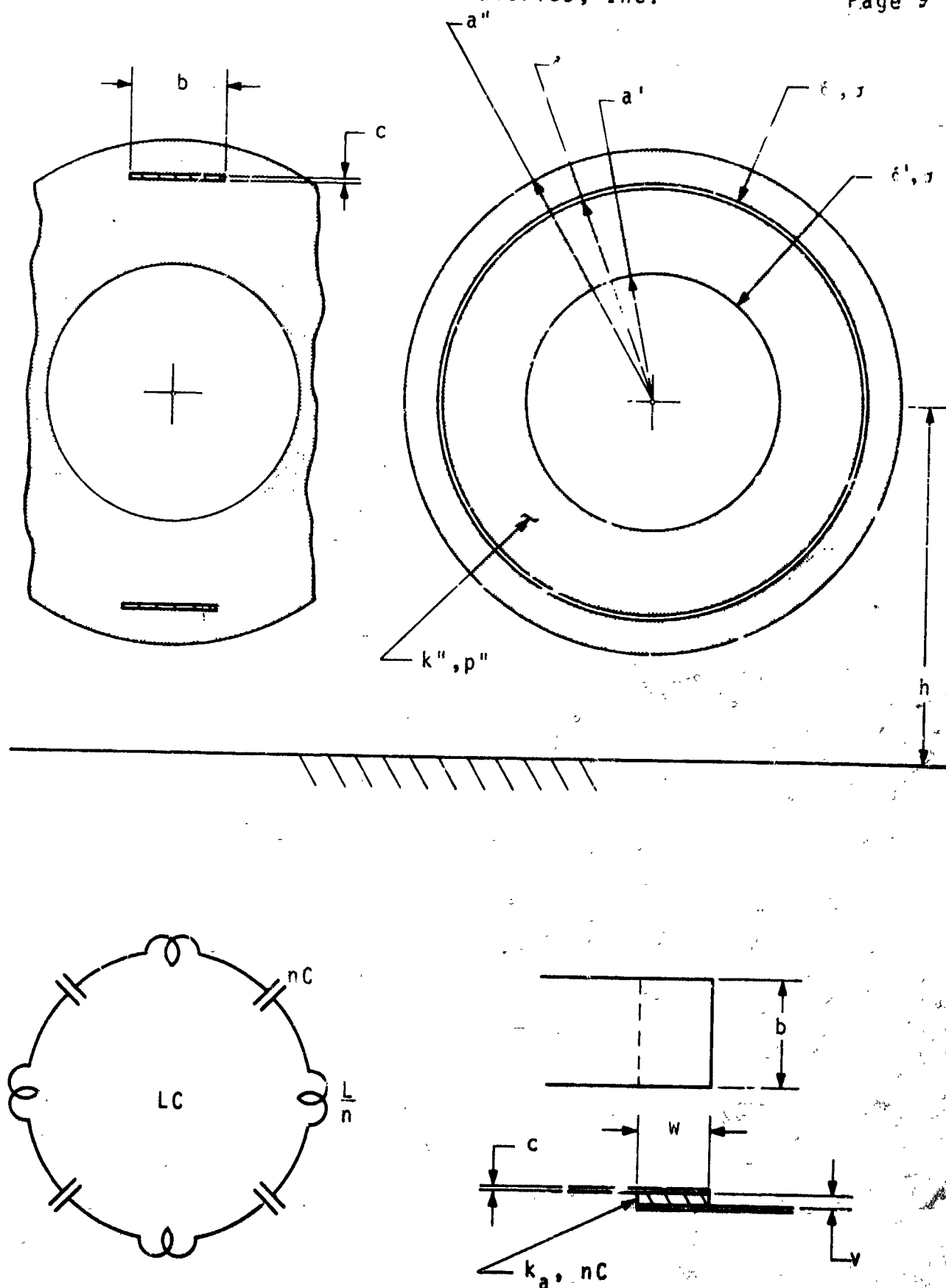


Fig. 1 - Diagrams for explanation of some symbols.

- v = capacitor thickness
 w = capacitor length
 n = number of sections in loop
 δ = skin depth
 σ = conductivity
 μ_o = magnetic permeability of free space = $4\pi \times 10^{-7}$ henry/meter
 ϵ_o = electric permittivity of free space = 8.85×10^{-7} farad/meter
 k = dielectric constant
 λ = wavelength
 f = frequency of operation
 f_o = frequency of resonance in free space
 ω = $2\pi f$ = radian frequency
 R = resistance
 X = reactance
 Z = $R + jX$ = complex impedance
 L = inductance
 C = capacitance
 M = mutual inductance
 R_o = wave resistance of free space = 377 ohms
 R_s = skin resistance = $1/\delta\sigma$
 p = R/X = power factor
 e = efficiency
 ρ = magnitude of reflection coefficient of a plane wave at a dielectric interface, the ratio of the amplitude of electric or magnetic-field intensity
 τ = magnitude of transmission coefficient of a plane wave crossing a dielectric interface, the ratio mean of the amplitude ratios of electric and magnetic-field intensity
 F^2 = transmission coefficient outward through a dielectric interface, the ratio of power density in radial wave (watts/square radian)
 ψ = angle of reflection, measured from plane of interface
VP = "vertical polarization", electric field parallel to plane of angle of incidence

HP = "horizontal polarization", electric field perpendicular to plane of angle of incidence.
CP = circular polarization
LP = linear polarization
VMD = vertical magnetic dipole
HMD = horizontal magnetic dipole
RPF = radiation power factor
DPF = dissipation power factor
TPF = total power factor
Sub l = radiation property if located in free space
Sub k = radiation property if immersed in dielectric medium
Sub c = property of conductor
Sub a = property of alumina
Sub v = VP
Sub h = HP
Superscript ()' = property of spherical core
Superscript ()" = property of dielectric sphere
Superscript ()* = property without core

B. Symbols Describing Quantities Associated with Mechanical Behavior.

Units as specified.

W = weight of projectiles, (lb (force of gravity on earth))
m = mass of projectile (lb-sec²/in.)
 ρ_m = mass density of projectile, (lb-sec²/in⁴)
E = modulus of elasticity, (lb/in²)
V = velocity of compressive wave propagation in projectile material, (in/sec)
T = period of free vibration of projectile, (seconds)
 μ = Poisson's ratio for an elastic material
 V_i = impact velocity of projectile, (in/sec)
g = ratio of peak acceleration at impact to acceleration of gravity on earth
s = dynamic compressive stress in projectile, (lb/in²)
 α = maximum deformation of bodies in collision, (inches)
D = diameter of circular area of contact, (inches)

y = depth of penetration of projectile nose into target, (inches)
t_t = total time of acceleration time history, (seconds)
 $\delta = \frac{1}{\pi}$ times the ratio of linear deformation over pressure (in²/lb)
 γ = material parameter of projectile
 ν = material parameter of projectile
sub p = property of projectile
sub t = property of target

III. Specifications.

The electrical, physical and environmental specifications presented in the NASA statement of work are summarized in Table I. These specifications have been augmented by some changes and interpretations agreed to during the course of this work.

The entire telemetry assembly, including the acceleration sensor, modulator, transmitter and battery, is expected to be packaged within the central 2½-inch diameter spherical volume. A metal spherical shield will enclose these components and thereby provide a core contributing a constant predictable effect on electrical behavior. A light-weight frangible impact-limiter shell may be added about the penetrometer sphere; however, consideration of this shell is not within the scope of the WL study.

For the purpose of this study, a 4-inch diameter penetrometer sphere was considered reasonable. Based on the results of the impact-deformation experiments performed at NASA-Langley, it was tentatively decided that no antenna hardware would be mounted within 3/16 inches of the surface of the sphere. This is equal to the extent of the maximum expected surface deformation at impact on a hard surface.

With regard to the average-gain specification of -14 db (relative to a dipole), it is assumed that this includes dissipation in the antenna. It is also assumed that the essential criterion for pattern gain is that the gain always exceed a certain minimum level. From the total variation of 4 db which is allowed, it is inferred that the minimum allowable level is 2 db below the -14 db average level, or -16 db relative to the peak gain of a dipole. This corresponds to an antenna efficiency of 5%.

Electrical Specifications

Frequency: Fixed frequency between 240 and 250 Mc.

Pattern: Omnidirectional when operating in free space.

Pattern measured about all directions in free space shall vary less than 4 db from maximum to minimum. For antenna locations at or below the impacted surface, radiation is not required at elevation angles less than 10^0 from horizontal.

Gain: Antenna gain, averaged over the spherical radiation pattern shall be at least -14 db with respect to a reference dipole.

Bandwidth: Broadband antenna operation is an objective. Maximum frequency deviation of the transmitter is ± 0.03 Mc.

Reflection: Less than 6 db SWR.

Power: 100 milliwatts, from a 50-ohm coaxial line.

Physical Specifications

Shape: Spherical, encapsulated within a fiberglass-reinforced epoxy-resin sphere.

Size: Between three and five inches, diameter.

Antenna weight: Less than two ounces, including transmission feed line and coupling structure.

Material: Any compatible with the encapsulation.

Environmental Specifications

Impact: Withstand 150 feet-per-second impact on a hard surface.

Vibration: Withstand 20-G random-frequency vibration between 5 and 2,000 CPS for two minutes duration in each of three orthogonal directions.

Immersion: Perform satisfactorily while immersed up to two diameters in porous soil.

Temperature: Capable of operation at any temperature between 0^0C and 60^0C .

Pressure: Capable of operation within the range of pressures from atmospheric to zero (free space).

Table I. Specifications.

In addition to the requirement of operation in free-space, the antenna must perform its function during all conditions of impact, including high-shock deformation at impact on a hard surface at nearly 150 feet per second, and immersion in surface materials. A quantitative determination of the physical properties of the lunar surface is more important if the surface is dust or porous soil rather than hard. Hence, frequency stability and nearly-constant radiation efficiency during the immersion process is more important than at the instant of impact with a hard surface. The extreme conditions of impact and immersion cannot both occur: if the impacted surface is hard enough to cause maximum deformation, the penetrometer will not become immersed below the surface; if the surface is granular or powdery such that the penetrometer becomes immersed, the maximum deformation does not occur.

IV. Study of Alternative Antennas.

A. Available Types.

The choice of the type of antenna is severely limited by the size. The entire antenna is contained in a sphere which is "small" in the sense that its radius (a) is much less than one wavelength ($\lambda/2\pi$). On the basis of a typical size,

	a	=	50 mm	=	2 inches
At 250 Mc:	λ	=	1.25 m;	$2\pi a/\lambda$	= 0.24
At 600 Mc:	λ	=	0.50 m;	$2\pi a/\lambda$	= 0.63

In this size, a simple dipole is the most effective radiator by a large margin.

The small antenna may be an electric dipole or a magnetic dipole (made in the form of a loop). It is known that either of these kinds has about the same limitation on its radiation (Ref. 4). This limitation is described in terms of the "radiation power factor" ($RPF = p_1 = R_1/X_1$) determined by the radiation resistance (R_1) and the reactance (X_1) in free space. The theoretical upper limit for

either kind can be computed on the assumption of a spherical antenna of ideal configuration filled with ideal material:

Theoretical upper limit: $p_1 = (2\pi a/\lambda)^3$

This is the volume sphere ratio of the antenna over the radiansphere.

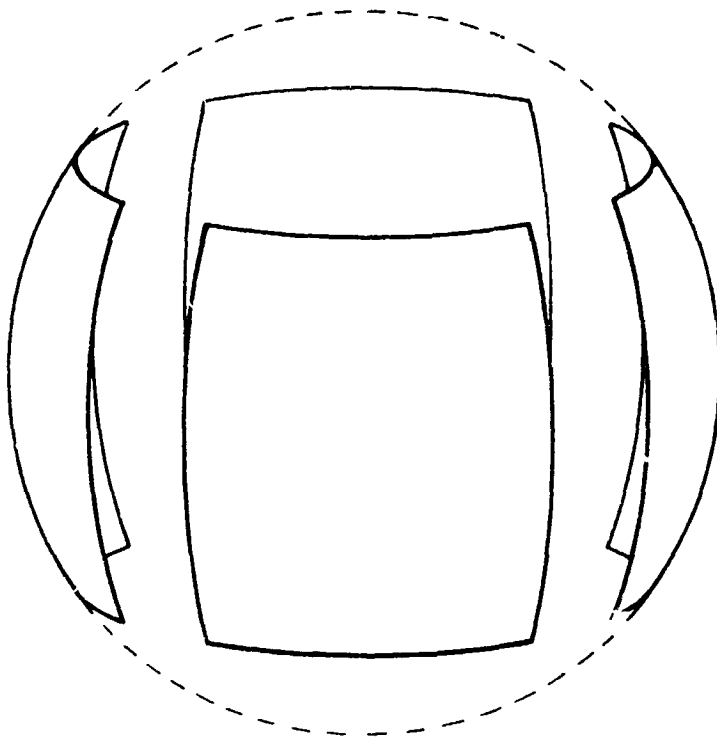
The advantages of a higher RPF have been explained previously (Ref. 4). In the present application, these advantages appear in the following ways.

- (1) Greater radiation efficiency in the presence of the dissipation power factor (DPF) of conductor and dielectric losses.
- (2) Lesser reflection coefficient with any detuning ratio ($\Delta f/f$) which may be caused by manufacturing tolerances, by deformation, or by immersion in a dielectric medium.

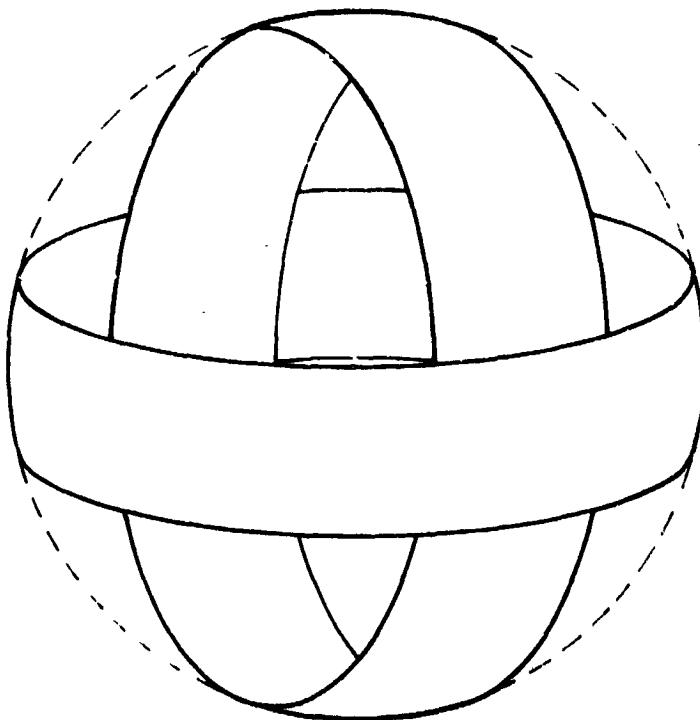
Both factors lead to radiation of a greater fraction of the power available from the transmitter.

A practical dipole falls short of the theoretical limit in two respects. Both the configuration and the filling fall short of the ideal. Fig. 2 shows a practical configuration of each kind. Each is made of thin sheet conductor covering about half of the spherical surface, which is near optimum for maximum RPF, while leaving the inside volume substantially free of conductor. As will be seen, the filling in either case (the dielectric or the absence of magnetic filling) decreases the RPF to about 1/3 the theoretical limit. Some further decrease is caused by the surface conductor shape, and also by the conductive spherical core partially filling the space inside of the antenna.

Since a dipole has a doughnut pattern of radiation, spherical coverage requires a pair of crossed dipoles, as shown in Fig. 2. These can be utilized in various ways. In the subject application, a single transmitter is required to transmit continuously over the coverage sphere. This necessitates coupling to the pair of dipoles with equipartition of power and with time-quadrature



(a) Electric dipoles (electrodes).



(b) Magnetic dipoles (loops).

Fig. 2 - Small dipoles in a pair crossed for spherical coverage.

relative phase. It happens that this can be accomplished simply by a directional coupler made of a small lumped circuit.

B. Considerations.

In making a choice between the two kinds of dipole, there are various requirements and other factors to be taken into account, as will be briefly stated here. Each of these considerations may or may not influence the choice, as will be seen either here or in the further discussion.

(1) The size is limited to a sphere that is "small", meaning that its radius is less than one radianlength ($a < \lambda/2\pi$). Therefore the antenna impedance includes radiation resistance much less than its reactance, so the latter has to be tuned out and the RPF is much less than unity.

(2) Spherical coverage can be obtained by a crossed pair of small dipoles of either kind, excited in time quadrature by the transmitter circuit. The power radiated in all directions over the sphere varies within a ratio of 1:2. The polarization varies radically with direction, so that the spherical coverage requires a diversity receiver responsive to any two orthogonal kinds of polarization. (The alternative is transmission on two channels with time sharing or frequency separation.)

(3) Equipartition of power between two crossed dipoles of either kind, under a wide range of conditions, can be assured by the use of a directional coupler for quadrature excitation. The conditions vary from free space to complete immersion in a dielectric medium of moderate density. They also include manufacturing tolerances of antenna detuning from the operating frequency.

(4) The antenna is imbedded (encapsulated) in a dielectric sphere (radius = a ", dielectric constant = k "). The presence of this material, and its substantial dissipation (p "), have a major effect on a capacitive antenna or electric dipole, but little effect on an inductive antenna or magnetic dipole.

(5) The antenna is protected by a small thickness of dielectric skin or shell which is the outer part of the dielectric sphere.

(6) Inside of the antenna, the dielectric sphere contains a concentric metal-shielded spherical core of somewhat smaller size.

(7) The antenna is to continue operation without excessive detuning after immersion in a dielectric medium of moderate dielectric constant. An electric dipole would experience much more detuning than a magnetic dipole.

(8) There is an unavoidable increase in radiation power factor on immersion in the dielectric medium. With practical materials inside of the spherical volume, the increase is somewhat greater for a magnetic dipole. This increase of RPF has the undesirable effect of changing the impedance but also has the desirable effect of increasing the radiation efficiency for the same DPF.

(9) Maximum radiation power factor is obtained by optimum utilization of the spherical space. This is realized, in either kind of dipole, by using thin sheet conductor covering about half of the spherical surface. This principle is adapted to either kind of dipole, as shown in Fig. 2.

These considerations will be discussed further in order to determine the relative merits of the alternative types.

C. Alternative Kinds of Dipoles.

Fig. 2 shows the outer configuration of the two possible kinds of "small" antenna. Each kind is shown in the form of a pair of crossed dipoles suitable for spherical coverage. Each is proportioned approximately for optimum utilization of a spherical space.

Fig. 2(a) shows the electrodes for a pair of crossed electric dipoles. The four patches have such size and shape as to obtain maximum product of capacitance and radiation resistance, the RPF being proportional to this product. The former requires area of conductor; the latter requires space between the conductors. Each dipole is completed by connecting a tuning inductor between one pair of opposite electrodes. The internal circuit is then coupled to the two inductors with relative phase in time quadrature.

The RPF of the electric dipoles could be further increased slightly by using several open-ended wires in place of the conductive

sheet. This expedient would further decrease the obstruction of magnetic field. One possible configuration is a "spider" of wires to form each electrode. Another is a spiral of wire occupying the space of each electrode and made of the length of wire which, with the connection between electrodes, would resonate the dipole at the operating frequency. The latter would take the place of a separate tuning inductor.

Fig. 2(b) shows the conductors for a pair of magnetic dipoles or loops. The strips of sheet conductor have such width as to obtain maximum quotient of radiation resistance over inductance, the RPF being proportional to this quotient. Decreasing inductance requires strip width, while increasing radiation resistance requires space for magnetic field linking the loops. (A further advantage could be obtained by a filling of magnetic material, such as ferrite, but this seems inconsistent with the severe mechanical requirements.) Each loop is completed by inserting tuning capacitors in series at one or more points. The internal circuit is then coupled to the two loops with relative phase in time quadrature.

For reference in further consideration, Table 2 gives a comparative outline of various properties of small dipoles of both kinds. Some of these properties are discussed above; others will receive attention below. Several of the factors are nearly the same for both kinds. This is true of the conductor area, also of the RPF in free space or in the dielectric medium.

The detuning effect of immersion is greatly different. The electric dipole has a concentrated electric field which is directly sensitive to the surrounding dielectric, which increases the capacitance. The magnetic dipole has a concentrated magnetic field which is relatively insensitive to the surrounding dielectric properties. In the latter case, the dielectric slightly increases the apparent tuning capacitance by acting as a small shunt capacitance.

The effect of dielectric loss in the filling material is also greatly different. This effect cannot be reduced in the electric dipole, but can in the magnetic dipole by dividing the loop into a number of sections separated by series capacitors.

Electric DipolesMagnetic Dipoles (Loops)Optimum Shape

Two pairs of electrodes covering
about 1/2 of spherical surface.

Two loops of strip covering
about 1/2 of spherical surface.

Radiation Power Factor in Free Space

Upper limit in spherical volume.

$$P_1 < \left(\frac{2\pi a}{\lambda}\right)^2 \frac{1}{1 + \frac{1}{2} k''}$$

$$P_1 < \left(\frac{2\pi a}{\lambda}\right)^2 \frac{1}{1 + 2}$$

(dielectric filling, $k'' = 3.5$)

(non-magnetic filling)

Radiation Power Factor, Effect of Immersion

$k = 3$ in dielectric medium (2.5 to 3.5)

$k'' = 3.5$ in dielectric sphere.

$$P_k/P_1 = k^{3/2} \frac{2 + k''}{2k + k''} = 3.0$$

$$P_k/P_1 = k^{3/2} = 5.2$$

Detuning Effect of Immersion

$$\frac{\Delta C}{C} = \frac{2(k - 1)}{2 + k''} = 0.73$$

$$\frac{\Delta C}{C} = \frac{k - 1}{3} \left(\frac{2\pi a}{\lambda}\right) = 0.16$$

$$\frac{\Delta f}{f} = -0.24$$

$$\frac{\Delta f}{f} = -0.08$$

Dissipation in Dielectric Filling

Largely effective in antenna
reactance, because most of
antenna capacitance is in
this dielectric

Effect can be reduced by
number of series capacitors,
but minimum set by induced
current in dielectric.

Tuning and Coupling

Pair of inductors,
require space inside
2 (or 4) small coils.
Wire connections to
electrodes.

Integral series capacitors,
require no space inside.
Small wires inductively
coupled to loops.

Table 2. Comparison of electric and magnetic dipoles.

The circuit aspects of tuning and coupling are practical problems that will be discussed separately for each kind of dipole.

D. Electric Dipoles.

Referring to Fig. 2(a) and Table 2, there is a crossed pair of electric dipoles, each one made by connecting two opposite electrodes through a wire and a very small tuning inductor.

The RPF in free space is greatly decreased, below the theoretical limit, by the dielectric filling. Otherwise, the electric dipole without dielectric filling would have RPF double that of the magnetic dipole without magnetic filling. The dielectric filling removes this advantage.

A serious problem of the electric dipole is the detuning by immersion. In the simple spherical model, the capacitance is increased by the factor 1.73, so the frequency of resonance is decreased by the factor 0.76. The relative change is decreased by the electrode configuration at the metal core, but not as much as the RPF is decreased by these properties, making the design even more sensitive to detuning by immersion.

The major part of the dipole capacitance is in the dielectric material filling the sphere. This material may be chosen for mechanical strength rather than low loss. Therefore the radiation efficiency may be greatly reduced by the DPF caused by losses in the filling material. This may be the most serious problem of the electric dipole.

E. Magnetic Dipoles (Loops).

Referring to Fig. 2(b) and Table 2, there is a crossed pair of magnetic dipoles, each one formed by a loop of thin metal strip. In the practical form to be described, each loop is tuned by inserting in series a number of capacitors which are made an integral part of the loop.

The RPF in free space falls far short of the theoretical limit, by the lack of a magnetic filling. This adverse effect is comparable to that of the dielectric filling in the electric dipole.

A striking advantage of the magnetic dipole is the small amount of detuning caused by immersion. The induced currents in the surrounding dielectric have the effect of a small amount of capacitance in shunt with the loop. This causes a small increase in the apparent value of tuning capacitance. The formula for this effect is an adaption of the previously derived formulas for a magnetic dipole surrounded by a conductive medium (Refs. 8, 9, 11). The effect is proportional to the radius of the dielectric sphere in which the loop is located. In the simple spherical model, the capacitance is increased by the factor 1.16, so the frequency of resonance is decreased by the factor 0.92. The relative change is decreased by the electrode configuration and the metal core, and in about the same ratio as the RPF is decreased by these properties, making the design no more sensitive to detuning by immersion.

The formula for detuning by immersion is based on the ideal case of many series capacitors inserted in the loop for tuning to resonance. Then the individual capacitors become so large that the surrounding dielectric makes no appreciable addition to their capacitance. In practice, if the loop is divided into n parts separated by series capacitors, a simple model gives the following approximate formula for the direct effect of adjacent dielectric.

$$\begin{aligned}\frac{\Delta C}{C} &= \frac{k-1}{6} \left(\frac{\pi}{n} \frac{2\pi a}{\lambda} \right)^2 \\ &= 0.012 \quad \text{if } n = 4, \quad 2\pi a/\lambda = 0.24\end{aligned}$$

$$\frac{\Delta f}{f} = -0.006$$

The actual effect is somewhat greater but the resulting amount of detuning is still negligible in comparison with other effects of immersion.

Another advantage of many series capacitors is the reduction of dissipation in the dielectric filling near the loop conductor. This is important because the filling material may be chosen for mechanical strength rather than low loss. The DPF added in the tuned circuit from the dissipation p'' in this material near the loop is approximately,

$$\Delta p = p'' \frac{k''}{6} \left(\frac{\pi}{n} \frac{2\pi a}{\lambda} \right)^2$$

$$= 0.02 p'' \quad \text{if } n = 4, \quad 2\pi a/\lambda = 0.24$$

The dielectric loss from this cause may be reduced as far as required, by increasing n .

Induced dielectric current in the filling material also reflects some of its loss into the loop reactance. The DPF added in the tuned circuit from this effect is,

$$p = p'' \frac{k''}{15} \left(\frac{2\pi a}{\lambda} \right)^2$$

$$= 0.014 p'' \quad \text{if } 2\pi a/\lambda = 0.24$$

This is equal to the preceding formula if

$$r = \pi \sqrt{5/2} = 5.0$$

Since this effect by induced currents cannot be decreased by increasing n , there is little to gain by $n > 5$.

The coupling from the transmitter to each loop presents no unusual problem. It can be done by inductive coupling with a small wire, not requiring any conductive junction with the loop strip; this is regarded as an advantage.

E. Recommendation of Crossed Loops.

Crossed dipoles with quadrature excitation are required for spherical coverage, such excitation being obtainable in a small directional coupler. The preceding considerations lead clearly to a preference for magnetic dipoles or loops as compared with electric dipoles, for the substantial reasons to be listed here. There is no factor which clearly favors electric dipoles.

(1) An integrated tuned antenna can be formed by a loop of thin metal strip with a number of capacitors inserted in series for tuning, independent of any conductive connections with the inside of the sphere.

The utilization of the entire space for the inductor enables minimum dissipation and maximum radiation efficiency. No extra space is required for tuning the antenna.

(2) In free space, there is much less effect of dielectric loss in the filling material, enabling greater radiation efficiency. This advantage is obtained by the number of series capacitors, made possible by the form of the self-tuned loop antenna.

(3) During immersion in a dielectric medium, there is much less detuning. This advantage also is obtained by the number of series capacitors.

The principal problem in the loops is probably the mechanical construction of the series capacitors structurally integrated with the metal strip. As early as 15 years ago, a smaller metal-strip loop with an integral single series capacitor was adopted for use in a proximity fuze subject to severe stresses. This is regarded as a typical problem of electrical and mechanical design coordination.

V. Mechanical Problems of Impact.

The mission of the penetrometer device places severe requirements on the performance during impact. It is during this period that telemetry is essential. Survival for future operation is not enough; reliable operation during impact deceleration must be assured.

Primary protection for the penetrometer components is provided by packaging them within the sphere of fiberglass-reinforced epoxy-resin encapsulant. The antenna structure within the encapsulant is particularly susceptible to mechanical distortions and stresses because of its proximity to the impacting surface. However, the reaction of distortions of the antenna on the telemetering modulation is not of primary significance; techniques can be employed to buffer the circuit from antenna reaction. The antenna distortions resulting from impact are analyzed in Appendix II, and the effect on electrical performance is assessed in Section VIII.

The principal problem of impact is maintaining the integrity of the antenna structure, thereby assuring continuous operation

without the generation of noise modulation by intermittent failure. For the crossed-loop antenna configuration proposed for the present application, there are three potentially weak points: any connection to the loop radiator, the strip conductor which forms the loop, and the capacitors in the loop.

A connection to the loop radiator could be accomplished by a flexible wire, but there is proposed a non-contacting loop-coupling; the latter method is superior mechanically and, as shown in Section VII, is a good electrical design.

An analysis of the mechanics of impact on a hard surface is presented in Appendix II. The estimates of stress and deformation under the extremes of impact provide a basis for the selection of materials and their location. For the strip conductor in particular, materials of adequate strength and extensibility are required to survive the strain a few tenths of an inch below the surface of the encapsulant. The ceramic capacitor materials have great strength, but must be protected from shock transmitted through the encapsulant and the strip conductors. By the proper choice of these materials, structural configuration, and location within the encapsulant, the stresses transmitted to the dielectric capacitor and its associated bonding surfaces can be restricted to a tolerable limit. It is proposed that the metal strip be thin enough to comply with the strain in the encapsulant, and also thin enough to avoid breaking the bond at the dielectric faces of the capacitors. These considerations are discussed in more detail with regard to the particular antenna configuration in Section VII.

For the ultimate mechanical design and demonstration of performance, it will be necessary to perform impact reliability tests.

VI. Electromagnetic Problems of Environment.

A. Polarization Diversity.

Crossed dipoles, oriented in space quadrature, are necessary for full spherical coverage. A single dipole has a radiation pattern in free space that is a sine function of revolution (doughnut shaped),

omnidirectional in only one plane, and having radiation nulls along the dipole axis. With two crossed dipoles, the second dipole radiates in the direction of the null of the first dipole, and vice versa.

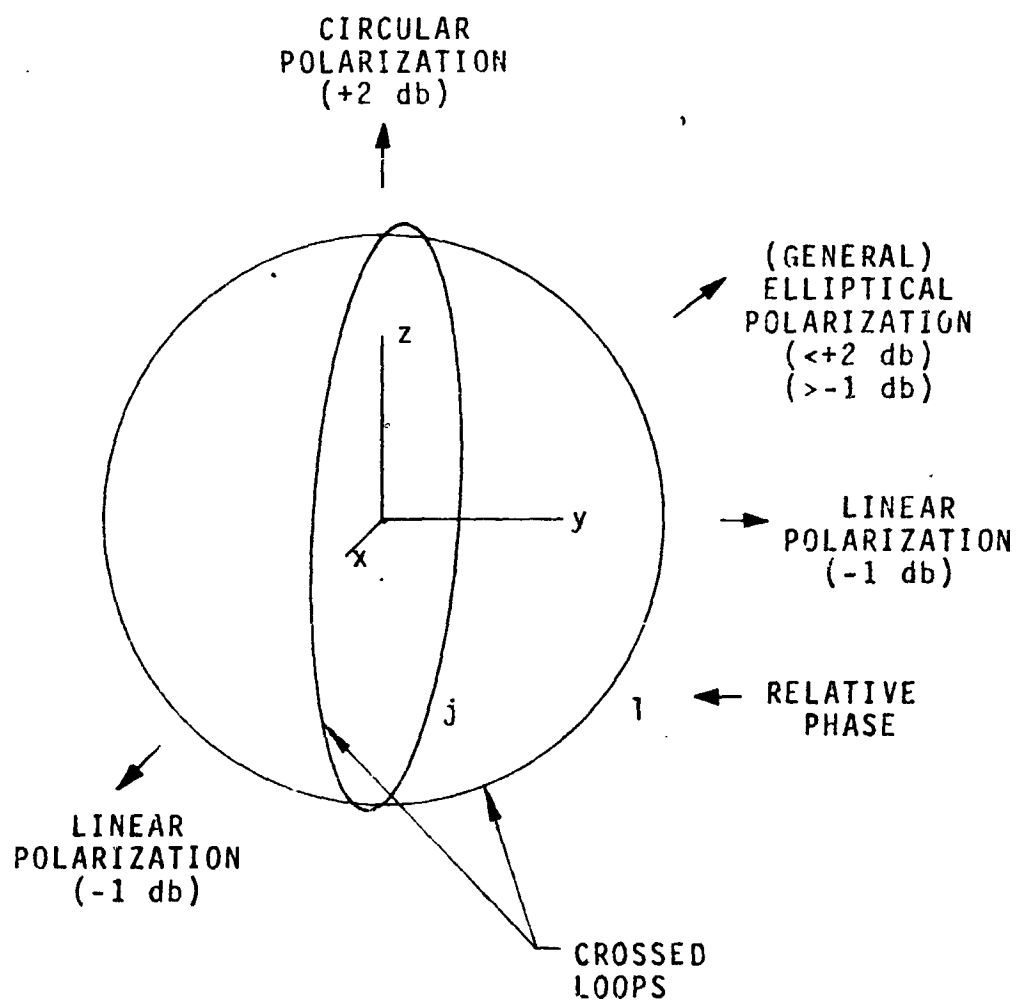
Spherical coverage can be achieved from the crossed-dipole arrangement in a number of ways. In the present application, a single antenna is required to transmit simultaneously over the entire sphere. This is accomplished by exciting both dipoles with equal power in time-quadrature phase relation. The resulting pattern (Fig. 3) is similar to that of the well known turnstile antenna with radiation in all directions with various polarizations: linear, right and left-handed circular, and elliptical.

For the reception of the transmitted signal from the crossed-loop transmitter in any orientation, a single receiving antenna with any particular polarization has certain limitations. Transmission nulls will occur at certain directions when the receiving antenna is cross-polarized to the radiated signal. In fact, some polarization loss is inevitable at all directions in space except at the directions where the polarization of the radiation signal and the receiving antenna happen to be matched.

In order to receive all the power radiated, at any direction in space, a diversity receiver with two orthogonally polarized antenna is required. With this receiver arrangement, the total variation of the received signal about all directions in space is about 3 db, the unavoidable variation of a simple turnstile antenna.

B. Radiation Before Impact.*

The free-space pattern of the crossed-loop antenna is modified by reflection at the approaching surface. The resulting overall pattern depends on the relative intensity and polarization of the direct, incident and reflected signals, and their combination at the diversity receiver. It is not possible to present a single representative radiation pattern for the condition before impact because such a pattern depends on the relative orientation of the antenna and the ground. In the present application, the antenna is not stabilized relative to the ground so that the orientation is unknown, and changing. Those factors that are significant in



(Power relative to an isotrope)

Fig. 3 - Crossed loop antennas fed in quadrature for spherical coverage.

formulating the radiation before impact will be presented so that some generalizations can be made as to what can be expected; in particular some estimates regarding the maximum degradation in performance will be presented.

The geometry for the condition of radiation before impact, from an antenna in free space (1) above a dielectric medium (k), is shown in Fig. 4. The radiation pattern for a polarization-diversity receiver at an elevation angle ψ is the combination of the direct and reflected signals in each of two orthogonal polarizations (VP and HP).

The effect of the dielectric interface on the radiation before impact is formulated in terms of the reflection coefficients ρ_v and ρ_h corresponding to the two orthogonal polarizations.

$$\rho_v \exp -j\theta_v = \frac{k \sin\psi - \sqrt{k - 1 + \sin^2\psi}}{k \sin\psi + \sqrt{k - 1 + \sin^2\psi}}$$

$$\rho_h \exp -j\theta_h = \frac{\sin\psi - \sqrt{k - 1 + \sin^2\psi}}{\sin\psi + \sqrt{k - 1 + \sin^2\psi}}$$

Perfect dielectric, free of dissipation, is assumed. For VP, there is no reflection at the Brewster angle ψ_0 , for the condition:

$$\sin^2\psi_0 = \frac{1}{k + 1}$$

The reflection coefficients for $k=3$ are plotted in Fig. 5. For the perfect dielectric, the phase angle of the reflection is 0 or π radians.

The radiation pattern in the presence of the reflection from the air-dielectric interface is the resultant interference pattern of the direct and reflected components of the same polarization; at the diversity receiver, the two orthogonal component polarizations are summed, independent of their relative phase. For each polarization there is the usual lobe pattern of alternating minima and maxima. Below the Brewster angle, the angular location of the minima and maxima for VP and HP will coincide because the phase of the reflection coefficient is the same; above the Brewster angle,

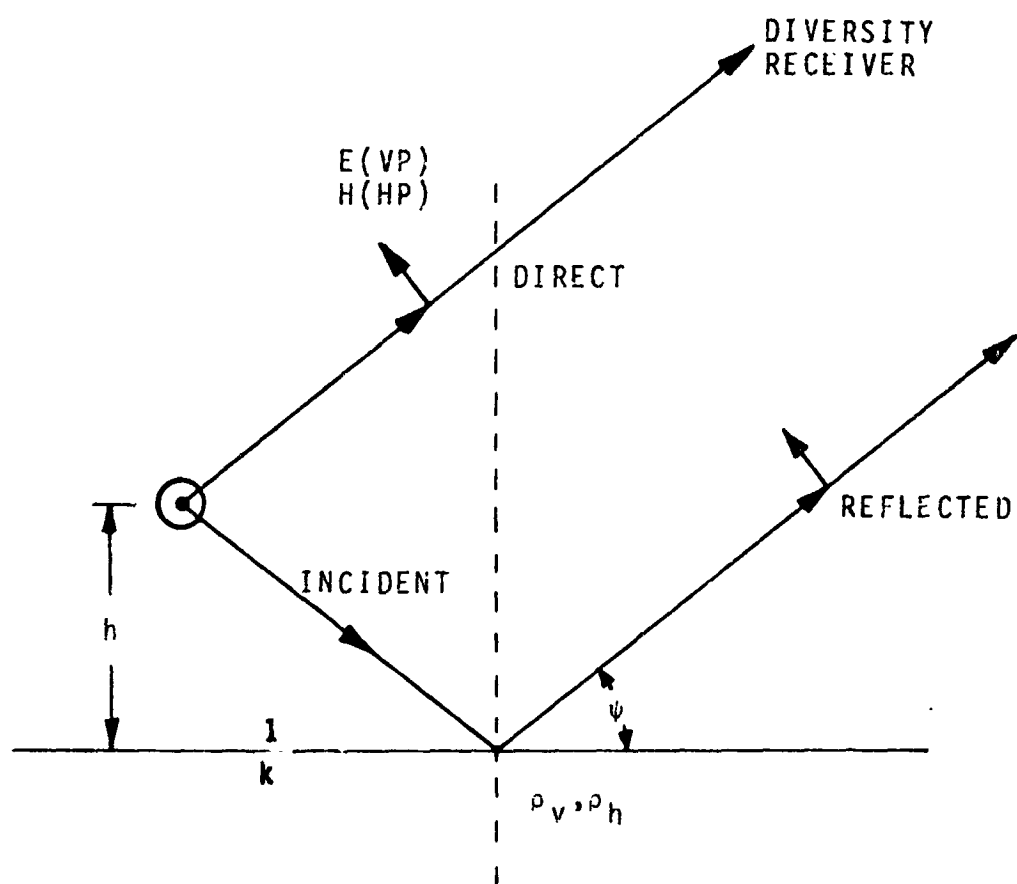


Fig. 4 - Radiation before impact, with reflection from surface.

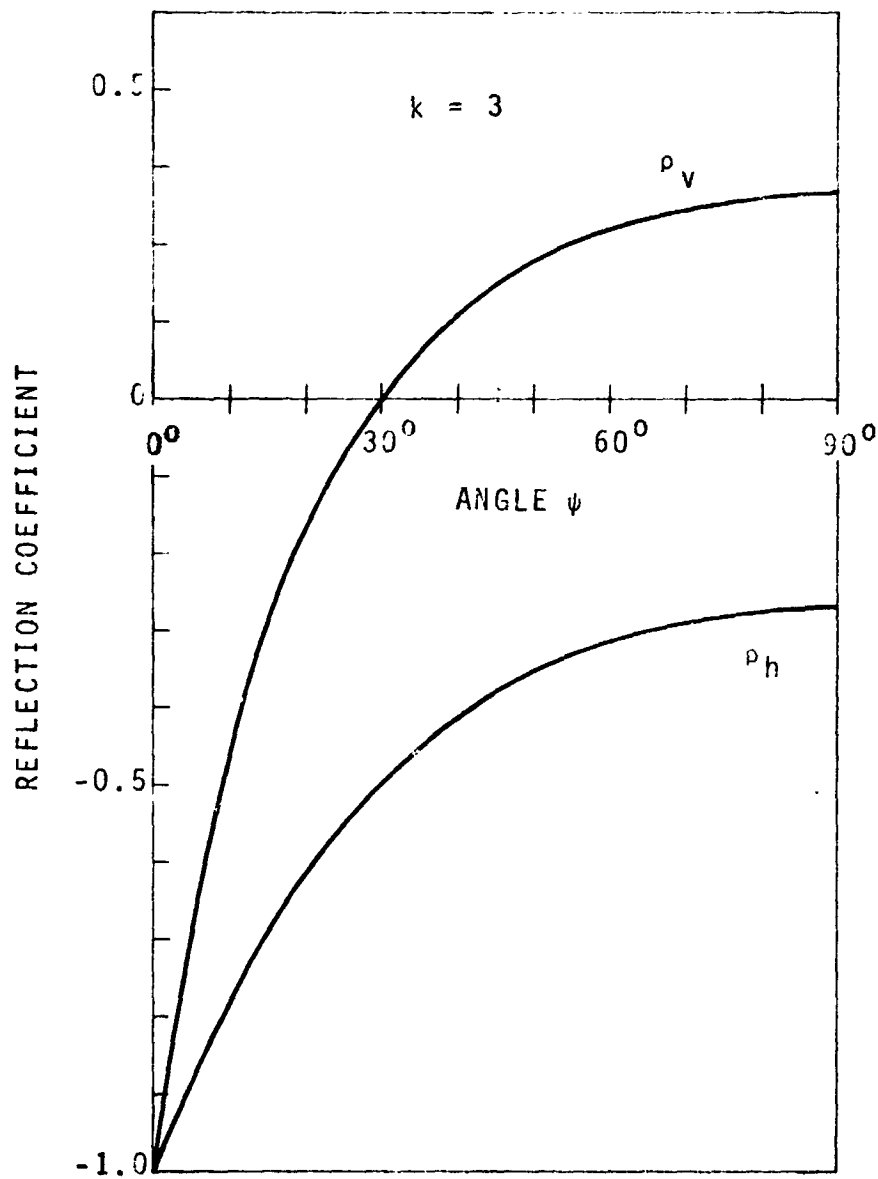


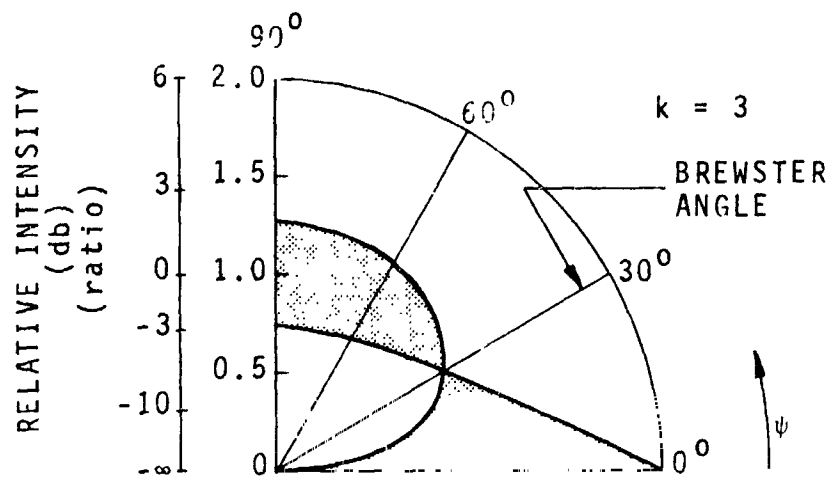
Fig. 5 - Reflection coefficient at dielectric surface.

where the reflections are out of phase, the minima in one polarization will coincide with the maxima in the other, and vice versa. The envelope of the limits of the lobe pattern can be defined in terms of $1 \pm |\rho|$; such envelopes are plotted in Fig. 6 for VP, HP and CP radiation from the antenna above a reflecting interface. These results are representative of the condition for an assumed isotropic radiator where the direct and incident amplitudes are equal and the same polarization.

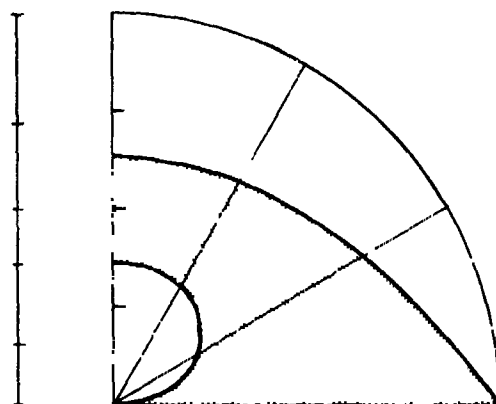
The patterns of radiation intensity and polarization of the crossed-loop antenna are substantially more complex than the simple cases described above. While the total radiation power for diversity reception is omnidirectional over the sphere within 3 db, the pattern of intensity for any particular polarization varies greatly. This can be illustrated by the polarization pattern of the crossed-loop antenna which is shown in Fig. 7. The polarization pattern is a pictorial representation of the polarization ellipse on a stereographic projection of the radiation sphere (Ref. 15).

Three polarization patterns are shown in Fig. 7 which are merely representations for three particular orientations of the crossed-loop antenna relative to the projection plane. For this case, there is a symmetry which simplifies analysis; the intensity and polarization for the direct and incident radiation are equal for each elevation angle. The azimuth direction is represented by the vertical axis of the projection; positive and negative elevation angles are located on either side of the horizontal axis, respectively. The envelope of each polarization component may be determined as presented earlier (Fig. 6) by consideration of the relative intensity of the appropriate elevation pattern. The resultant envelope of the intensity at the polarization-diversity receiver can then be computed by summing the orthogonal components keeping in mind that minima and maxima of HP and VP coincide below the Brewster angle, and alternate above this angle.

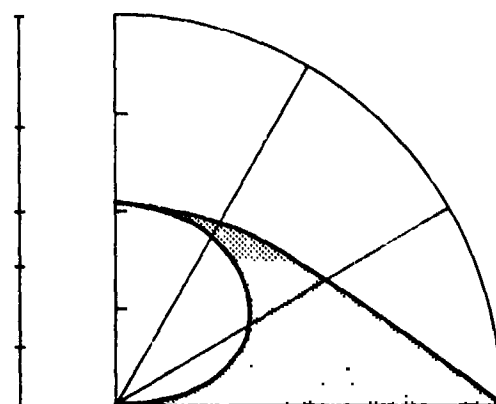
In general, the direct and incident radiation of the crossed-loop antenna may be represented by any two points on the projection of the radiation sphere, depending on the elevation angle and the relative orientation of the antenna. A solution of the problem in such general terms is beyond the scope of this presentation.



(a) vertical polarization

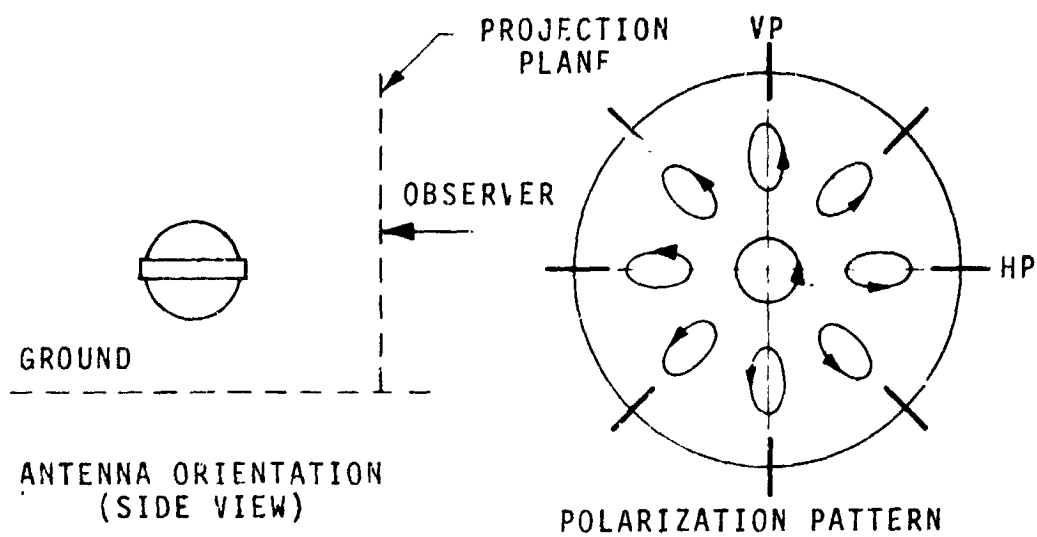


(b) horizontal polarization

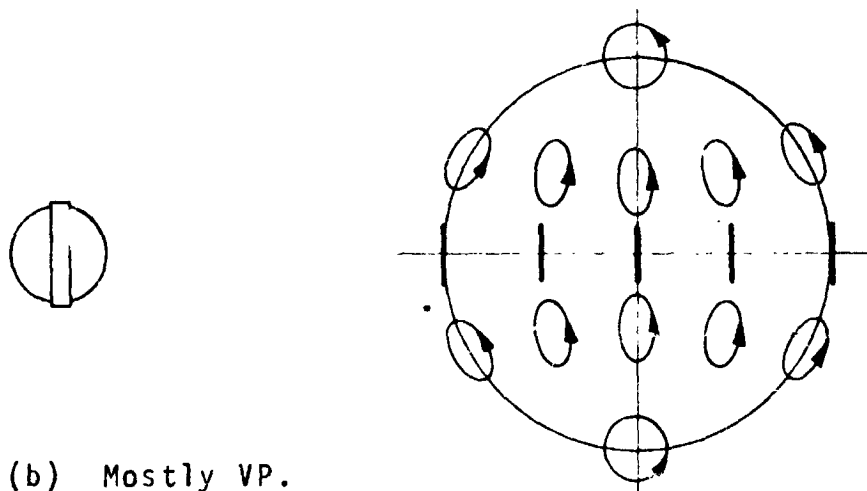


(c) circular polarization

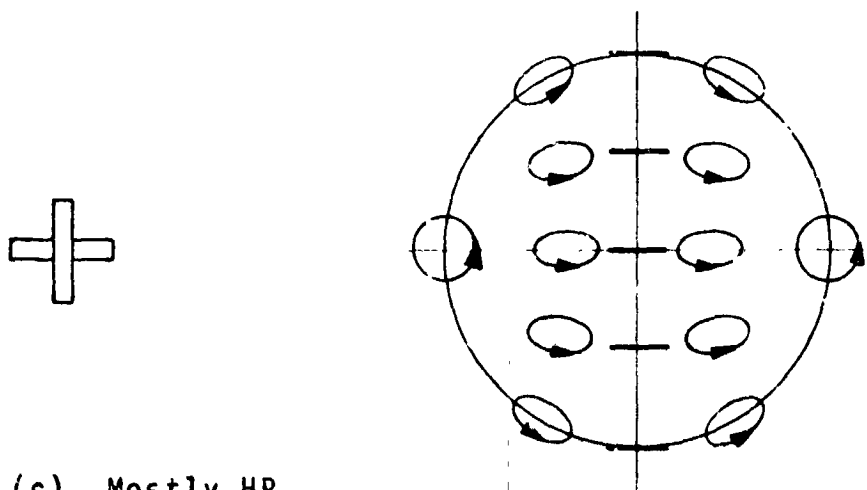
Fig. 6 - Pattern envelope with reflection from surface.



(a) HP and VP.



(b) Mostly VP.



(c) Mostly HP.

Fig. 7 - Polarization patterns of crossed-loop antenna.

The illustrations in Fig. 7, however, do indicate a possible worst case, which is of interest in the evaluation of the overall radiation of the crossed-loop antenna before impact.

The maximum degradation of the overall radiation by pattern interference can be estimated by considering the condition illustrated in Fig. 7(c), where, in the plane of interest the polarization of the crossed-loop antenna radiation is entirely horizontal. This is the condition for deepest minima (maximum reflection coefficient), with no opportunity for signal augmentation by diversity reception of crossed-polarized components. Under these conditions, the interference minima relative to the intensity of a single loop have been presented in Fig. 6(b); for the crossed-loop configuration, an additional 3 db loss must be added. Consequently, the estimated maximum degradation of intensity at the diversity receiver, relative to the peak intensity available is:

90°:	- (2.7 db + 3.0 db)	= - 5.7 db
60°:	- (3.3 db + 3.0 db)	= - 6.3 db
30°:	- (6.0 db + 3.0 db)	= - 9.0 db
10°:	- (13.0 db + 3.0 db)	= -16.0 db

C. Radiation at Impact.

The radiation is difficult to compute for the transitional conditions between free space and deep immersion. The given relations for free space will be supplemented by formulas for deep immersion. Then some comments will be made relative to the transitional conditions at impact.

Fig. 8 shows the geometry of radiation from a submerged antenna into the surrounding dielectric medium (k) and upward through the interface into free space (1). The reflected and transmitted waves are denoted by the reflection coefficient (ρ) and the transmission coefficient (τ).

The radiation efficiency through the interface, for vertical and horizontal polarization (F_v^2 and F_h^2), is to be formulated on the basis of transmission from a spherical wave in the dielectric outward by a spherical wave in free space. The radiation efficiency is the

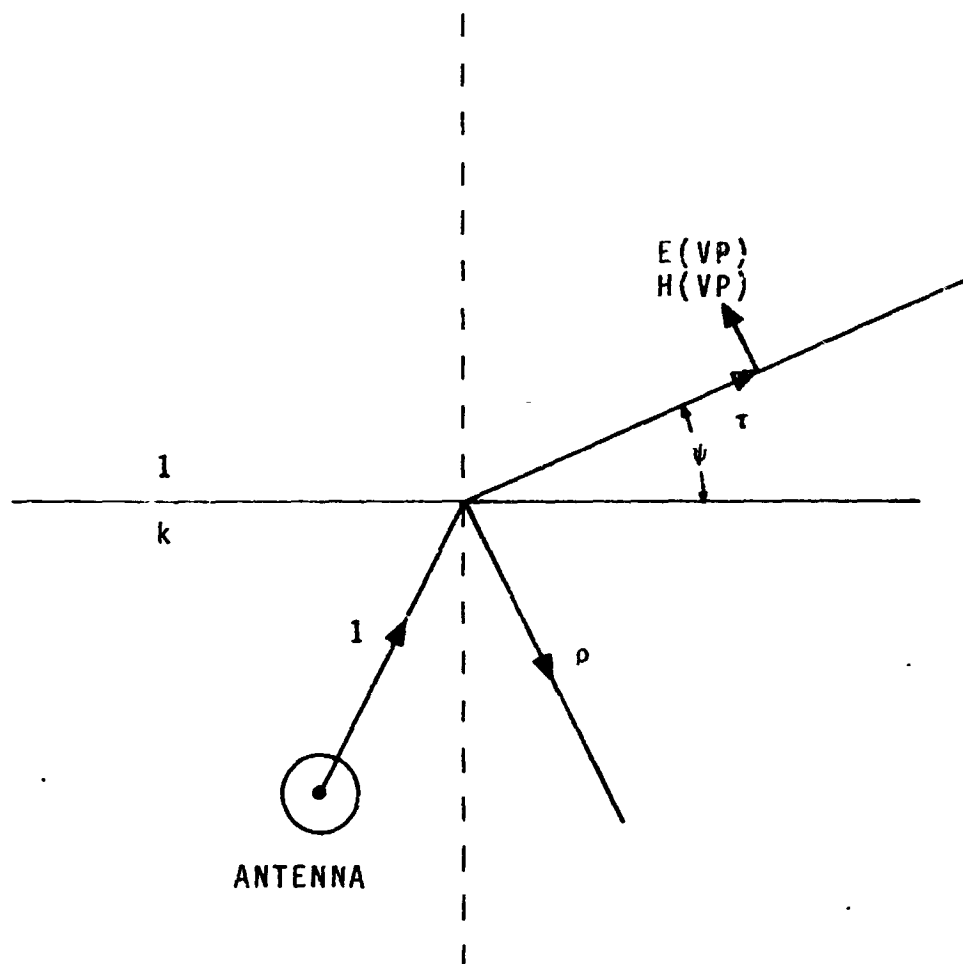


Fig. 8 - Transmission outward through the dielectric interface (ground).

ratio of power density per square radian (steradian) in these two spherical waves along a certain ray at an elevation (ψ) above the ground plane. Therefore this efficiency is decreased by the reflection at the interface and also by the spreading of the ray angle with refraction.

On this basis, the radiation efficiency through the interface is formulated as follows for VP and HP.

$$F_V^2 = \frac{4\sqrt{k} \sin^2 \psi}{(\sqrt{k-1} + \sin^2 \psi + k \sin \psi)^2}$$

$$F_H^2 = \frac{4 \sin^2 \psi}{\sqrt{k} (\sqrt{k-1} + \sin^2 \psi + \sin \psi)^2}$$

In either case, at perpendicular incidence ($\psi = \pi/2$),

$$F_V^2 = F_H^2 = \frac{4}{\sqrt{k} (\sqrt{k} + 1)^2}$$

Near grazing incidence ($k \psi \ll \sqrt{k-1}$), these ratios approach the limits,

$$F_V^2 = \frac{4\sqrt{k} \sin^2 \psi}{k-1} ; F_H^2 = \frac{4 \sin^2 \psi}{\sqrt{k} (k-1)} ; F_H^2/F_V^2 = 1/k$$

Fig. 9 shows a polar graph of these factors for a typical dielectric medium ($k = 3$). The interpretation of these factors should take into account also the radiation efficiency of the antenna into the medium, which is greater than that in free space. This results from the increase of RPF relative to DPF.

If the antenna radiation efficiency is very small in free space, it is greatly increased by immersion (by the factor $k^{3/2}$). Near the vertical direction, the resulting efficiency of radiation from the antenna outward above ground is actually increased by immersion. The net ratio of increase is subject to the upper limit:

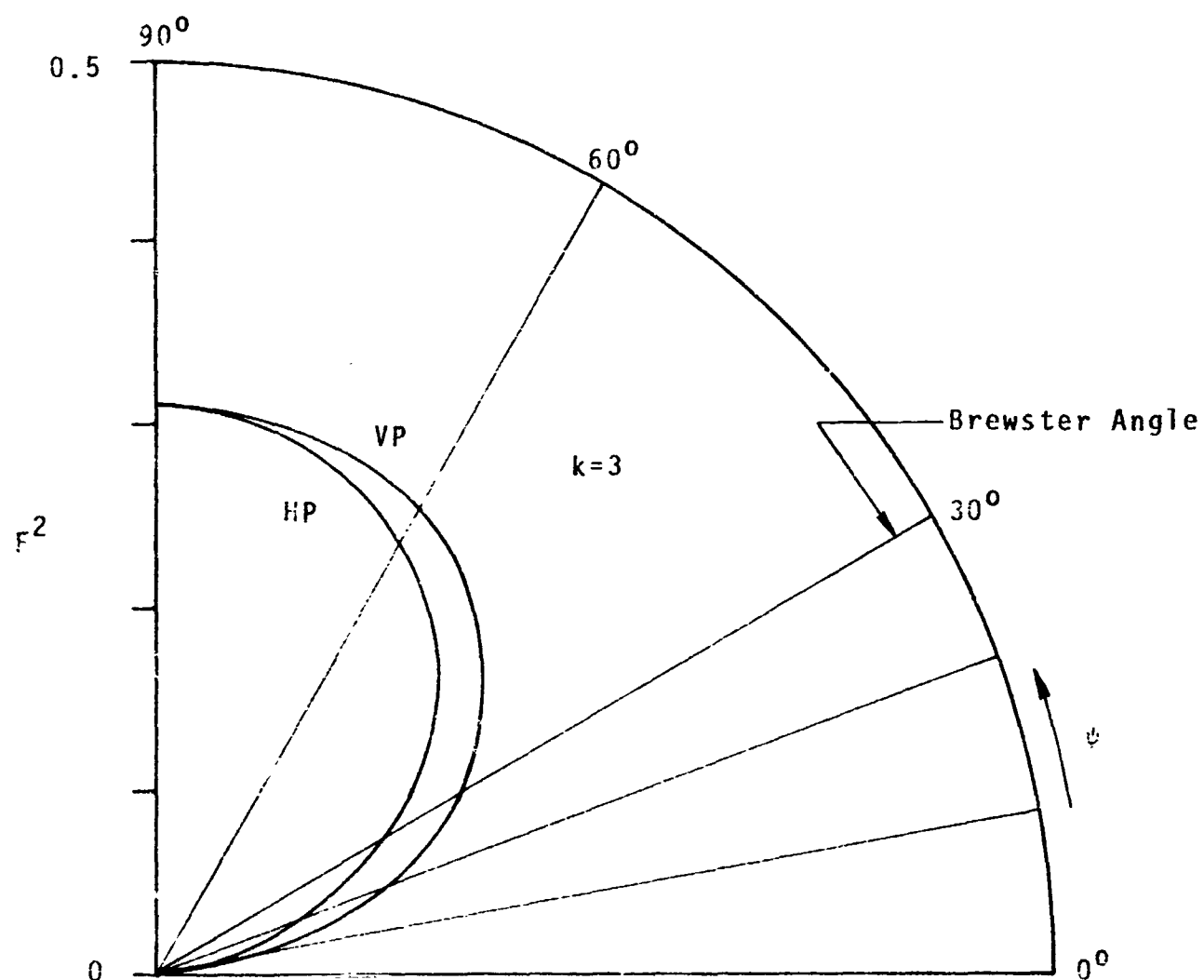


Fig. 9 - Variation of transmission efficiency outward through the dielectric interface.

$$k^{3/2} F_v^2 = k^{3/2} F_h^2 = \frac{4k}{(\sqrt{k} + 1)^2} < 4$$

In locations not far above or below the surface, the antenna behavior in free-space or in the medium is modified by the image reflected in the interface.

The transitional location may be defined as the condition of half-immersion. At this point, the radiation efficiency from the antenna outward above ground is intermediate between that in free space and that in deep immersion. There seems to be no simple formulation for this condition.

The following example illustrates these effects. It is based on an antenna having a radiation efficiency of 0.50 in free space.

Dielectric medium (ground):

$$\text{Radiation efficiency in the ground: } \frac{3^{3/2}}{1 + 3^{3/2}} = 0.84$$

Transmission efficiency through interface:

$$\psi = \pi/2 = 90^\circ : F_h^2 = F_h^2 = 0.31$$

$$\psi = \pi/18 = 10^\circ : F_v^2 = 0.055$$

$$F_h^2 = 0.027$$

Radiation efficiency from submerged antenna outward above ground:

$$90^\circ: 0.84 \times 0.31 = 0.26$$

$$10^\circ \text{ VP: } 0.84 \times 0.055 = 0.046$$

$$10^\circ \text{ HP: } 0.84 \times 0.027 = 0.023$$

Estimated radiation efficiency from half-submerged antenna:

$$90^\circ: \sqrt{0.50 \times 0.25} = 0.36$$

$$10^\circ \text{ VP: } \sqrt{0.50 \times 0.046} = 0.15$$

$$10^\circ \text{ HP: } \sqrt{0.50 \times 0.023} = 0.11$$

By way of summary, the conditions governing radiation around the time of impact may be stated briefly.

(1) Above the ground, the radiation efficiency is that in free space, modified by the image in the surface.

(2) In the ground, the radiation efficiency in the dielectric medium is greater, but reflection at the surface decreases the radiation efficiency outward above ground. The former factor predominates near vertical incidence, the latter near grazing incidence.

D. Impedance Variation by Deformation.

As a magnetic-dipole antenna comprising crossed loops imbedded within an epoxy-resin sphere is impacted on an impenetrable surface, a slight transitory change of shape and size of the antenna occurs. The magnitude and character of this transitory change is a function of the antenna velocity before impact, the physical properties of the surface impacted and of the epoxy-resin sphere, and the orientation of either loop with respect to the point of impact. A change of shape or size of the antenna loop causes a change of inductance and hence detuning. Antenna detuning, in turn, appears as reflection in the line and a corresponding loss in transmitted power. Furthermore, depending on the loading sensitivity of the transmitter frequency, the change of antenna impedance shifts the transmitter frequency and generates spurious modulation. This is detrimental because it introduces an error in the telemetered information.

The antenna orientation in which one loop is horizontal and the other is vertical at the moment of impact results in the greatest deformation, detuning and reflection. At impact, the shock wave stresses the horizontal antenna loop uniformly, producing a transitory increase of loop circumference. The maximum relative increase of loop circumference has been estimated at 3 mils (Reference, Appendix II). Such deformation will result in an increase of loop inductance of 9.5 mils as calculated in Section VII.A, which follows.

The vertical antenna loop is subjected to a transitory localized flattening at the point of impact, with the circumference

remaining nearly constant. The electrical effect of this deformation has been evaluated experimentally, first by the measurement of loop inductance, and later by a more precise method of impedance measurement. The loop was deformed in the manner to be expected during impact; the loop inductance is reduced by deformation as indicated in Fig. 10.

The antenna-detuning loss resulting from these inductance variations is presented in Section VIII.B.

E. Impedance Variation by Immersion.

As the magnetic dipole antenna approaches the air-dielectric interface prior to impacting the ground, both resistance and reactance of the dipole antenna change with antenna height. This change of resistance and reactance also depends on the relative orientation of the dipole, the operating frequency and the electromagnetic properties of the ground. A theoretical analysis of the impedance change of a very small dipole, valid for location from far above the ground (free space) to the point of contact with the ground, is presented in Reference 13. This analysis can also be extended in some degree to represent the case of a dipole below the surface of the ground.

The theoretical analysis of antenna-impedance variation for antenna locations from far below the surface (far submerged) to contact the surface, is similar to the free-space analysis. As the antenna approaches the dielectric-to-air interface from either above or below, the coefficient of reflection from the interface goes through similar variation but of opposite polarity. This reflection causes the variation of antenna impedance, relative to the limiting value of radiation resistance far above or below the surface.

The radiation resistance (R_k) and the change of reactance (ΔX_k) of a small loop antenna far submerged is related to the radiation resistance (R_1) of the same antenna in free space by the following simple formulas.

$$R_k = R_1 k^{3/2} ;$$

$$\Delta X_k = R_1 (k-1) \frac{\lambda}{2\pi a}$$

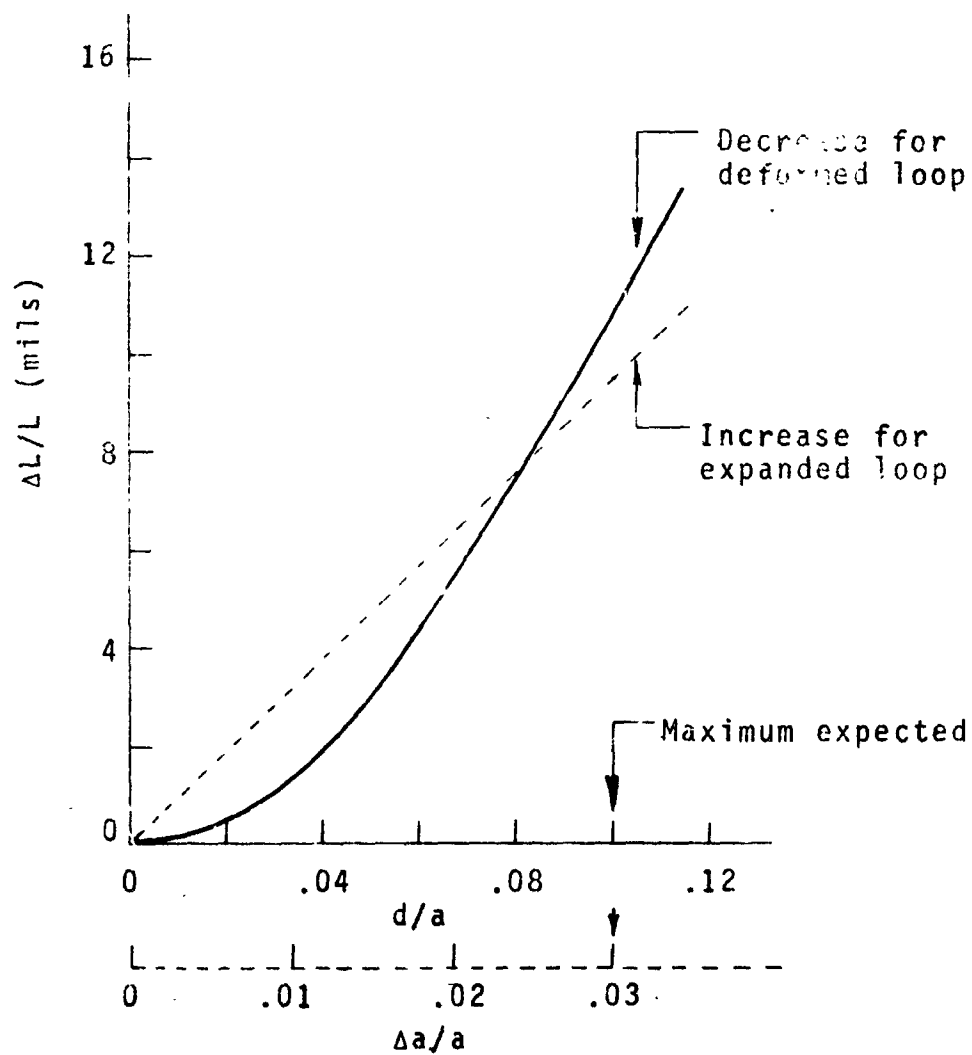
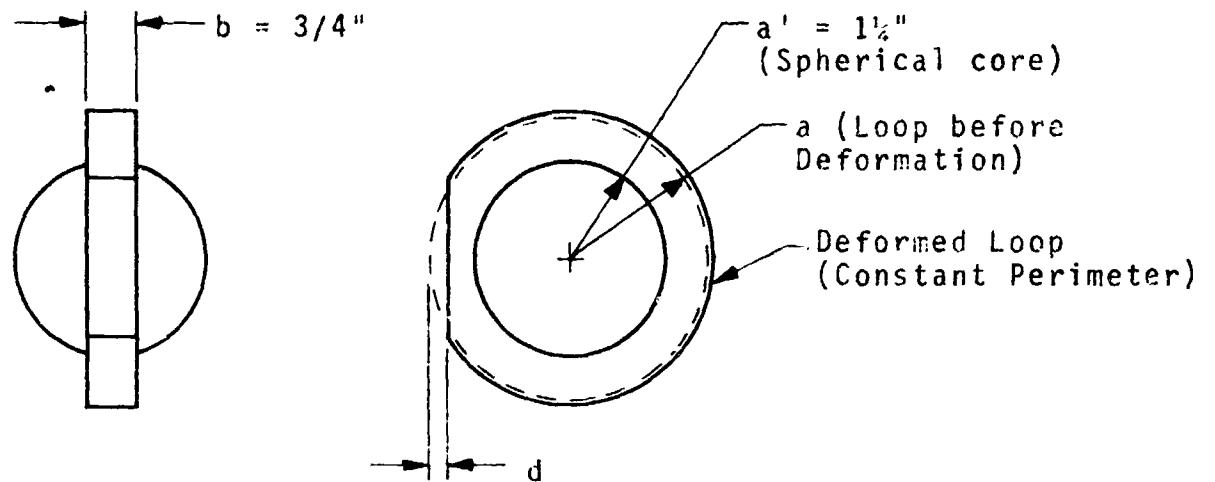


Fig. 10 - Decrease of loop inductance for impact deformation.

From the data presented in Reference 13 for a very small magnetic dipole in free space, approaching a non-conducting dielectric surface of $k = 4$, the solid curves on the left portion of Fig. 11 are constructed. These curves represent the loci of the radiation resistance and the change of reactance, both normalized to the free-space radiation resistance of a magnetic dipole. Shown are curves for a dipole with a vertical axis (horizontal loop) or a horizontal axis (vertical loop), denoted VMD and HMD, respectively.

The point at the upper right corner of Fig. 11 represents the relative antenna impedance for the same antenna far submerged. The antenna impedances for various depths are determined from the corresponding magnitude of the interface reflection above the surface, reversing the reflection phase, and renormalizing to the radiation resistance far submerged. The resulting impedance loci are the solid curves on the right portion of Fig. 11. The validity of this calculation begins to fail as the depth decreases to become comparable to the radianlength. The dashed lines are an estimate of the actual impedance variation in the transition region.

Auxiliary coordinate scales for dielectric constants of 2.5 (dry sand), 3.0 and 3.5 (alumina grit) are shown added to the figure. These simple scale changes are approximately valid, assuming that the general shape of the loci apply for the slightly lower dielectric constants.

For any location of a loop antenna, either far above, near, or far below the dielectric surface, the variation of the antenna impedance from the free-space impedance can be determined from the appropriate antenna location along the loci shown in Fig. 11. For present purposes, the end points and the intermediate trend are the significant facts, and these are independent of the loop orientation.

The calculation of antenna impedance for the limit of deep submersion was empirically checked by submerging a model of the loop antenna in loosely packed dry sand, measuring the antenna impedance and comparing it to the measured free-space impedance of that same antenna. Simulation of an infinite dielectric media was limited by the size of the available container for the sand, the container being 0.6λ on a side. To partially compensate for the small container size during the test, the submerged antenna was located offset by one-

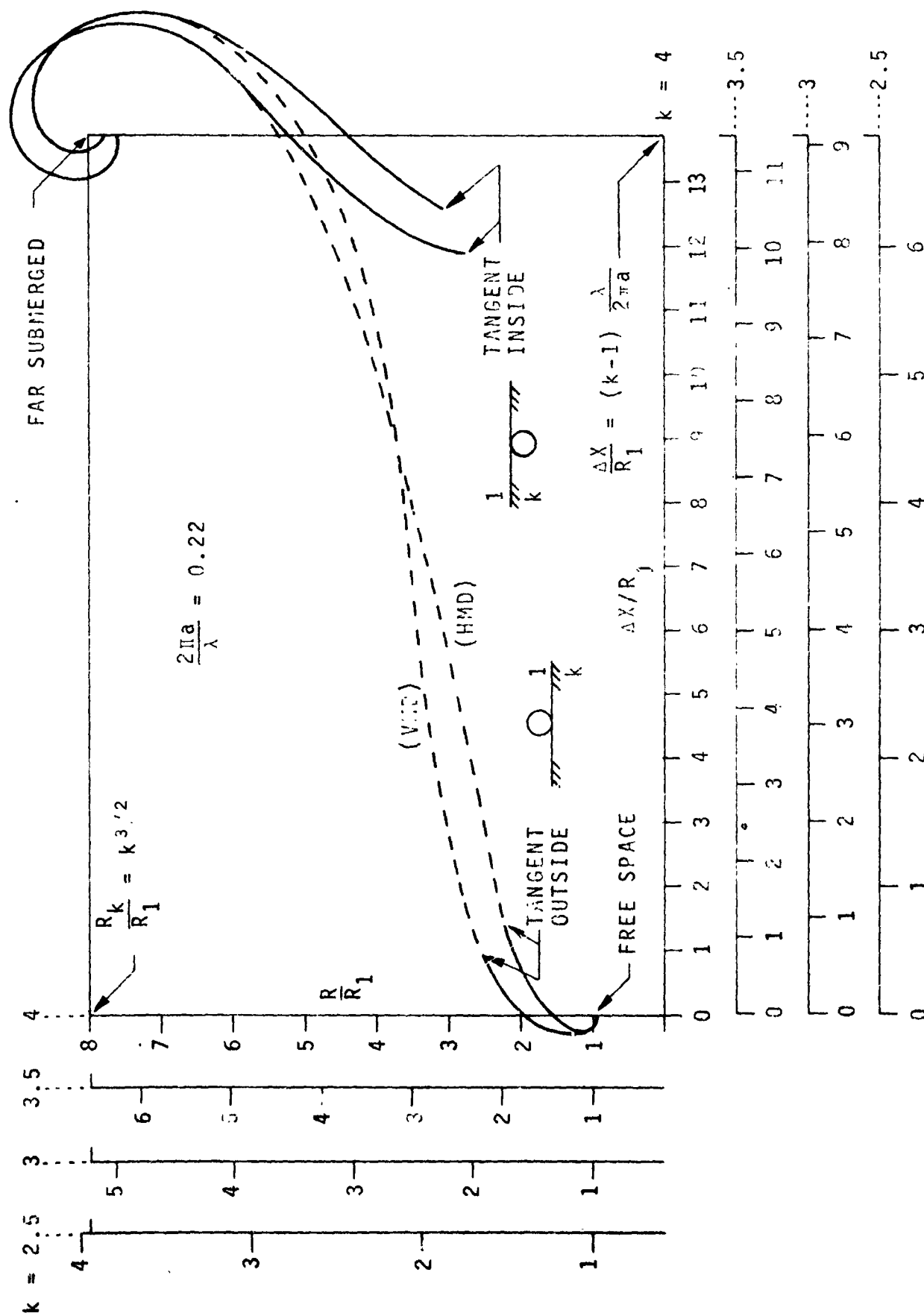


Fig. 11 - Variation of loop impedance from free space to far submerged.

quarter wavelength from the container center in three directions, thereby partially cancelling the reflection from the three pairs of opposite sides. With this size limitation, the theoretical and experimental values for the end points agreed within 20% for the change of reactance and 10% for the radiation resistance.

The variation of antenna impedance at immersion causes antenna detuning, line reflection and resulting frequency pulling of the transmitter. Considerations regarding impedance matching for this changing antenna impedance are presented in Section VII.

VII. Study of Design of Crossed-Loop Antenna.

A systematic design of the crossed-loop antenna requires a fundamental study and assessment as a basis for the design of a practical configuration. This section first presents the method of computing the component values of the antenna equivalent circuit. From this equivalent circuit the performance of the antenna is to be computed and presented in Section VIII. Also presented in this section are methods of coupling to the antenna, methods of quadrature excitation of the crossed loops, and a discussion of the mechanical design of the antenna.

For the purpose of this study, a typical antenna model is chosen to be evaluated for use in the penetrometer. The antenna comprises a pair of orthogonal loops, alumina tuning capacitors and a conducting spherical core, all encapsulated within a fiberglass-reinforced epoxy-resin sphere. The properties of the components of the typical antenna model are as follows:

a	=	42 mm	=	1-21/32 inches
a'	=	32 mm	=	1-1/4 inches
a''	=	51 mm	=	2 inches
b	=	19 mm	=	3/4 inch (about a/2)
c	=	0.2 mm	=	0.008 inch
w	=	12.6 mm	=	1/2 inch
v	=	1 mm	=	0.038 inches

$$\begin{aligned}
 n &= 4 \\
 k_a &= 9.6 \text{ (alumina in capacitors)} \\
 k'' &= 3.5 \text{ (dielectric sphere)} \\
 f_o &= 250 \text{ Mc} \\
 \lambda &= 1.2 \text{ m} = 47 \text{ inches} \\
 \delta &= 4 \text{ } \mu\text{m} \text{ (skin depth in silver or copper at 250 Mc)} \\
 R_s &= .004 \text{ ohm (skin resistance of silver or copper at 250 Mc)}
 \end{aligned}$$

These values are used in the example calculations in this section.

A. Self-Tuning.

The inductance of a one-turn air-core loop of thin metal strip is computed from the equation.

$$L^* = \mu_o a \left(\ln \frac{32a}{b} - 2 \right) = 0.12 \text{ } \mu\text{h.}$$

This equation is a modification of that presented in Reference 2 for the condition of a flat-strip inductor; the equivalent wire radius is $b/4$. The validity of this calculation was verified by measuring the inductance of such a loop with an inductance meter (Ref. 3).

The actual loop antenna used in the penetrometer is not hollow with respect to magnetic field. In the center of the penetrometer package are the telemetering components, enclosed by a metal spherical shield.

With this metal shield or core placed in the center of the loop, the loop inductance is reduced because the volume available for the magnetic flux within the loop is reduced. The reduction of the inductance is determined from consideration of the loop imaged in the conducting spherical core. The mutual inductance between the actual loop and its image (Ref. 12) is approximately

$$M = \pi \mu_o a \left[\frac{1}{2} \left(\frac{a'}{a} \right)^4 + \frac{3}{16} \left(\frac{a'}{a} \right)^8 \right] = 0.030 \text{ } \mu\text{h.}$$

which includes the first two terms of the equation presented in Reference 5. The effective inductance of the loop, with the spherical core in place, is then

$$L = L^* - M \frac{a}{a^2} = 0.079 \text{ } \mu\text{h.}$$

The validity of these equations was verified by measuring the inductance of loops of various radii, around the metal core. The results of these tests, as shown in Fig. 12, indicate very close agreement with the calculated values.

Approximately 4.5% further reduction of loop inductance occurs because of the magnetic-flux shielding of the second loop.

The loop inductance is tuned to resonance at the operating frequency by inserting series capacitors in the loop. The required capacitance of each capacitor is

$$C = n/L\omega^2$$

In terms of the physical dimensions of each capacitor,

$$C = k_a \epsilon_0 \frac{bw}{v}$$

The actual capacitance added in series with the loop must be somewhat different than this value in order to account for incidental effects. From the results of the tests performed on an encapsulated two-loop antenna, for $n = 4$, the actual capacitance should be about 4/5 the value calculated above.

The choice of the number of capacitors to be inserted in the loop is based on the following considerations:

- (1) Limitation of the DPF added in the tuned circuit from p'' in the filling material near the loop (Reference, Section IV).
- (2) Practical thickness and cross-section area of the capacitors.
- (3) Even value of n for convenient overlap of orthogonal loops.
- (4) Diminishing benefit beyond a certain number (Reference, Section IV, Table 2).

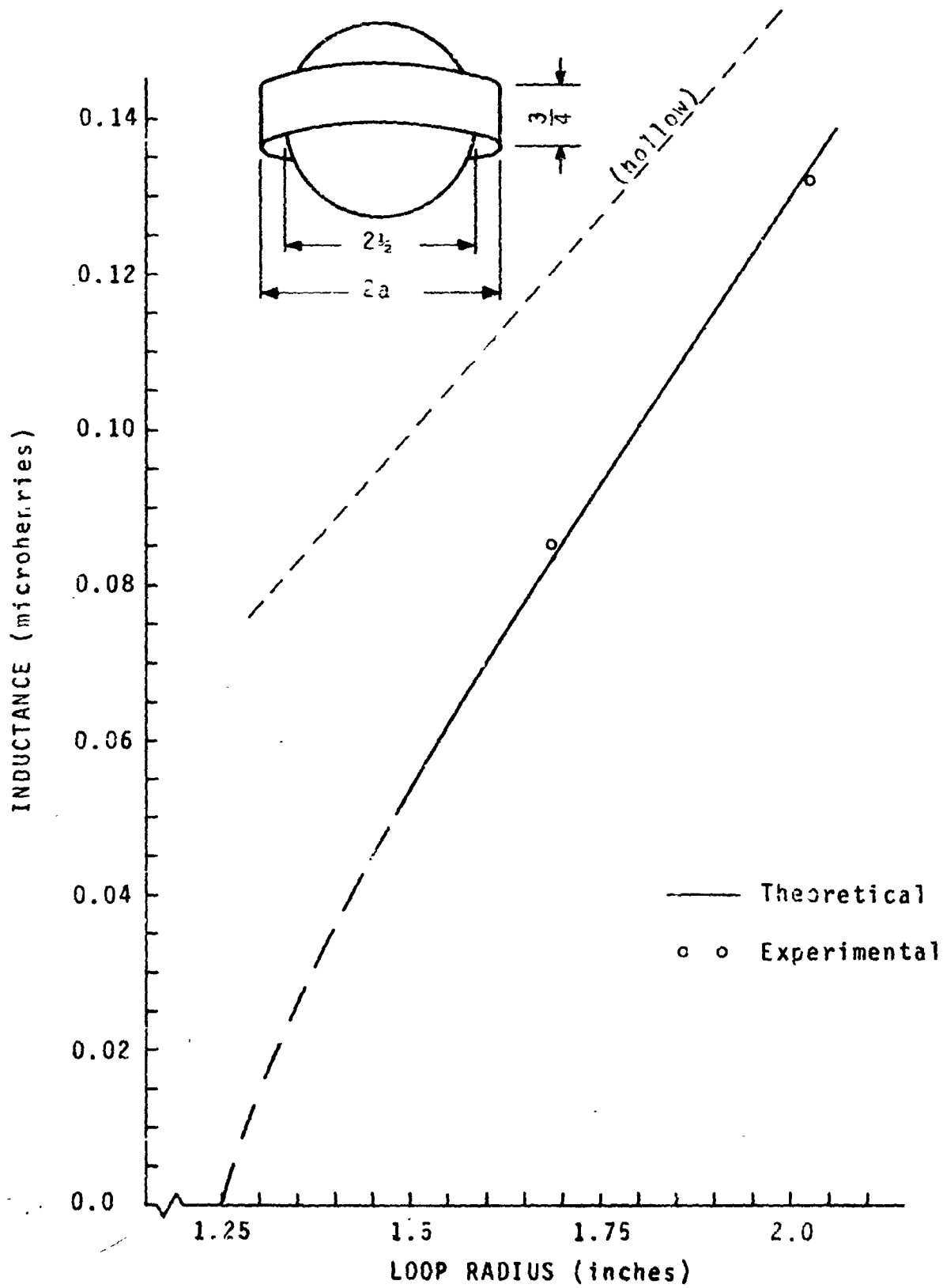


Fig. 12 - Inductance of a loop about a metal sphere.

jhl

Based on these factors, the choice of four series capacitors is considered to be a fair compromise.

Sintered alumina (99.5% pure) and fused silica both have electrical properties well suited for the dielectric in the capacitors. The DPF of each material is very low, 0.0001, and each is capable of being metalized. Metalizing is necessary to form the parallel plates of the capacitor and to facilitate soldering to the metal-strip loop sections. Alumina is stronger than fused silica (Reference, Table 3) and does not cleave as readily when stressed. The dielectric constant of alumina is 9.6 as compared with 3.8 for fused silica. A high dielectric constant is preferable in order to concentrate the energy within the capacitors. This is desirable because the DPF of the adjacent encapsulant material is about 0.03, much greater than that tolerable in the tuned loop as a whole.

The dielectric constant of sintered alumina increases with temperature by 1% over the full range of temperatures from 0°C to 60°C, which would cause detuning of ± 2.5 mils from the mean. This amount is substantial but could be tolerated. The dielectric constant of fused silica varies only 1/6 as much.

The choice of dielectric material involves the trade off of physical and electrical properties. For the purpose of this study, alumina is chosen because of its high dielectric constant and its superior mechanical properties.

As a consequence of the low total power factor (TPF) of the antenna, tuning to resonance is critical and some means of trimming must be provided. By grinding the side of one or more of the capacitors (or by drilling small holes), a fine adjustment of the antenna tuning is available. This adjustment can be made after the loop is fabricated (and possibly even after the complete antenna is encapsulated) to compensate for fabrication tolerances and the effect of the local environment in the operational configuration.

B. Radiation Efficiency.

The equivalent circuit of the loop antenna is a series circuit comprising the inductance of the antenna loop, the effective

<u>Electrical Properties</u>	<u>Alumina (99.5%)</u>	<u>Fused Silica (Corning 7940)</u>
Dielectric constant (k) (10^{-6} /deg. C)	9.6	3.8
Thermal coef. of k (10^{-6} /deg. C)	180	27
Power Factor (mils)	0.1	0.05
<u>Mechanical Properties</u>		
Flexural strength (lb/in ²)	46,000	14,000
Compressive strength (lb/in ²)	300,000	150,000
Hardness (knoop)	1,800	560
Modulus of elasticity (lb/in ²)	52×10^6	10.5×10^6
Shear modulus (lb/in ²)	22×10^6	4.5×10^6
Poisson's ratio	0.21	0.16
Coef. of expansion (in/in °C)	9.8×10^{-6}	0.6×10^{-6}

Table 3. Electrical and mechanical properties of alumina and fused silica.

capacitance of the series capacitors, radiation resistance, and a dissipation resistance to represent all the causes of dissipation in the antenna.

The radiation efficiency of the antenna is the ratio of the radiated power over the total power expended in the antenna circuit. This is calculated as the ratio of radiation resistance over total resistance, or the ratio of RPF/TPF.

The RPF is the ratio of radiation resistance over loop reactance. The radiation resistance of a loop antenna, without a central core, from Reference 6, is

$$R_1^* = \frac{\pi}{6} R_0 \left(\frac{2\pi a}{\lambda} \right)^4$$

With the metal core in place, the radiation resistance becomes

$$R_1 = R_1^* \left[1 - \left(\frac{a'}{a} \right)^3 \right]^2$$

Combining this expression with the one previously derived for L gives the following expression for the RPF of the loop antenna with core.

$$\begin{aligned} P_1 &= R_1 / \omega L = \left(\frac{2\pi a}{\lambda} \right)^3 \frac{\pi}{6} \frac{\left[1 - \left(\frac{a'}{a} \right)^3 \right]^2}{\left[\ln \frac{32a}{b} - 2 - \frac{\pi}{2} \left(\frac{a'}{a} \right)^3 - \frac{3\pi}{16} \left(\frac{a'}{a} \right)^7 \right]} \\ &= 1.2 \text{ mils} \end{aligned}$$

This value is 1/9 of the upper limit of the free-space RPF for this size spherical volume (Reference, Table 2) because the configuration and filling of this antenna fall short of the ideal in respect to magnetic filling and surface utilization.

The calculation of the RPF was empirically verified by the following method. A model of a loop antenna was fabricated and the total power factor of the antenna was determined by impedance tests for the following conditions: (1) the antenna radiating in free space, and (2) the antenna located within a "radiation shield" located at a radius of one radianlength, thereby removing the radiation resistance (Ref. 10). From the difference of the results of

these tests, the RPF is calculated. The theoretical RPF agreed with the observed value within 10%.

The loop-conductor power factor is the portion of the DPF caused by the skin resistance of the antenna loop.

$$P_C = R_C / \omega L$$

$$\text{where } R_C = R_S \frac{a}{(c+b)} \frac{2}{\pi} \left(\ln \frac{4\pi b}{c} + \pi \right) = 0.69 \text{ mils} \quad (\text{Ref. 1})$$

(copper or silver plated loop)

This equation is valid for c/b less than 1/2.

The sphere-conduction power factor, the portion of the DPF caused by the skin resistance of the central core is

$$P'_C = R'_C / \omega L$$

The skin resistance of the conducting core, as effective in the loop circuit, can be calculated by the "incremental inductance rule" (Ref. 2).

$$R'_C = \frac{3\pi}{2} \frac{R'_S}{\omega} \left[\left(\frac{a'}{a} \right)^2 + \left(\frac{a'}{a} \right)^6 \right] = 0.1 \text{ mils}$$

(copper or silver-plated core)

Fabrication procedures may require holes in the central core shield for the flow of epoxy resin to the inside of the core. Holes as large as one-half inch diameter are quite acceptable. If as much as half the original surface area is occupied by holes, and the edges of the holes are not too sharp, p'_C is increased to approximately 0.2 mils.

The DPF of the alumina in the capacitors is stated on the data sheet from Coors Porcelain Company, as 0.1 mils at 25°C.

The dissipation factor of the fiberglass-reinforced epoxy resin (encapsulation) also contributes to the DPF of the antenna. A dissipation factor of 35 mils is a typical value for epoxy resins. This insulation power factor is lowered by the type and quantity of fiberglass added for reinforcing. An insulation power factor of 30 mils is used for the purpose of calculations in this report.

Only a fraction of the total stored energy of the antenna circuit is stored in the insulation, as noted in Section IV of this report. Hence, an effective power factor from this cause is calculated as follows:

$$p'' (\text{eff.}) = p'' \frac{(\text{Energy stored in insulation})}{(\text{Total energy stored in capacitors and insulation})}.$$

The ratio of the energy stored in the insulation over the total energy stored in the capacitors and the insulation, is estimated as 0.03. based on this estimate, the effective power factor contributed by the insulation is 0.9 mils¹.

The radiation efficiency of the loop antenna is calculated from

$$e = \frac{RPF}{RPF + DPF} = \frac{P_1}{P_1 + p_c + p'_c + p_a + p'' (\text{eff.})}$$

The relative distribution of the available power at the antenna to useful radiation and various dissipations is presented in Table 4, giving a TPF of 3.1 mils.

$$BW = (RPF + DPF)f_o = (TPF)f_o.$$

For the antenna model, TPF = 3.1 mils so the 3-db bandwidth is 0.78 Mc. This bandwidth is an indication of the sensitivity to detuning by tolerances and environment. It is adequate for the intended FM.

There are three basic methods of increasing the radiation efficiency of the antenna; namely, increase the size outside of the core, increase the operating frequency, and decrease the dissipative

¹The results of tests (Ref. 7) performed on an encapsulated antenna indicate that the estimate of the ratio of the energy in the insulation over the total stored energy was in error and should be approximately 0.10. This observation was too late for verification and changes throughout this report. The results and conclusions presented in this report are based on the estimated value presented in the text.

<u>Power Factor</u>	<u>Symbol</u>	<u>Value (mils)</u>	<u>Distribution</u>
Radiation	p	1.2	0.39
Dissipation in antenna loop	p_c	0.7	0.23
Dissipation in central core	p'_c	0.2	0.06
Dissipation in alumina capacitors	p_a	0.1	0.03
Dissipation in insulation	$p''(\text{eff.})$	0.9	0.29
Total		3.1	1.00

Table 4. Distribution of available antenna-circuit power.

losses. The first two methods have the further advantage of increasing the bandwidth of the antenna, thereby increasing the antenna stability. Decreasing the dissipative losses, on the other hand, decreases the already narrow bandwidth. A quantitative study of a frequency, size trade off is presented in Section IX of this report. In addition, a quantitative study of antenna efficiency core-size trade off is presented in Appendix I.

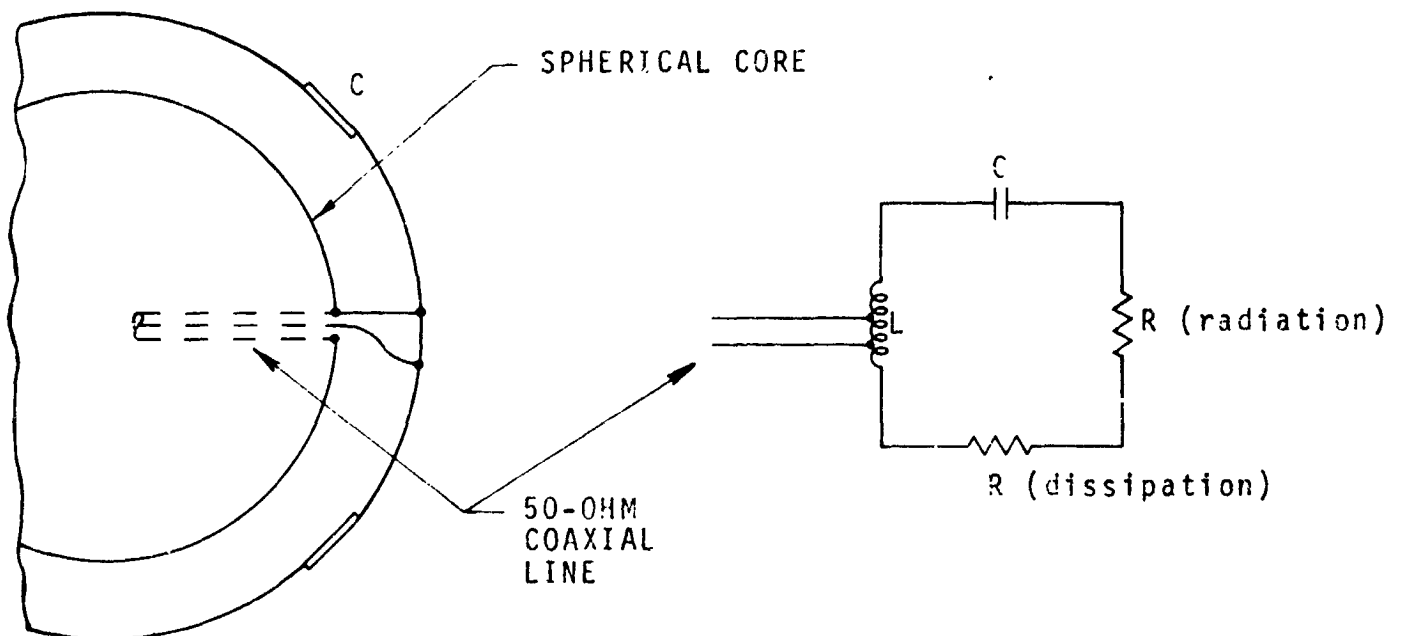
C. Impedance Matching.

The loop antenna described is to be coupled to the transmitter feed, a 50-ohm coaxial line. The resistive portion of the antenna impedance must be transformed to this 50-ohm impedance level.

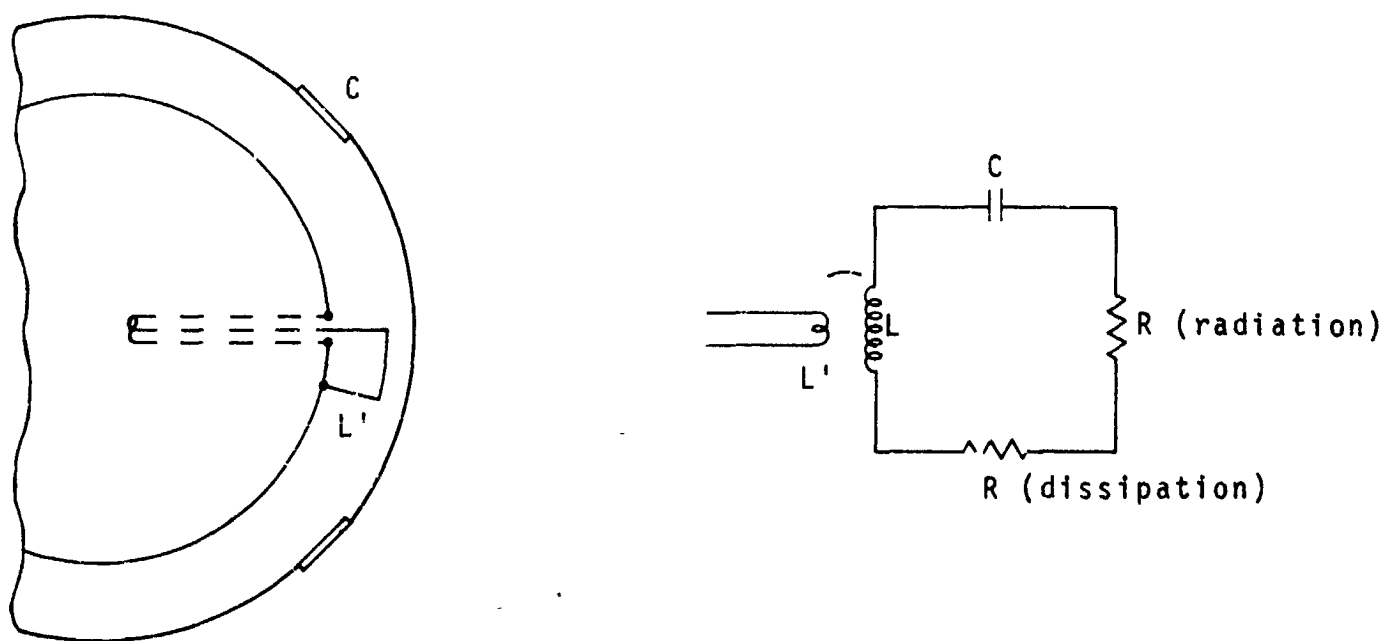
Two methods of coupling to the loop antenna are shown in Fig. 13. In both methods, the outer conductor of the coaxial line is bonded to the central core of the antenna. In the electrical-contact type, the coaxial-line center conductor, and another wire from the central core, are connected at spaced points to the conducting strip which forms the loop antenna. The spacing of the contact points on the loop, and the resulting area enclosed by the connecting wires, are chosen to transform the antenna resistance to the 50-ohms impedance of the coaxial line. In the magnetic-coupling type, shown in Fig. 13(b), the center conductor of the coaxial line is extended to form a small loop returning to the central core. This is a non-contacting arrangement which is preferable in view of the hazard to the integrity of direct connections after severe impact.

A mockup comprising the loop antenna, magnetic-coupling loop, and spherical core, as shown in Fig. 14, was constructed to evaluate this coupling method. The size of the coupling loop was adjusted for 50-ohm input resistance at f_0 when radiating into free space. The design was found to be straightforward, capable of transforming the antenna resistance as required, and not unduly critical to dimensional variation.

For the proposed application, the penetrometer must operate immersed in a dielectric media. If the antenna model is adjusted for match in free space, and then is far submerged in a dielectric medium of $k = 3$, a 3.8-db reflection loss is anticipated in accordance with



(a) Electrical-contact type.



(b) Magnetic-coupling type.

Fig. 13 - Methods of coupling to loop antenna.



Fig. 4 - Loop antenna and core with magnetic-coupling loop.

the previous calculations of impedance effects. A compromise antenna detuning in free space is possible so that equal reflection loss in both free space and total immersion is obtained. For this compromise tuning condition, a 2-db reflection loss remains for either extreme of free space or far submerged operation. Since the free-space condition is more critical (with lesser bandwidth and more sensitivity to detuning) it is proposed to match for that condition and accept whatever reflection loss may be caused by submersion. Much less reflection loss is expected in the most interesting phase of transitional submersion.

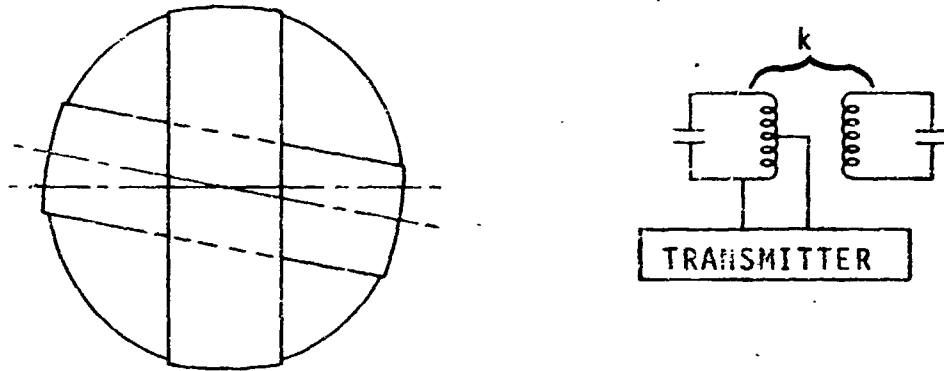
D. Quadrature Coupling.

In order to obtain spherical coverage, the two orthogonal antenna loops are intended to radiate equal power with time-quadrature relative phase. One general method of feeding the antenna loops is presented in Ref. 14 whereby the transmitter is directly coupled to one antenna loop; then, by one of the three techniques shown in Fig. 15, the second loop is excited by coupling with the first loop. At resonance, the coupling between the two loops naturally accomplishes the desired quadrature-phase relation. The "critical" value of coupling equalizes the radiated power from the pair of loops.

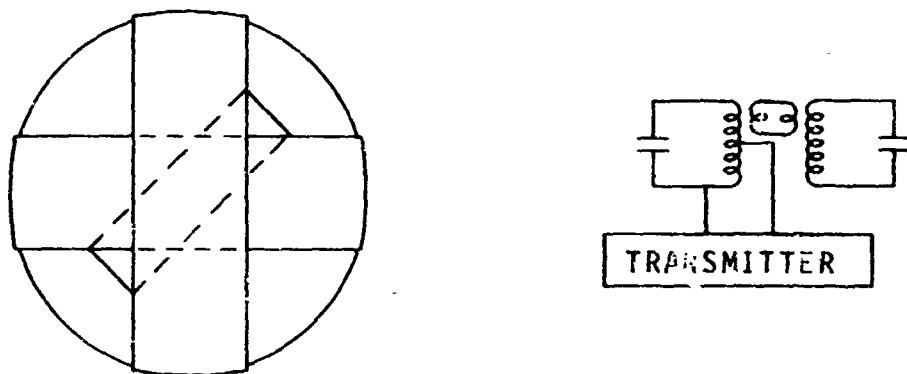
This antenna-feed method has a definite limitation in the penetrometer application because of the environmental variation. Since both antenna loops are detuned as the penetrometer approaches a dielectric surface, the critical-coupling adjustment for equal power in each antenna and the resonance condition for quadrature phase no longer exist. Consequently, the uniformity of the resulting radiation pattern would fall far short of the theoretical turnstile pattern.

A more satisfactory method of loop excitation is to feed directly both antenna loops. This is accomplished as shown in Fig. 16. The transmitter is connected to one port of a four-port 3-db quadrature directional coupler. The two equal-amplitude quadrature-phase outputs of the coupler go to two coupling loops, one for each of the orthogonal antenna loops. The fourth port is terminated in a 50-ohm dummy load.

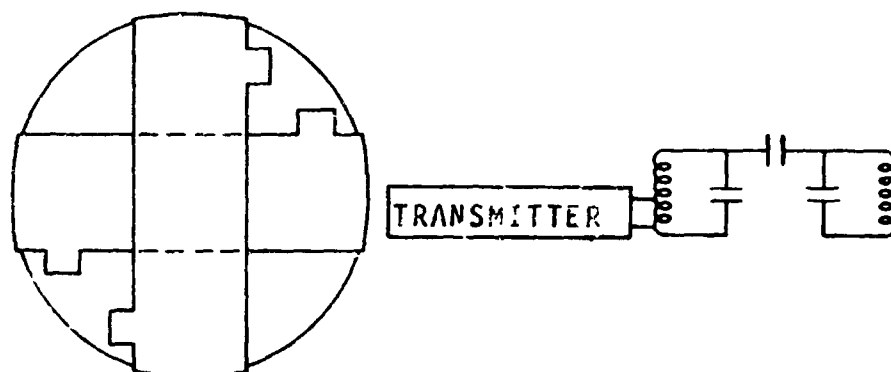
The directional-coupler method provides equal power incident on each antenna loop, independent of detuning of either antenna.



(a) Magnetic-field coupling by non-orthogonal loops.



(b) Magnetic-field coupling by auxiliary coupling loop.



(c) Electric-field coupling.

Fig. 15 - Techniques for quadrature coupling of crossed loops.

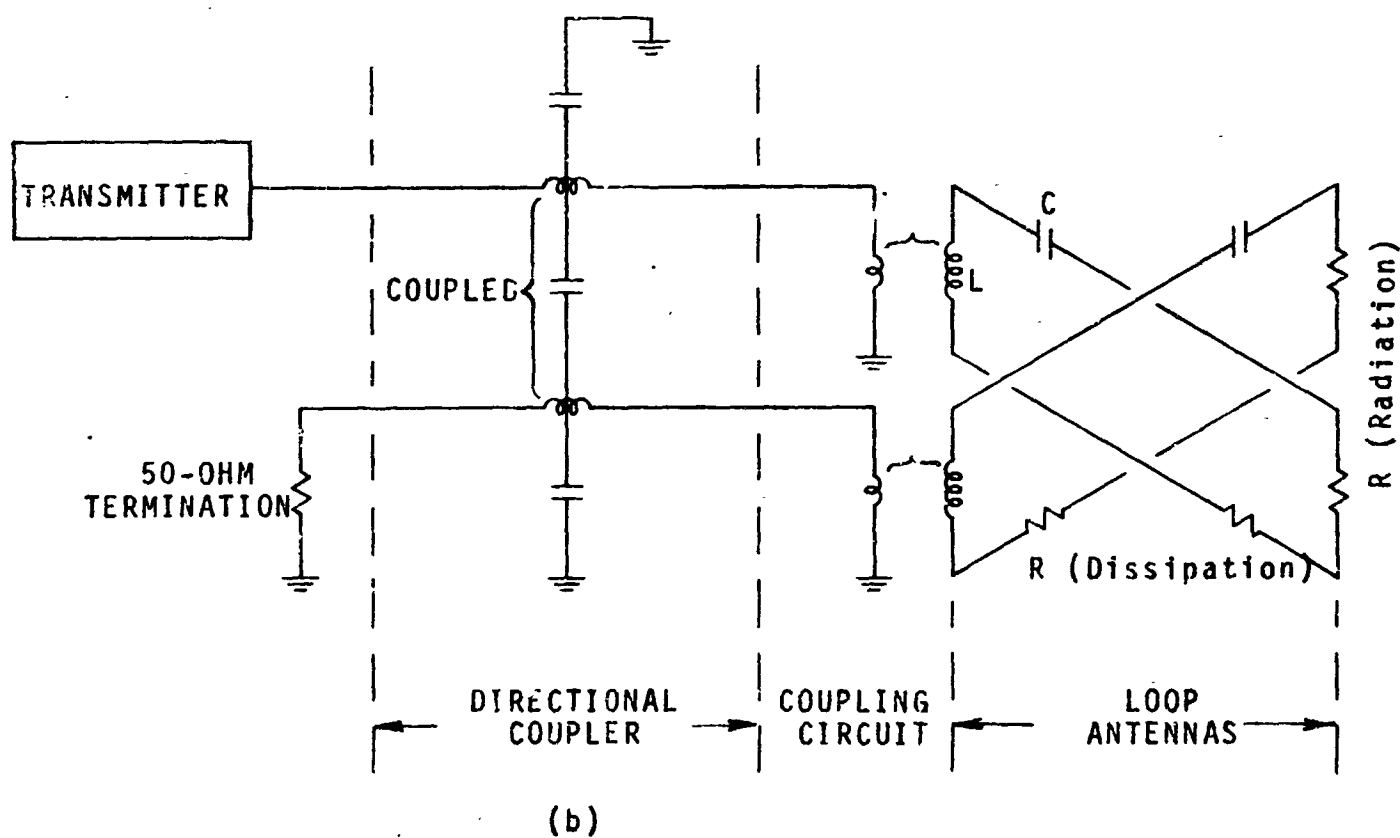
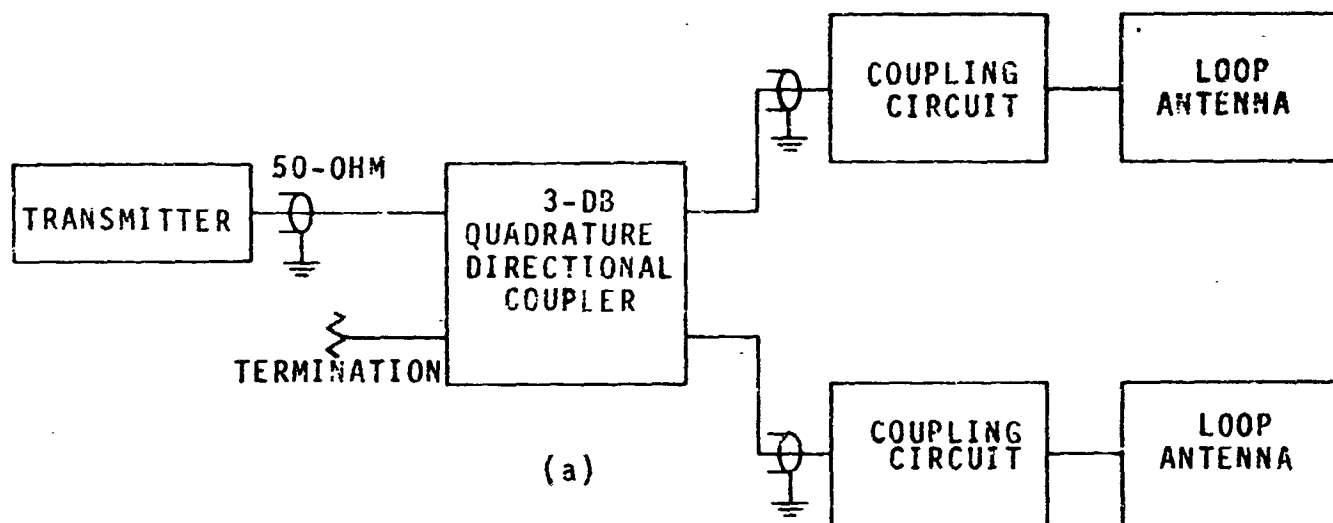


Fig. 16 - Circuit of antenna and quadrature feed.

Therefore, the power radiated from each antenna depends on the matching and tuning of that particular antenna only. In addition, for equal reflection from both antennas, the reflected waves are dissipated in the 50-ohm termination rather than returning to the transmitter. The net reflection from the effective transmitter load is thereby reduced and the loading-stability requirement of the transmitter is eased.

For determination of the electrical requirements, it was assumed that the directional coupler is to cause no more than 1-db additional variation of the radiation pattern. (The turnstile pattern provides 3-db variation.) Amplitude inequality and quadrature phase error of the directional coupler both cause variation of the radiation pattern. Allowing 1/2-db variation to each, the amplitude ratio from the directional coupler must be within 1 db and the phase difference between the two signals must be $90^\circ \pm 6^\circ$.

A model of the 3-db directional coupler has been constructed within an enclosure of inside dimensions $1/2 \times 1/2 \times 5/8$ inches, as shown in Fig. 17. The equivalent circuit is shown in Fig. 18. The coupler comprises a double coil and three capacitors. Four coaxial connectors facilitate cable connections to each port; three external ports are necessary, the fourth can terminate inside. At 245 Mc, the output signals from this model are similar within 0.2 db, the reflection at each of the ports is within 2 db SWR, and the directivity is 18 db. A slight adjustment of the component values could perfect the matching and directivity. This adjustment was not performed since the performance of this model proves the feasibility of designing and assembling a suitable directional-coupler package within such a small volume.

Directional couplers that meet the electrical specifications are also commercially available and reasonably priced. They are packaged within a case $9/16 \times 9/16 \times 13/32$ inches.

E. Mechanical Structure.

The crossed-loop antenna is depicted in Fig. 19 and consists of two beryllium-copper bands, each soldered to four Alumina 995 ceramic capacitors. The metal bands are $3/4$ -inch wide x .008-inch thick and are perforated to increase the structural support offered

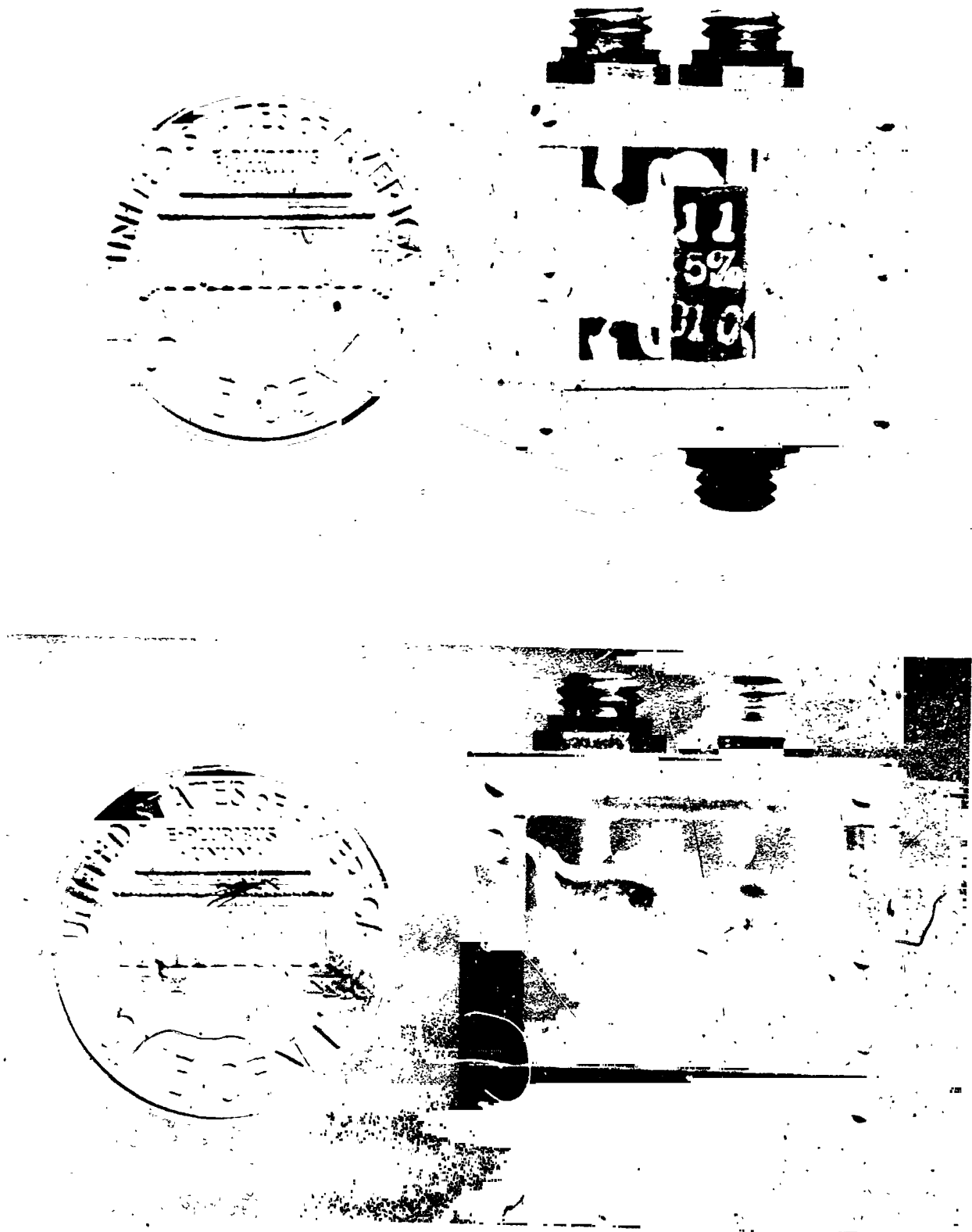
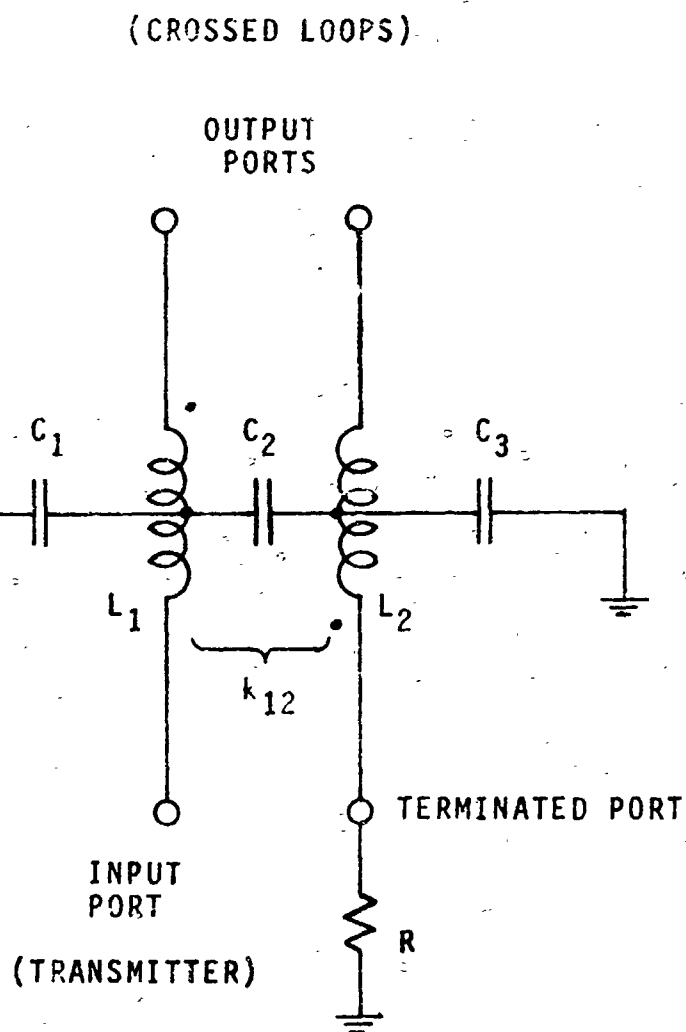


Fig. 17 - Miniature directional coupler.



$$\begin{aligned}L_1, L_2 &= .071 \mu\text{h} \\k_{12} &= 0.71 \\C_1, C_3 &= 8.3 \text{ pf.} \\C_2 &= 20 \text{ pf.} \\R &= 50\Omega\end{aligned}$$

(Values of L and C include effects of leads, etc.)

Fig. 18 - Circuit of the quadrature directional coupler.

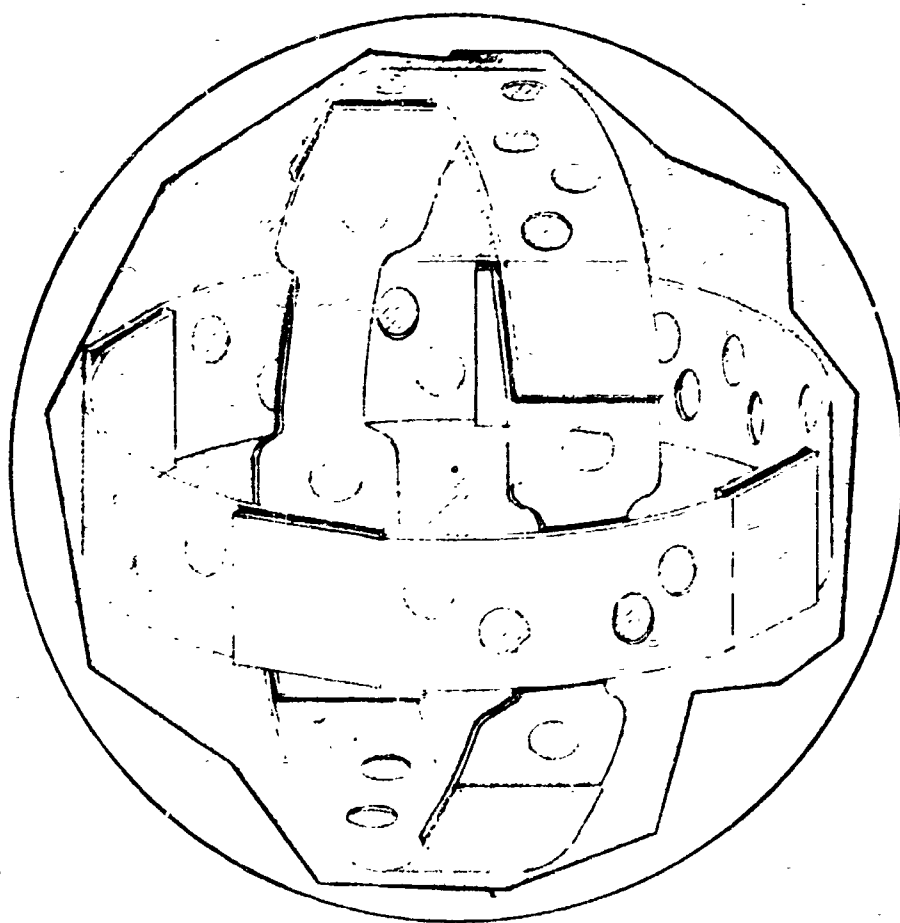


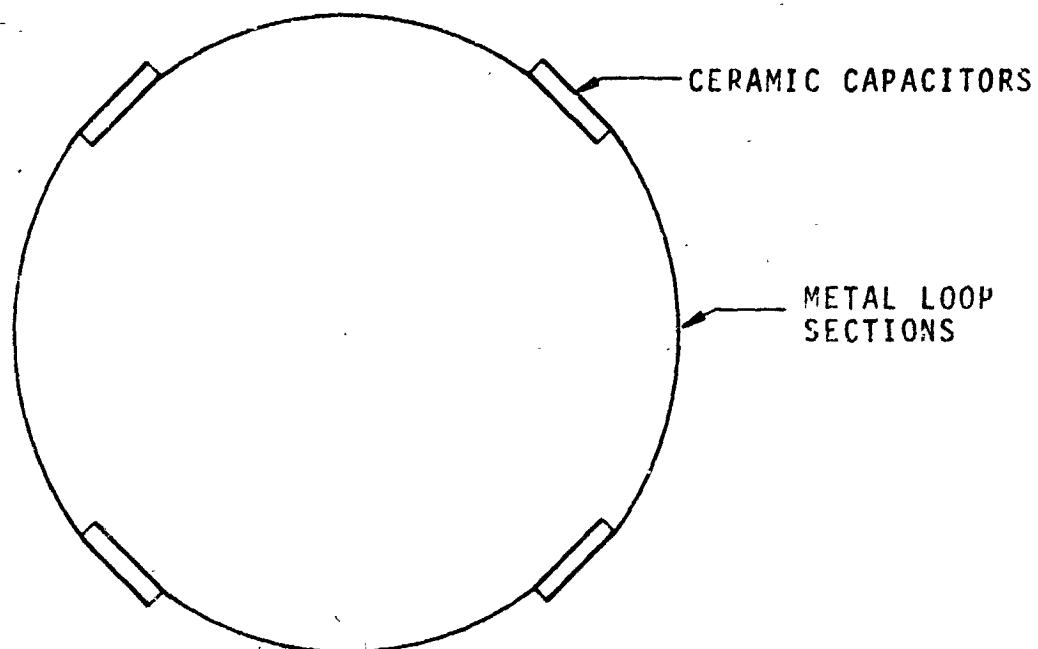
Fig. 19 - Configuration of crossed antenna loops.

by the encapsulant. The mean diameter of each loop is 3.31 inches. The capacitors are 3/4 inch x 1/2 inch x 1/32 inch thick, and are nickel flashed on each face. In order to facilitate soldering, the ceramic capacitors are silver plated (.0002-inch thick) over the nickel flash.

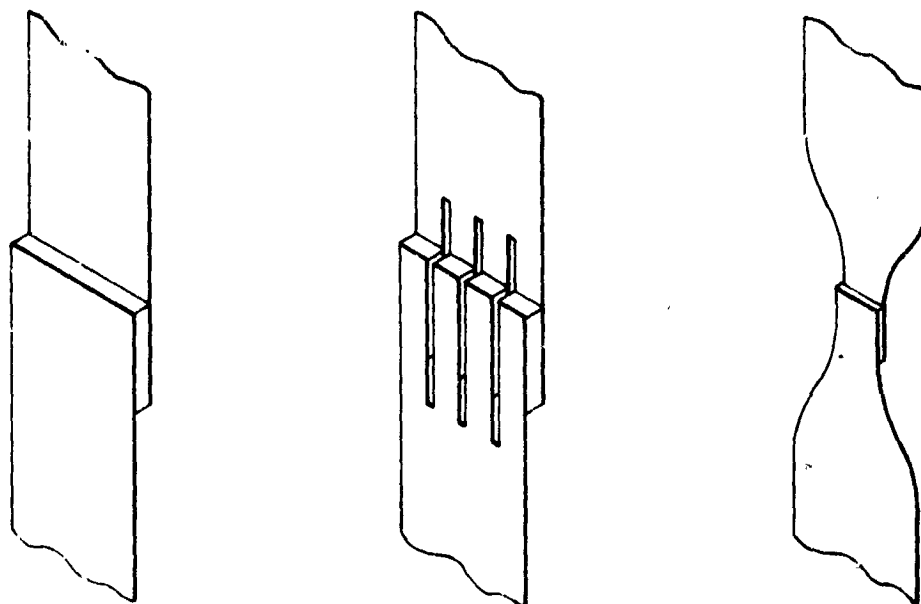
Shown in Fig. 20 is the general configuration of the capacitors and metal sections assembled to form an antenna loop, and some alternative configurations for the capacitors. The configuration on the left is the simplest but may be prone to cracking as a result of localized impact deformation. The other two configurations can withstand greater impact deformations but are more difficult to fabricate. To achieve the strongest possible joint between the metal bands and the capacitors, it was expected that they would be joined by hard soldering. However, the high temperatures (about 1200°F) reached during this soldering process produced thermal stresses which caused the ceramic capacitors to crack. As a result, soft soldering was used for the preliminary antenna model. In order to preclude the existence of high thermal stresses, it is expected that the hard soldering process could be used if the coefficient of thermal expansion of the alloy used for the metal bands is near that of the alumina. Table 5 shows the significant properties of Alumina 995 and several alternative antenna-band materials. Note that the low-expansion nickel alloy (42%) has a coefficient of thermal expansion very near that of the alumina. It is proposed that future antenna models be fabricated with a low-expansion alloy in an effort to permit the use of hard soldering.

Preliminary models of the fiberglass-reinforced epoxy-resin spheres were fabricated using two mixtures of Dow Chemical resins and curing agents as in Table 6. Mixture I was suggested by NASA-Langley at the beginning of this design study program, and Mixture II was devised through consultation between Hazeltine and Dow Chemical. In both cases approximately 30%, by weight, of the sphere is composed of 1/4-inch long chopped-strand fiberglass.

Dow Chemical has discontinued producing the QX-3483.2 experimental hardner. Thus, Mixture II is proposed as a possible equivalent substitute. Spheres made from both mixtures were impacted against a concrete slab at 50 feet per second. Both materials



(a) Capacitors assembled in loop.



(b) Alternative configurations of capacitors.

Fig. 20 - Capacitor-assembly configuration.

Material	Yield Point lb/in ²	Tensile Strength lb/in ²	Modulus of Elasticity lb/in ²	Coefficient of Expansion Per Deg. C
Alumina 995*			52×10^6	6.8×10^{-6}
Beryllium-Copper (Annealed)	25-30,000	70,000	19×10^6	16.7×10^{-6}
Phosphor-Bronze (Annealed)	19-20,000	47,000	16×10^6	17.8×10^{-6}
Low-Expansion Nickel (Annealed)				
36% Nickel	40,000	71,000	21×10^6	1.3×10^{-6}
42% Nickel	39,000	68,000	22×10^6	5.8×10^{-6}
42-50% Nickel	33,000	77,000	24×10^6	10×10^{-6}

* Flexural Strength 46,000 lb/in²

* Compressive Strength > 300,000 lb/in²

Table 5. Antenna-material properties.

<u>Mixture</u>	<u>Ingredient</u>	<u>Relative Weight</u>
I	DER-331 base resin	100
	DEH-20 curing agent	6
	QX-3483.2 hardener	30
II	DER-331 base resin	100
	DEH-20 curing agent	10.5
	DER-732 base resin	30

Table 6. Mixtures of epoxy resin and curing agents.

withstood this test, and manifested the same amount of minor surface abrasions. In order to fully qualify either mixture as structurally acceptable, impact tests at 150 feet per second should be conducted.

A photograph of the teflon-coated aluminum encapsulating mold is shown in Fig. 21. It is made in three parts, two main sections and a small removable cap, in order to facilitate positioning of the antenna, and to permit uniform packing of fiberglass strands prior to pouring the epoxy.

The assembly and fabrication steps required in the fabrication of preliminary models are outlined in Table 7.

VIII. Description of Proposed Antenna.

A. Configuration.

The results of the theoretical design study and the preliminary electrical tests demonstrate that the requirements for the antenna in a penetrometer package can be met with a pair of crossed loops assembled in a practical configuration as shown in Fig. 22. The acceleration sensor, transmitter, battery and directional coupler are mounted within a 2½-inch spherical volume and surrounded by a thin-walled spherical conducting shield. This spherical shield is fabricated from two hemispherical shells bonded along the seam. The shield material is not critical; beryllium copper is well suited. Holes as large as one-half inch diameter, covering as much as half the shield surface area are acceptable if required for a flow of encapsulant to within the shield during the molding process. A silver or copper plating on the shield material is desirable, and essential if the material is a poor conductor or magnetic.

The directional coupler should be incorporated into the transmitter, as assumed above. For flexibility of fabrication and packaging, however, the directional coupler and the transmitter may be separate units, connected with a length of semi-rigid coaxial line. From the output ports of the directional coupler, two lengths of semi-rigid coaxial line connect individually to the two coupling loops located on the outer surface of the spherical shield or core.



Fig. 21 - Encapsulating mold.

Assembly and Fabrication Procedure

1. Prepare a batch of fiberglass. Use Owens-Corning type 801, Amino Silane treated. This is a surface treatment which maximizes the wetting or adhesion capability of an epoxy resin to the glass fiber. Bake the glass at 140°C for 18 hours in order to remove entrapped moisture.

2. Position antenna concentrically in the mold by use of preformed epoxy spacers.

3. Tightly pack fiberglass into the mold and around the antenna.

4. Prepare the epoxy mixture by carefully weighing and then mixing together all epoxy components. Place mixture under vacuum for 15 minutes to remove entrapped vapors.

5. With the mold fully assembled, connect one port at the top of the mold to a vacuum pump and evacuate the air from the mold cavity.

6. Carefully and slowly meter in the epoxy mixture, holding the mold cavity under vacuum.

7. When approaching the final stage of pouring, open the top of the mold and add more glass to compensate for the "washing down" effect produced by the epoxy mixture when entering the mold.

8. When the mold is completely filled, cap the epoxy entrance port and sustain vacuum for 1/2 hour through the other port.

9. Remove vacuum line and apply 80 psig air pressure at room temperature for 10 hours.

10. Sustain 80 psig pressure and place mold in oven at 140°F for 16 hours.

11. Disassemble mold.

12. Grind off the protrusion left by the filling port of the mold. Polish this area to conform to the sphere.

Note: In order to prevent too rapid curing of the epoxy resin, the ingredients should be at a temperature below 70°F before mixing.

The mixing and molding process should be conducted at a cool, clean, dry, well ventilated work area.

Table 7. Assembly and fabrication procedure for preliminary models.

The outer conductor of the coaxial line is bonded to the core, and the inner conductor is bonded to the coupling loop. The far end of the coupling loop is also bonded to the surface of the core.

Two orthogonal four-section antenna loops are located concentric with the core, each in the plane of one of the coupling loops. Each antenna loop comprises four alumina capacitors inserted in a loop of metal strip. The alumina sections are metalized to form the capacitors and these capacitors are soldered to the corresponding sections of metal strip. Careful choice of solder, solder flux and after-solder cleaning is required to avoid contamination of the edges of the capacitor. The loop radiators are thin conducting strips, approximately .007-inch thick by 3/4-inch wide, possibly perforated with 3/16-inch holes for greater strength of encapsulant. If not made of high-conductivity nonmagnetic material, silver or copper plating is essential.

A physical interference occurs at the overlap region of the two antenna loops because of the cylindrical contour of the loops and the limited offset provided by the thickness of the capacitors. To provide a clearance between the two antenna loops, the inner loop width may be reduced at the overlap regions, as shown in Fig. 22. In addition, the two loops are prevented from contacting where they overlap by a spacer of low dielectric constant.

The whole assembly is encapsulated in a 4-inch diameter fiberglass-reinforced epoxy-resin sphere.

B. Anticipated Performance.

The performance of the crossed-loop antenna is calculated from the equivalent circuit of the antenna in free space and the variation of the circuit elements by impact and immersion. Transmission efficiency, reflection and bandwidth are of particular interest. The transmission efficiency is limited by the dissipation in the antenna, by the losses in the directional coupler and the coaxial feed lines, by antenna detuning and mismatch, by the inherent 3-db variation of the turnstile-type radiated pattern, by the reflection at the surface interface, and by the spreading of the ray angle with refraction.

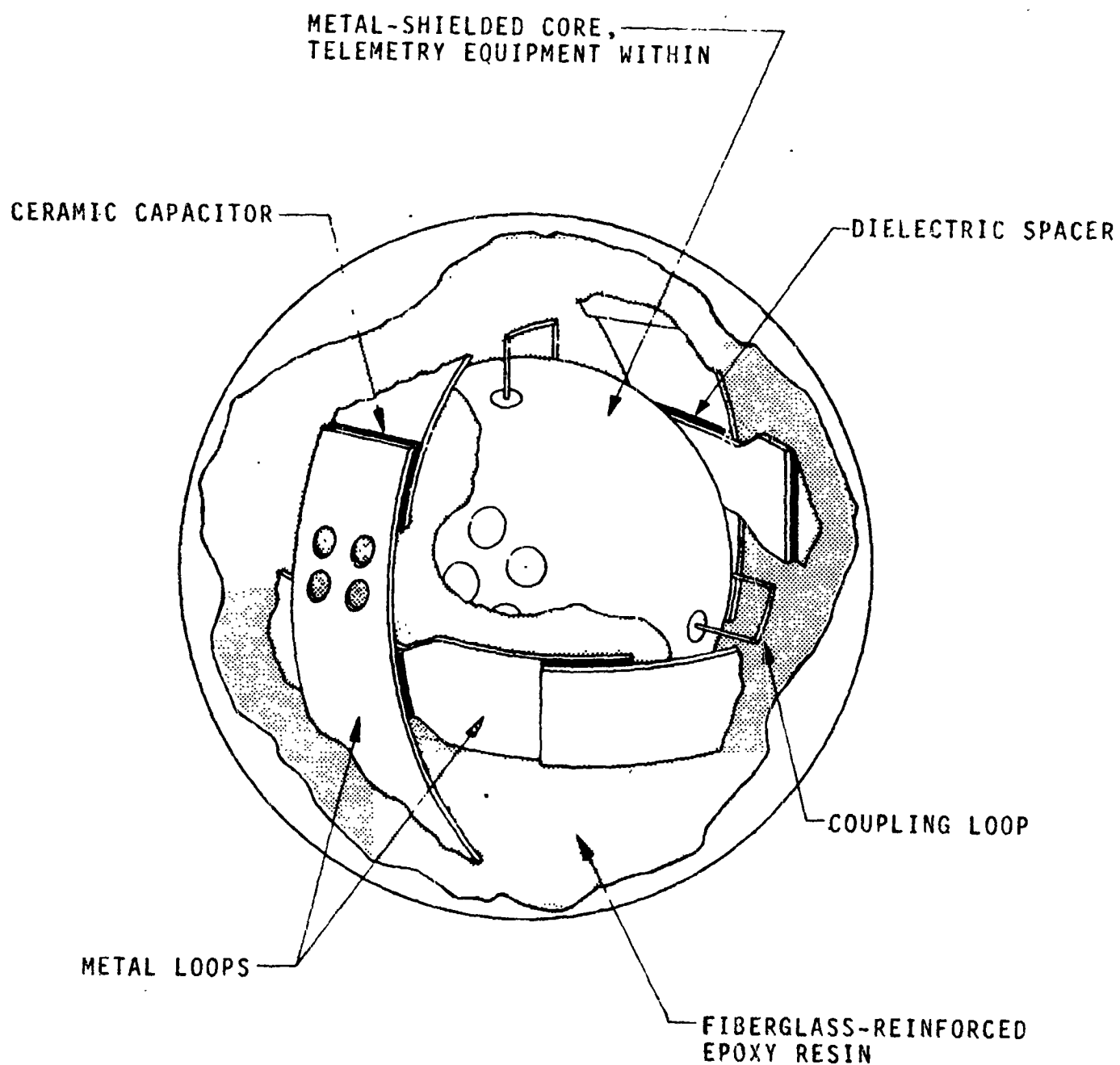

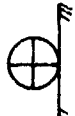


Fig. 22 - Cutaway view of crossed-loop antenna assembly.

In free space, the TPF of the 4-inch diameter antenna model is 3.1 mils, while the RPF is 1.2 mils. Hence, the transmission loss from antenna dissipation is 4.1 db. The dissipation loss from the directional coupler and the coaxial feed lines is expected to be about 0.5 db. Assuming perfect tuning and matching of the loop antennas for the nominal free-space conditions, the expected transmission losses are summarized in Table 8. A 1-db loss can result from the radiation pattern variation (Reference Fig. 3). The total of these free-space losses is less than 6 db, corresponding to an overall efficiency of 25%. This is considerably greater than the required antenna efficiency.

For the condition of landing on a soft surface and deep submergence below the interface, the corresponding transmission losses are also presented in Table 8; it is assumed that $k = 3$, and the antenna is oriented with one loop vertical and the other horizontal. The antenna-detuning loss becomes 3.8 db while the radiation efficiency increases to 1.1 db. If the receiver is directly above the submerged antenna ($\psi = 90^\circ$), only the signal radiated from the vertical loop is received (horizontal-loop radiation null), and the loss from reflection and refraction at the interface is 5 db (Reference, Section VI.C). Hence, the total transmission loss for the submerged antenna is less than 11 db. When the receiver is at a low elevation, corresponding to $\psi = 10^\circ$, and oriented to receive only the horizontal-loop signal (near vertical-loop radiation null), the transmission loss increases to less than 22 db.

The other extreme landing condition is at contact on a hard surface; a surface with $k = 7$ is considered. The worst antenna performance is expected when the antenna is oriented so that one loop is vertical and the other is horizontal at the moment of impact. For $\psi = 90^\circ$, only the signal from the vertical loop is received. Interface losses are nearly 4 db, detuning loss from both antenna deformation (Reference, Section VI.D) and proximity to a dielectric interface is 3.0 db, and the total transmission loss is less than 10 db. For $\psi = 10^\circ$, the worst performance occurs when only the horizontally-polarized signal from the horizontal loop is received (near vertical-loop radiation null). Interface losses are about 14 db, detuning loss is 4.9 db, and the transmission loss is less than 22 db. These results are also presented in Table 8.

CONDITION	ψ	TRANSMISSION LOSS (db)						TOTAL
		DISSIPATION IN COUPLER AND FEED LINES	DETUNING	RPF TPF	RADIATION PATTERN	INTERFACE		
FREE SPACE	ANY	0.5	---	4.1	< 1	---	< 6	
SAR IMMERSION (soft)  k=3	90°	0.5	3.8	1.1	< 1	5	< 11	
	10° HP					16	< 22	
CONTACT (hard)  k=7	90°	0.5	3.0	1.4	< 1	4	< 10	
	10° HP		4.9			14	< 22	

(Total power relative to isotrope)

Table 8. Expected transmission losses for loop antenna.

At the antenna locations of free space and far submerged, the antenna reflection directed to the transmitter is less than 3 db SWR. For impact on a hard surface at 150 feet per second, the antenna reflection directed to the transmitter is expected to be about 13 db SWR at the moment of impact.

Associated with the relatively small TPF of the antenna is a correspondingly narrow bandwidth. The TPF 3-db bandwidth of the antenna model, operating in free space at 250 Mc, is 0.78 Mc. This is adequate to meet the requirements for FM.

Spherical coverage relies on quadrature phase difference between the two loops. A sufficient amount of particular detuning would nullify the phase difference. If this occurred, then in the direction of equal amplitude and like polarization, there might result a sharp null of total radiation. Before impact, the only expected departure from quadrature phase is that caused by the difference of reactance between the two loop orientations, as shown in Fig. 11. This difference appears to be insufficient to cause more than half destruction of the quadrature relation, under the most extreme conditions, and much less with the expected amount of DPF.

At impact on a hard surface, with maximum deformation, there may be as much as 20 mils difference of normalized inductance (Reference, Fig. 10). This amount of differential detuning would be capable of destroying the quadrature phase difference and creating a null of total radiation in two directions. The probability of these directions corresponding to the direction of the receiver, at the time when impact deformation results in the required detuning, is very small. It can be positively precluded, for any known amount of maximum deformation, by increasing the antenna DPF or the coupling between antenna and line.

IX. Antenna Efficiency, Frequency-Trade-Off Study.

The fundamental limitations of a small antenna have been discussed in Section IV of this report. The principal limitation is described in terms of radiation power factor, because a small RPF in the presence of significant dissipation limits the efficiency.

Furthermore, an antenna with a small RPF and high efficiency will have a narrow bandwidth. For the antenna being studied, the limited bandwidth is a severe disadvantage because this antenna must operate under conditions which cause it to be detuned from resonance. Also manufacturing tolerances would be very small for such an antenna. For these reasons, an investigation of alternatives with higher PPF has been conducted.

The radiation power factor can be increased by increasing the size of the loop relative to the wavelength. This can be accomplished by increasing the size for a particular frequency, the frequency for a particular size, or both. Calculations have been made for larger antennas and for increased operating frequency. The RPF and TPF were calculated for a loop about a metal core. The loop and the core are considered to be silver plated with one half the surface area of the core cut out by holes. The results of these calculations are given in Figs. 23 and 24 together with a sketch of the loop and core giving appropriate dimensions. The available increases of RPF and TPF (bandwidth) are clearly shown.

It would be expected that a proportionate increase in loop radius or frequency would have the same effect on the RPF. However because of the presence of the metal core this is not true. An increase in loop radius causes a greater increase of RPF than a proportionate increase in frequency.

The change of radiation efficiency which accompanies the increased RPF and TPF presented in Figs 23 and 24 is presented in Fig. 25. As expected, it increases rapidly as the loop radius is increased and less rapidly as frequency is increased.

With increasing size or frequency, the efficiency approaches a limit, but the RPF and TPF continue to increase. As a measure of this effect, Fig. 26 presents the reflection loss which would result if the antenna is operated 5 mils from resonance, an amount which could be expected either from manufacturing tolerances or from deformation on hard impact. This figure shows very clearly the advantage of an antenna with a bandwidth greater than that of the example selected for this study.

In its present application, this system will suffer some amount of detuning with proximity to a dielectric surface. A cursory

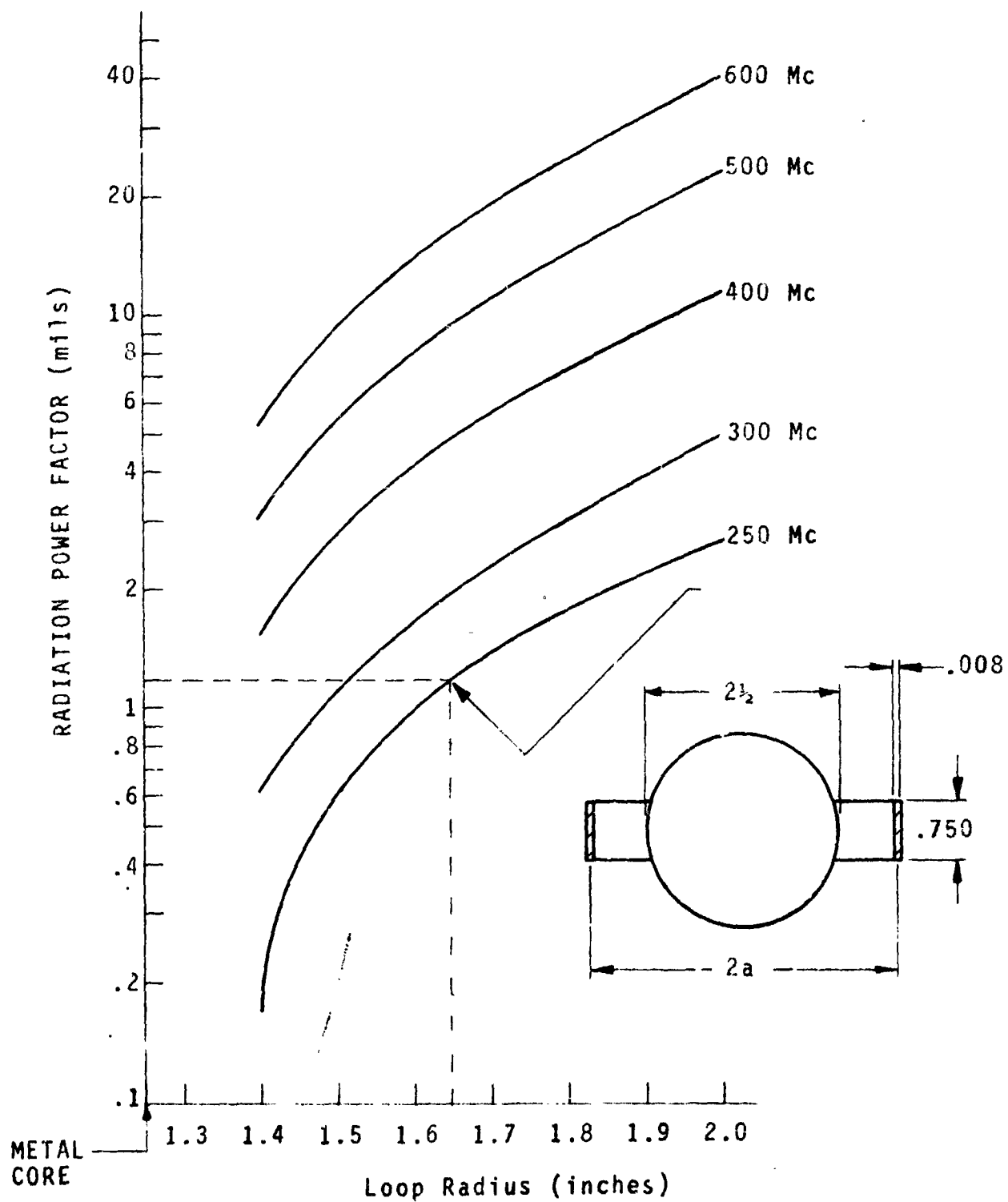


Fig. 23 - Radiation power factor for a loop antenna.

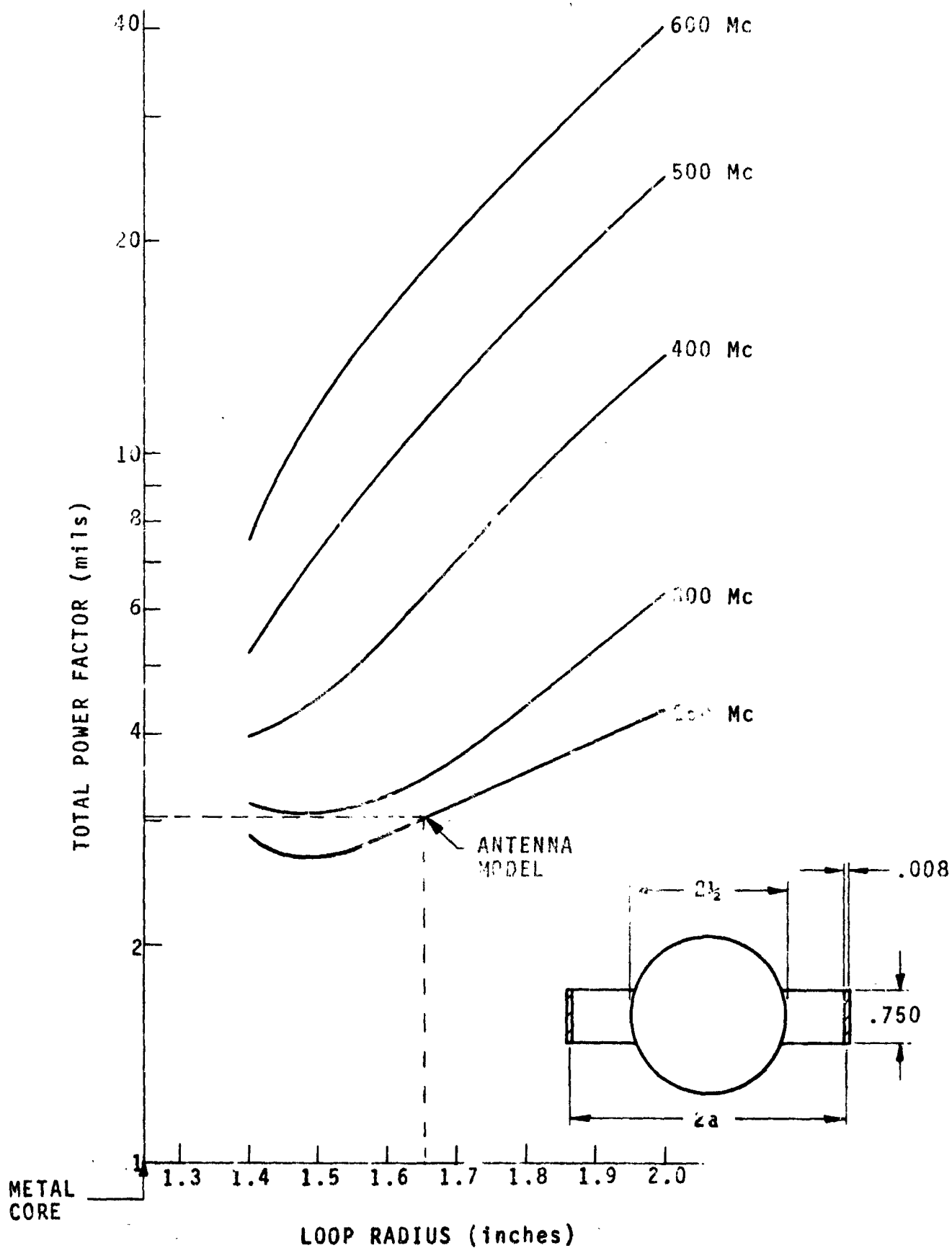


Fig. 24 - Total power factor for a loop antenna.

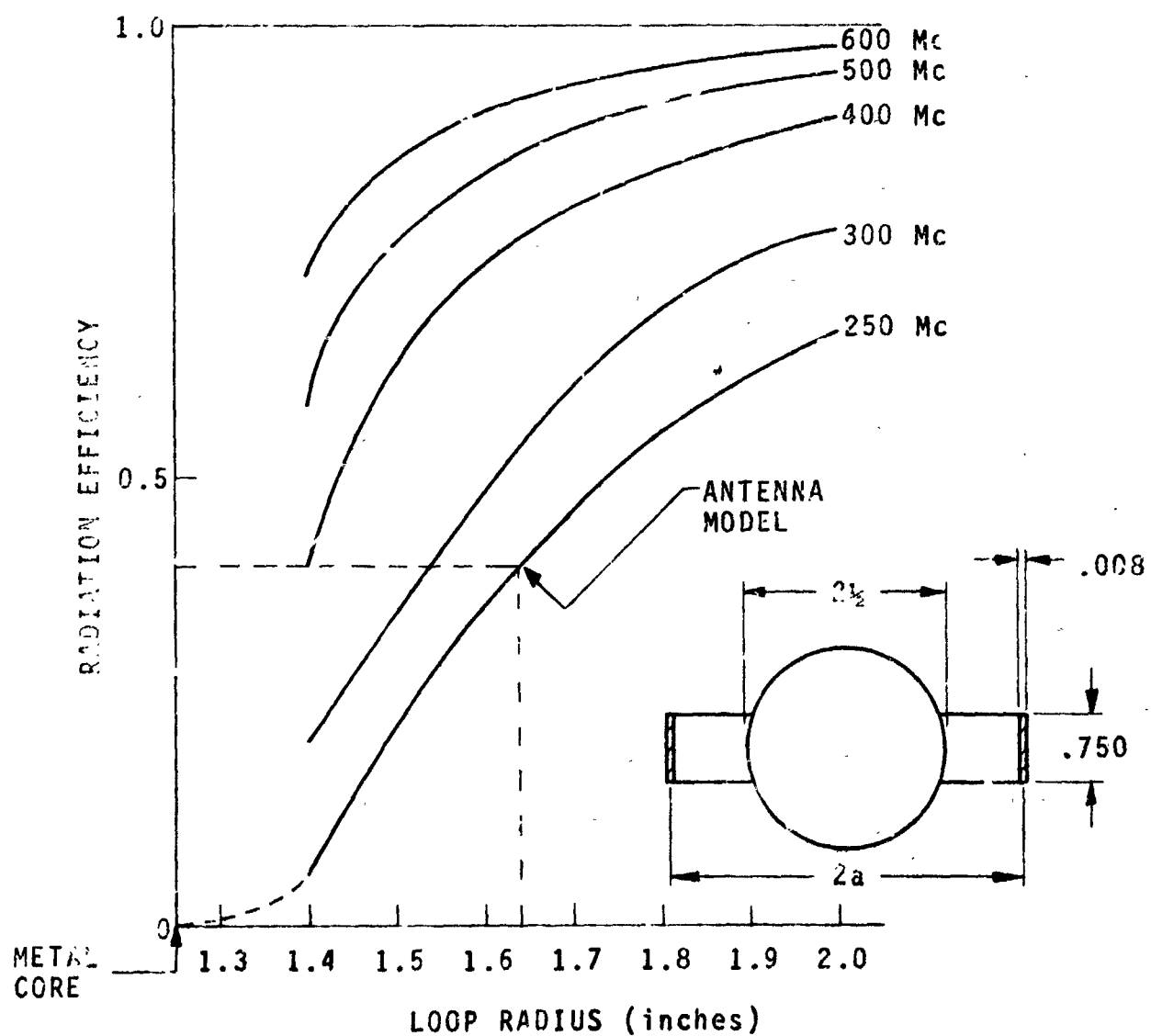


Fig. 25 - Radiation efficiency for a loop antenna.

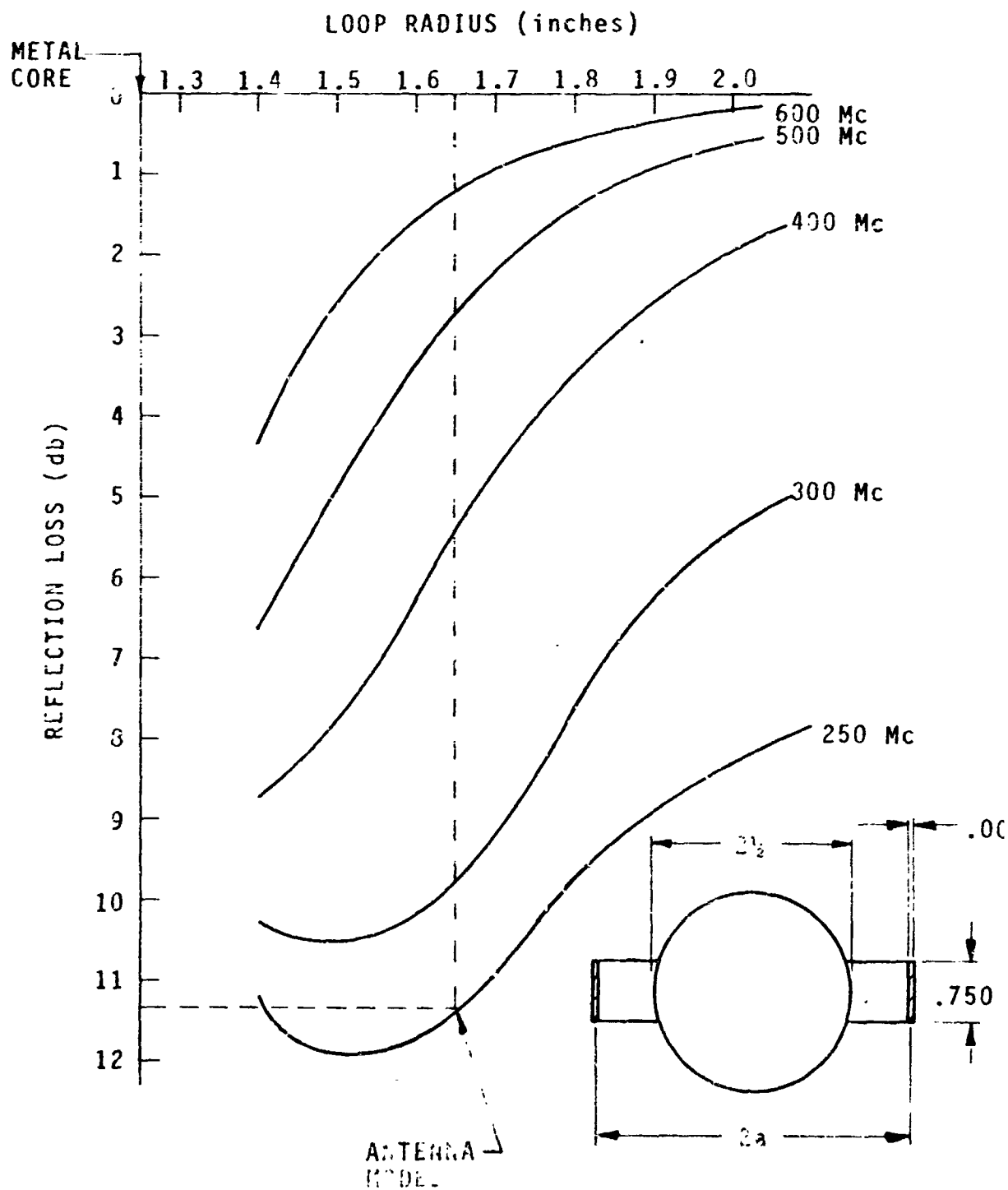


Fig. 26 - Reflection loss for operation 5 mils from resonance.

investigation was performed to determine whether the increased radiation loading which accompanies higher frequency or greater size could alleviate this problem. It is shown in Section VII.E that the magnitude of the reactive shift is directly proportional to the radiation resistance. Thus the reactive shift is greater proportionately with RPF but not DPF. It is concluded that this particular effect is not decreased by increasing size or frequency and would actually be increased if the DPF was not artificially increased in proportion to the RPF.

A directional coupler of the same type can easily be made for any frequency over the range considered. The coupling loop must be increased in area with greater TPF but the amount of increase appears to be readily available over the considered range of conditions.

X. Acknowledgments.

This work has been performed for the National Aeronautics and Space Administration under Contract NAS 1-4470, as a result of Wheeler Laboratories proposal Report 1249, dated 1964 AUG 26. The Wheeler Laboratories effort has been conducted under the direction of Langley Research Center, Langley Field, Va. The period of performance has been from 1964 DEC 21 through 1965 JUL 2.

The work described herein was performed by B. D. Cullen and L. G. Walshak under direction of H. A. Wheeler and H. L. Bachman. The portion of the work associated with mechanical properties was performed by C. J. Palazzo of Hazeltine Corporation, under the supervision of E. P. Kruzoff. The entire study was carried out under the supervision of R. E. Puttre.

This report has been written by several authors. The authors and the sections written by each are given below:

H. A. Wheeler	IV, VI.C
H. L. Bachman	V, VI.B
B. D. Cullen	II, IX, X, Appendix I
C. J. Palazzo	Appendix II
R. E. Puttre	I, III, VI.A, VI.D, VI.E, VII, VIII

XI. References.

- (1) J. D. Cockroft, "Skin Effect in Rectangular Conductors at High Frequencies", Proceedings of Royal Society (London), vol. 122, no. A790, pp. 533-542; Feb. 1929.
- (2) H. A. Wheeler, "Formulas for the Skin Effect", Proc. IRE, vol. 30, pp. 412-424; Sep. 1942.
- (3) H. A. Wheeler, "R-F Inductance Meter", Electronics, vol. 20, no. 9, pp. 105-107; Sep. 1947.
- (4) H. A. Wheeler, "Fundamental Limitations of Small Antennas", Proc. IRE, vol. 35, pp. 1479-1484; Dec. 1947.
- (5) W. R. Smythe, "Static and Dynamic Electricity", McGraw Hill, 2 ed., pp. 313-314; 1950.
- (6) S. A. Schelkunoff and H. T. Friis, "Antennas Theory and Practice", John Wiley and Sons, p. 323; 1952.
- (7) H. A. Wheeler, "Impedance Tests of Single or Coupled Resonators", Wheeler Labs. Report 665; Jan. 1955.
- (8) H. A. Wheeler, "Fundamental Limitations of a Small VLF Antenna for Submarines", IRE Trans., vol. AP-6, pp. 123-125; Jan. 1958.
- (9) H. A. Wheeler, "The Spherical Coil as an Inductor, Shield or Antenna", Proc. IRE, vol. 46, pp. 1595-1602; Sep. 1958. (Correction, vol. 48, p. 328; Mar. 1960.)
- (10) H. A. Wheeler, "The Radiansphere Around a Small Antenna", Proc. IRE, vol. 47, pp. 1325-1331; Aug. 1959.
- (11) H. A. Wheeler, "Useful Radiation from an Underground Antenna", Jour. of Research of NBS, vol. 65D, pp. 89-91; Jan.-Feb. 1961.

- (12) J. D. Jackson, "Classical Electrodynamics", John Wiley and Sons, p. 27-29; 1963.
- (13) L. F. Vogler and J. L. Noble, "Curves of Input Impedance Change due to Ground for Dipole Antennas", NBS Monograph 72; 1964.
- (14) J. E. Becker, A. J. Gianatasio, and H. A. Wheeler, "Development of Omnidirectional Transmitter Antenna - Technical Proposal to NASA", Wheeler Labs. Report 1249; Aug. 1964.
- (15) J. D. Hanfling, "Stereographic Mapping of Antenna Polarization", Wheeler Labs. Report 982; in preparation.
- (16) A. E. H. Love, "A Treatise on the Mathematical Theory of Elasticity", Dover, 4 ed.; 1927.
- (17) J. L. McCarty and H. D. Carden, "Impact Characteristics of Various Materials Obtained by an Acceleration-Time-History Technique Applicable to Evaluating Remote Targets", NASA Technical Note D-1269; Jun. 1962.

650729

NB 122W, 1597, 1626
1627, 1649, 1677

Robert E. Puttre

Appendix I. Antenna Efficiency, Core Size Trade Off.

All calculations presented in the body of this report have been based on an antenna with a 2 1/2-inch diameter core. This diameter is considered adequate for housing the components mentioned in Section III. However, an increase in this diameter might be necessary so calculations have been made to determine the effect this would have on antenna performance. The calculations have been performed for a silver-plated core which has one half the surface area cut out by holes. The RPF, TPF and radiation efficiency were calculated for several core diameters at a frequency of 250 Mc. The results are presented in Figs. A1.1, A1.2 and A1.3.

It can be seen from the graphs that if the core radius is increased by a quarter inch, for example, the loop radius must be increased by approximately this amount if the antenna performance is to be maintained. For greater loop diameters, the change of core radius has less effect. This is because a smaller fraction of the inside volume is occupied by the core.

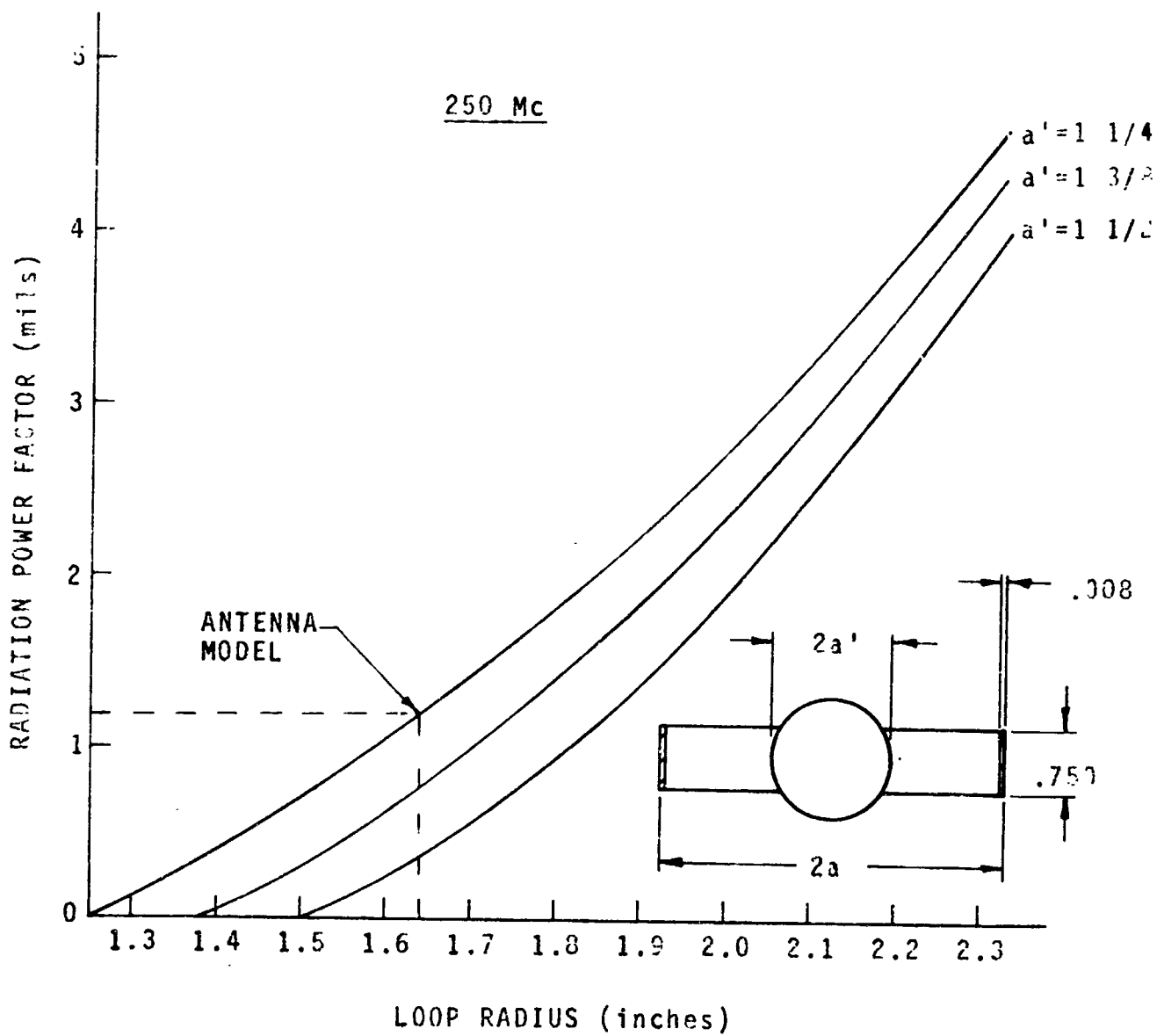


Fig. A1.1 - Radiation power factor for a loop about a sphere.

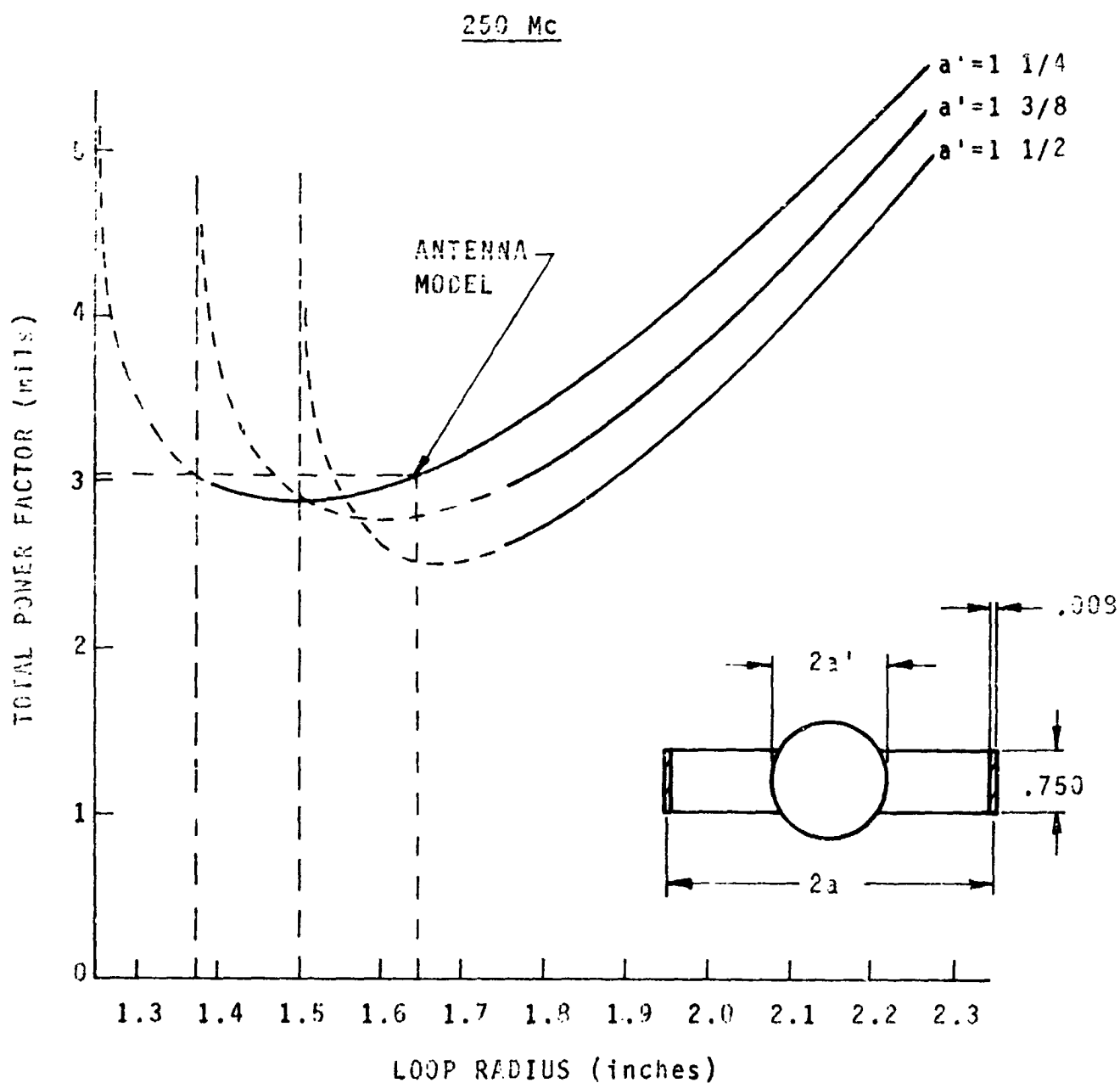


Fig. A1.2 - Total power factor for a loop about a sphere.

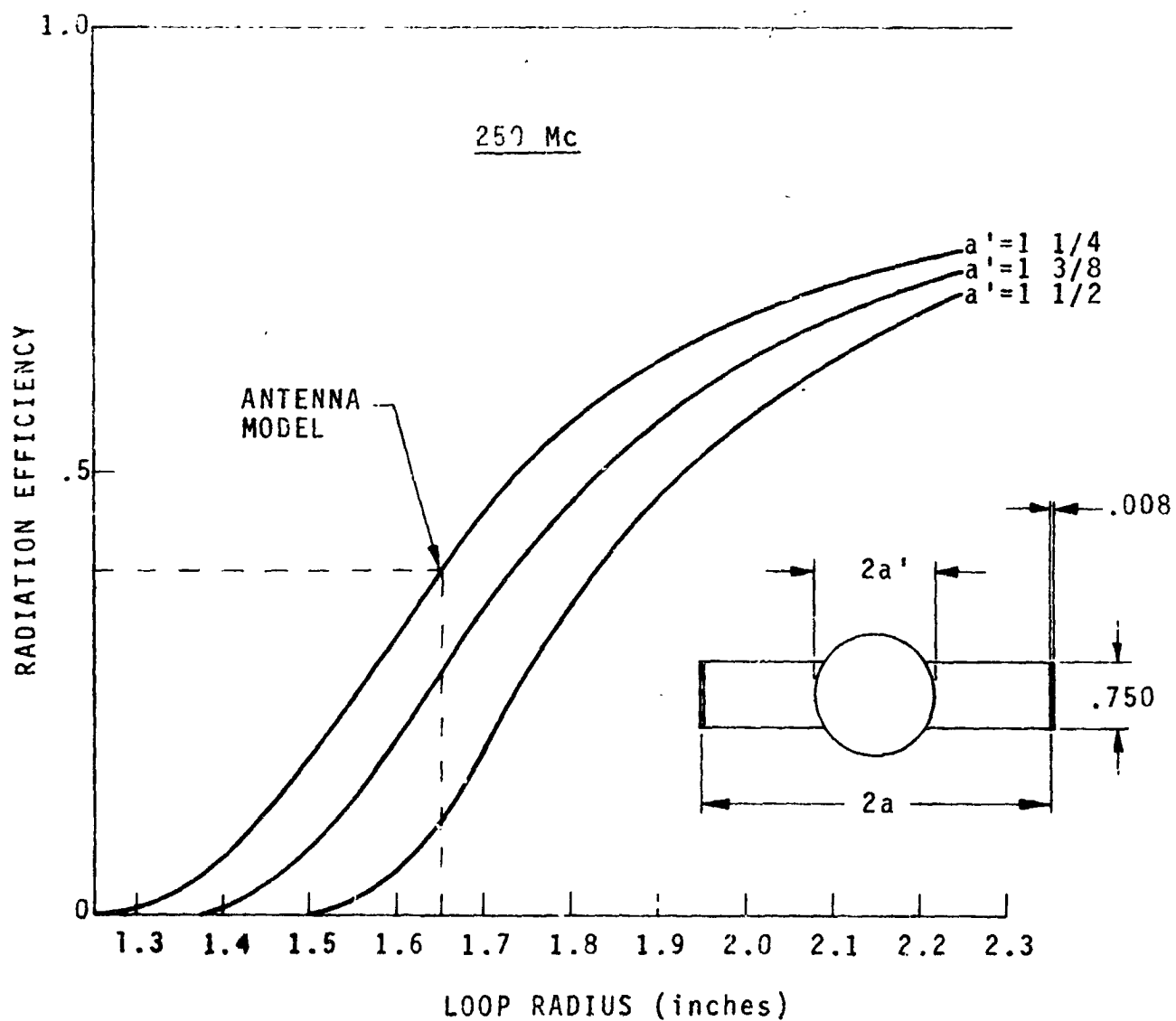


Fig. A1.3 - Radiation efficiency for a loop about a sphere.

Appendix II. Mechanics of Impact.

A. Introduction.

The spherical penetrometer (often referred to later as the projectile) must survive impact on a surface at velocities ranging between 50 and 150 feet per second. The package of an omnidirectional antenna encapsulated into a 4-inch diameter fiberglass-reinforced sphere weights 1.6 pounds; it is expected that the addition of other components will increase the weight to a maximum of 2 pounds. The mechanics of impact of this structure onto a hard concrete-like surface, or a soft sand-like surface will be analyzed to determine estimates of the loadings, deflections, stresses, and penetration of the penetrometer package.

B. Elastic Impact on Hard Surface.

The structural design of the projectile must be such as to permit the antenna to be fully operational during a "hard" impact. An attempt at deriving exact theoretical expressions of the mechanics of hard impact is a formidable, if not an impossible, task for the following reasons: (a) Fiberglass-epoxy resins are non-isotropic and extremely sensitive to geometry, molding procedures, and temperature; (b) These materials are strain-rate sensitive. Published quasi-static properties of non-metallic materials of this kind often bear little resemblance to their dynamic properties; (c) When the deflections of collision result in local crushing, the problem becomes discontinuous; (d) Dynamic deflections are not only time dependent but also non-linear.

In order to estimate the magnitudes of impact loads, deflections, and stresses experienced by the projectile, it is assumed that both the projectile and target are stressed within their respective elastic limits. The materials are assumed to be homogeneous and isotropic, and to conform to Hook's law; that is, the stress-strain characteristic curve is linear up to a point where deformations are permanent. The material properties of the projectile and target listed in Table A2.1 are applied to the analysis which follows.

Projectile and Target Structural Properties

	<u>*Projectile</u>	<u>**Target</u>
Modulus of Elasticity (lb/in ²)	1 x 10 ⁶	3.5 x 10 ⁶
Compressive Strength (lb/in ²)	18-26,000	2-6,000
Relative Deformation at Limit of Compressive Strength (ratio)	0.018-0.026	0.0006-0.0017
Poisson's Ratio	0.25	0.12
Weight Density (lb/in ²)	0.055	0.079

*Fiberglass-reinforced epoxy resin -- 32% (by weight) chopped strand glass fibers.

**Concrete plane surface.

Table A2.1. Projectile and target structural properties.

The theoretical method of analysis is Hertz's theory of elastic impact. In order for this theory to apply it must be shown that the local compression is a static effect; that is, the duration of impact must be a large multiple of the period of free vibration of the sphere.

The following expressions are used for determining peak impact acceleration loads, deflections, and duration of contact in accordance with Hertz's theory for elastic-impact (Ref. 16);

$$g = \frac{1}{386} \left[\frac{125}{72\pi^2} \frac{DV_i^6}{m^2(\delta_p + \delta_t)^2} \right]^{1/5}$$

$$\alpha = \left[\frac{15\pi}{8} \frac{V_i^2 (\delta_p + \delta_t) m}{\sqrt{2D}} \right]^{2/5}$$

$$t_t = 5.208 \left[\frac{(\delta_p + \delta_t) m}{\sqrt{DV_i}} \right]^{2/5}$$

where $\delta = \frac{1-\mu^2}{E\pi}$

Figures A2.1, A2.2 and A2.3 show the variation of these quantities with impact velocity.

In order for Hertz's theory to apply, it must be shown that $t_t > T$, where

$$T = \frac{1}{0.83} \frac{D}{V}$$

$$V = \sqrt{\frac{v_p + 2v_p}{\rho_m}}$$

$$\gamma = \frac{E\mu}{(1+\mu)(1-2\mu)}$$

$$v = \frac{E}{2(1+\mu)}$$

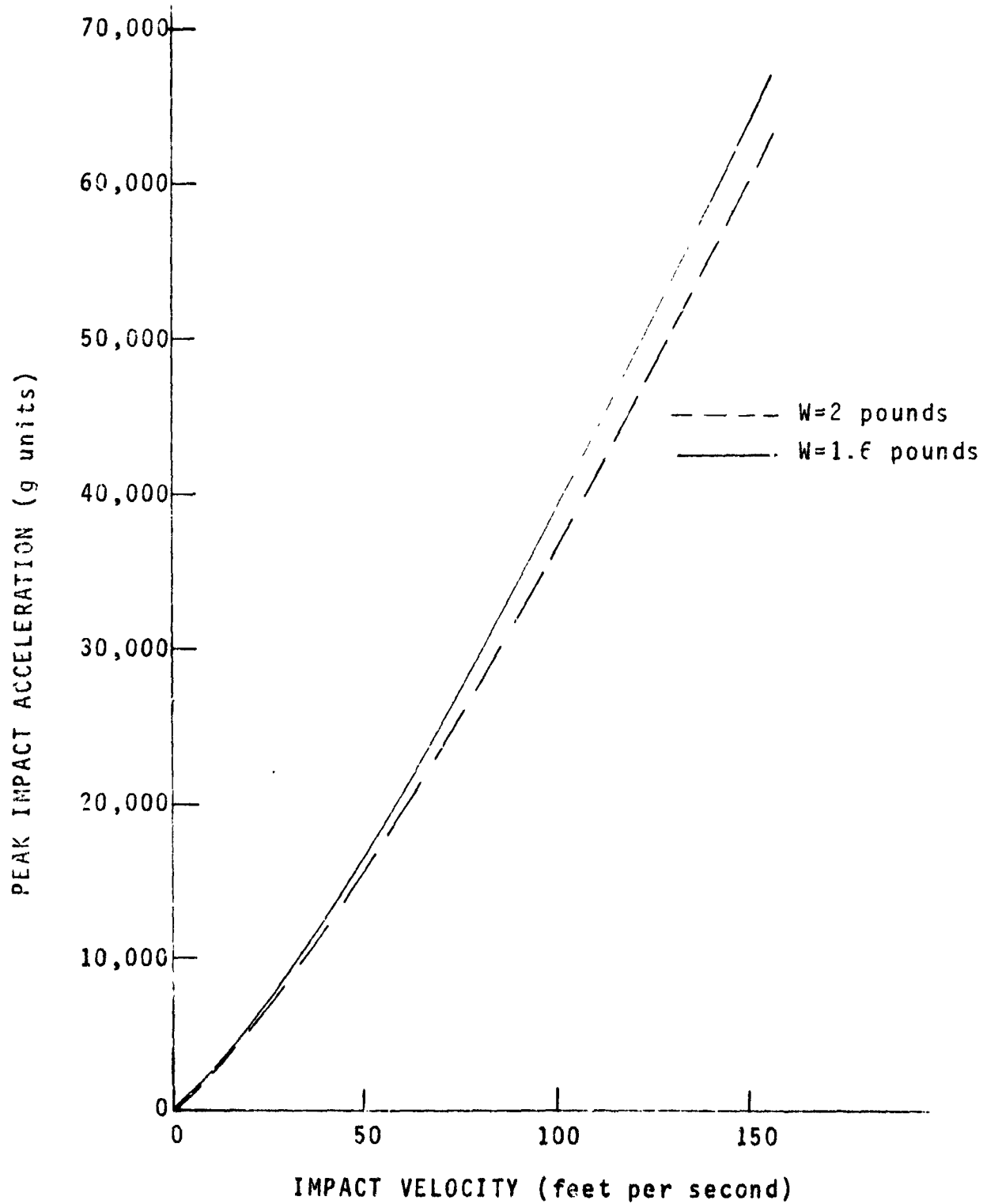


Fig. A2.1 - Peak impact acceleration of projectile.

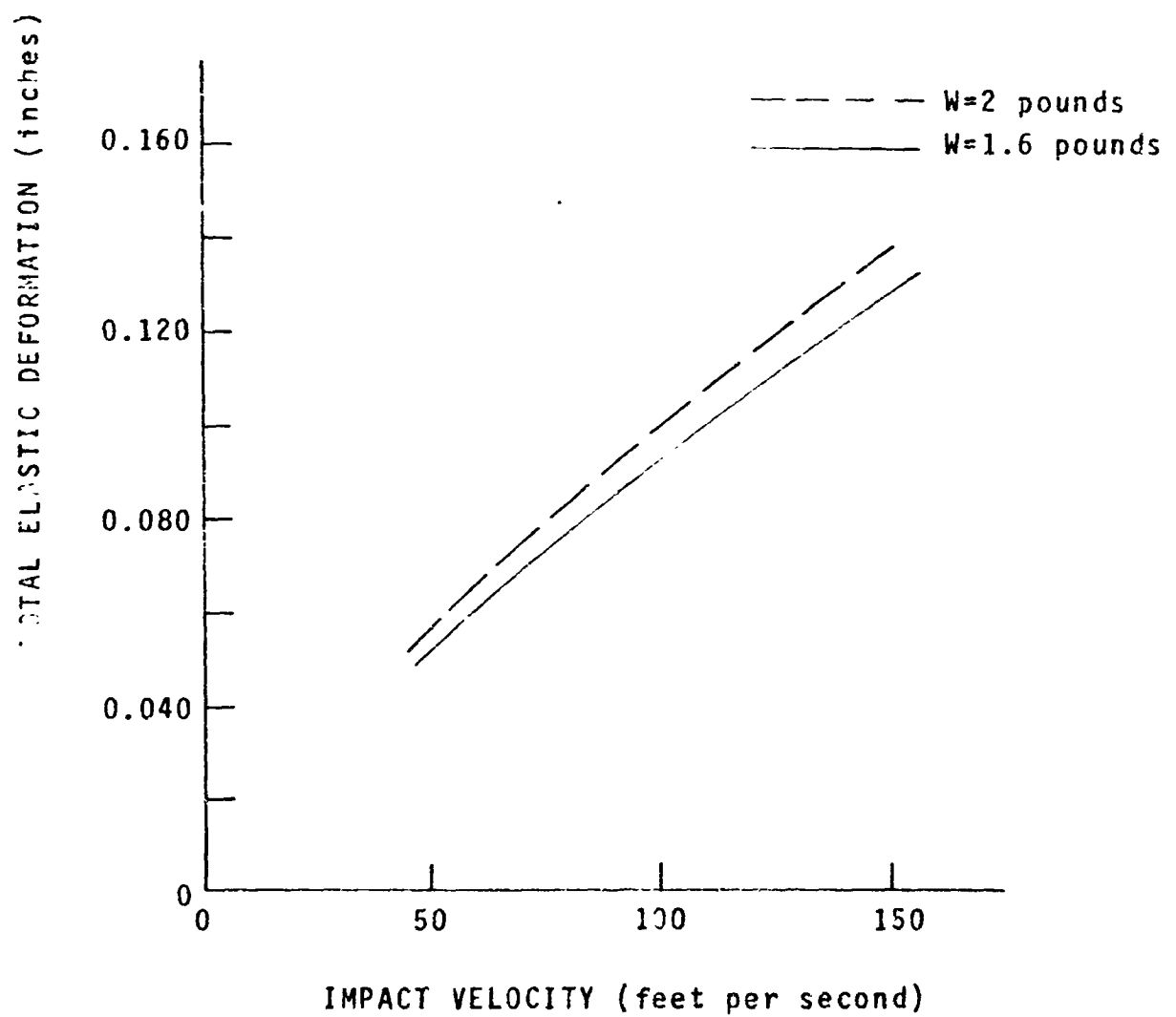


Fig. A2.2 - Total elastic deformation of projectile and target on collision.

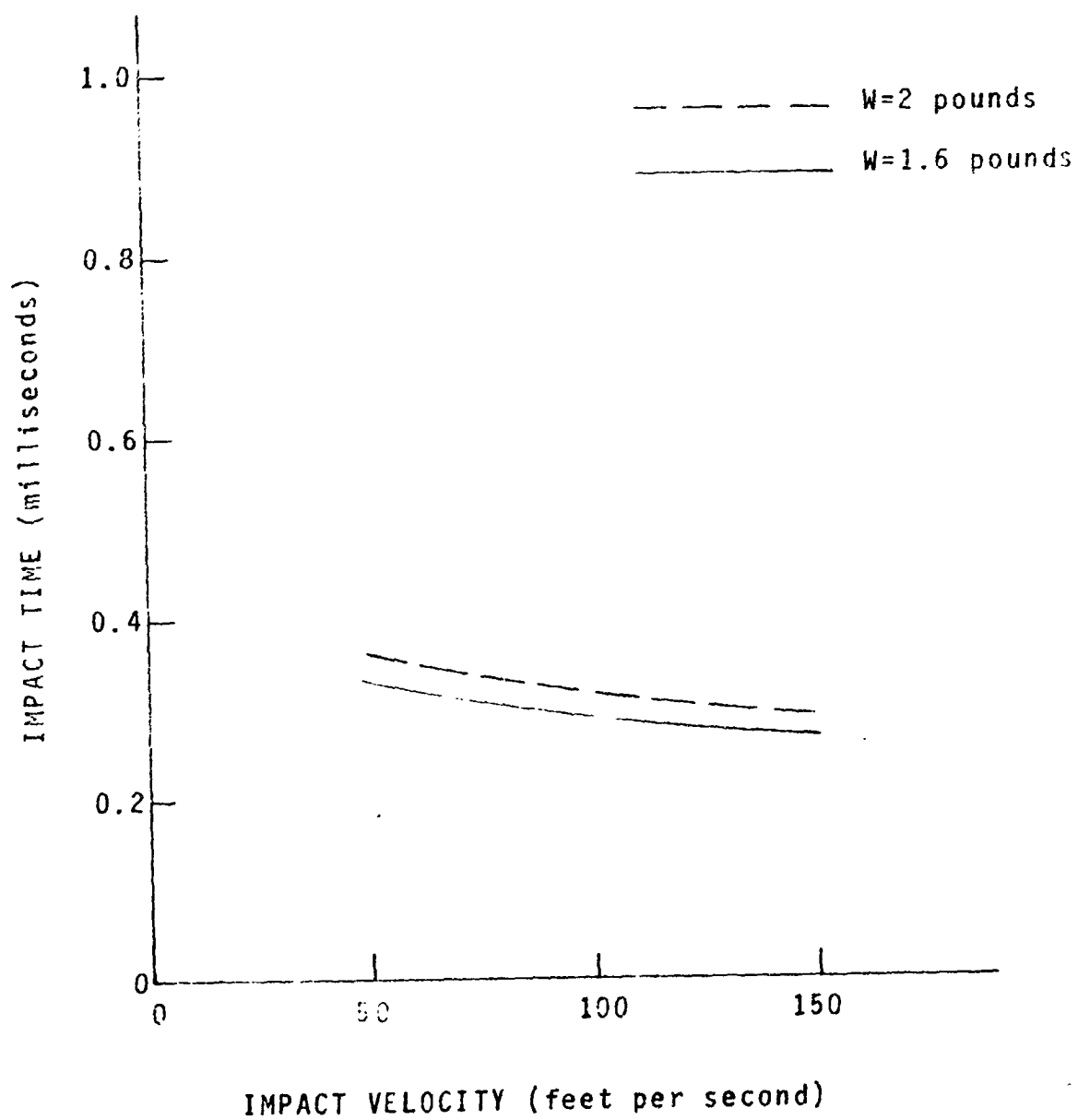


Fig. A2.3 - Total impact time of projectile.

The coefficient $\frac{1}{0.83}$ applies approximately for radial and spheroidal vibrations (Ref. 17). Substitution of E , ν , and ρ_m for the 4-inch diameter projectile yields $T = 0.5 \times 10^{-4}$, which is smaller than 3×10^{-4} , the minimum value of t_t from Fig. A2.3.

Estimates of dynamic stress levels experienced by the projectile are approximated by considering the dynamic compressive stresses developed in a fiberglass-epoxy free bar impacted at one end of a large mass moving at a velocity of V_i . Here

$$s \approx V_i \sqrt{\rho_m E_p} ;$$

Figure A2.4 shows s as a function of V_i .

An expression for the diameter of the circular area of contact is given by (Ref. 17).

$$D' = D \left[\frac{V_i}{V} \right]^{2/5} \left[\frac{5\pi (1 - \nu)^2}{16 (1 - 2\nu)} \right]^{1/5}$$

Figure A2.5 shows D' as a function of V_i .

Inspection of Fig. A2.4 and Table A2.1 suggests the possibility that some degree of structural breakdown of the projectile material can occur. Theoretically, at the first instant of contact, the stress intensity is infinitely high. However, as the compressive stress wave propagates through the sphere, it is expected that its intensity will be attenuated since the area over which the stress is distributed increases sharply immediately after contact of projectile and target. Thus, most of the expected damage to the projectiles should occur in the region of the contact area. This was demonstrated when a preliminary model of the fiberglass-epoxy sphere was impacted onto a concrete target at about 50 feet per second. Local surface abrasion resulted in a circle of contact of approximately 0.6 inch in diameter. This agrees reasonably well with the theoretical prediction of 0.52 shown in Fig. A2.5. The error is attributed to local pulverization of the concrete; small particles of concrete were found clinging to the sphere after testing. During impact, locally pulverizing of the hard, concrete-like target surface, which may have a maximum compressive strength of the order of 6000 psi, is expected.

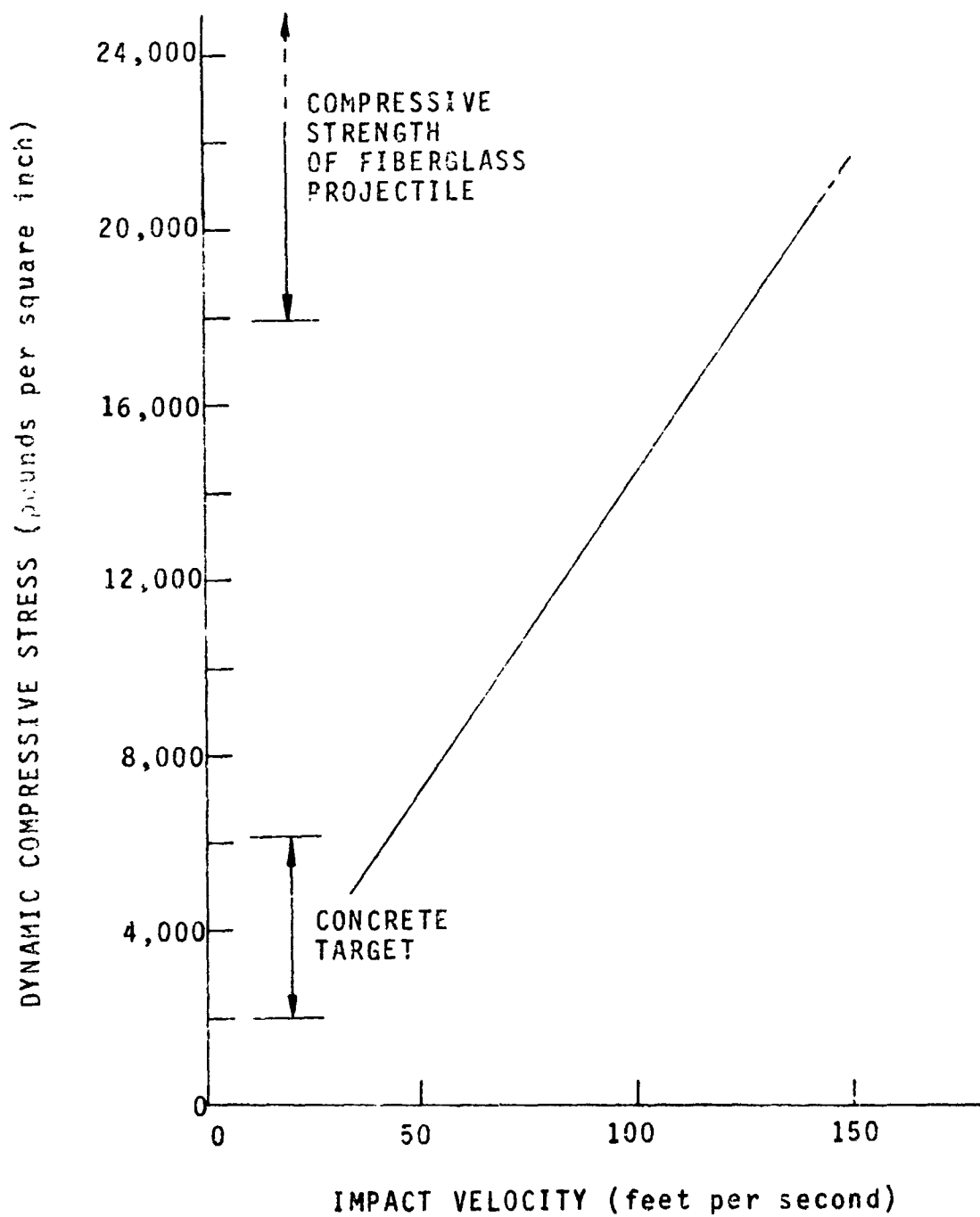


Fig. A2.4 - Dynamic compressive stress at impact.

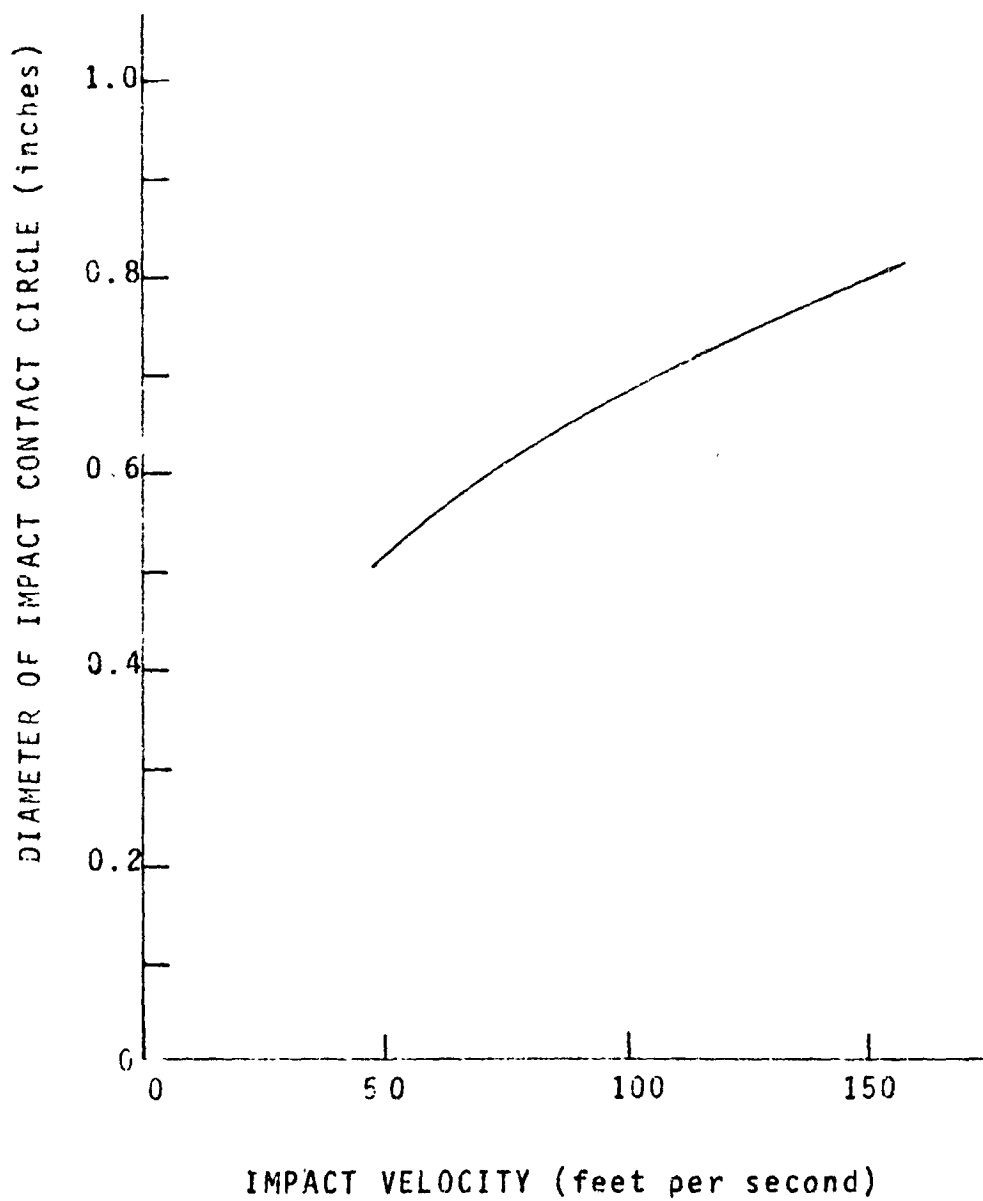


Fig. A2.5 - Diameter of impact contact circle.

Note that the relative compressive parameter α is the total elastic deformation of the projectile and the target. If both the target and projectile crumble locally, then at high V_i the actual α and D' will be greater than is shown in Figures A2.2 and A2.5, respectively.

C. Dynamic Deformation.

The evaluation of the maximum stresses resulting during impact was necessary for determination of the structural integrity of the projectile package. For evaluation of the electrical performance during impact, however, some estimate of the physical dynamic deformations of the projectile is needed.

With regard to impact deformations, consider an encapsulated cross-loop antenna so oriented that impact on a concrete target occurs when one loop is vertical and perpendicular to the target. Then the maximum local deflection experienced by this loop is as shown in Fig. A2.2.

By virtue of the fact that a compressive stress (Fig. A2.4) exists in the projectile during impact, the horizontal loop experiences an expansion. The maximum increase of the diameter and circumference of the horizontal loop is 0.3% and occurs when V_i is 150 feet per second.

D. Penetration.

When the projectile lands on a relatively soft target, the impact stress will be less than that determined for a hard target. The projectile will, however, penetrate into and below the surface of the target. For evaluation of the electrical performance of the antenna, some estimate of the penetration depth is needed.

The following expression (Ref. 17) offers an estimate of the penetration expected when the projectile is impacted on a loose No. 000 sand target.

$$y = \frac{5.2 m^{1/2} V_i^{2/3}}{D}$$

The coefficient 5.2 is twice the value expressed in Reference 16. The reason for this is that the projectiles discussed in Reference 16 are hemispherically-nosed cylinders. Since the shape of the projectile presently under consideration is a complete sphere, it is expected that its resistance to penetration is diminished by approximately a factor of 2. Figure A2.6 shows y plotted as a function of V_i .

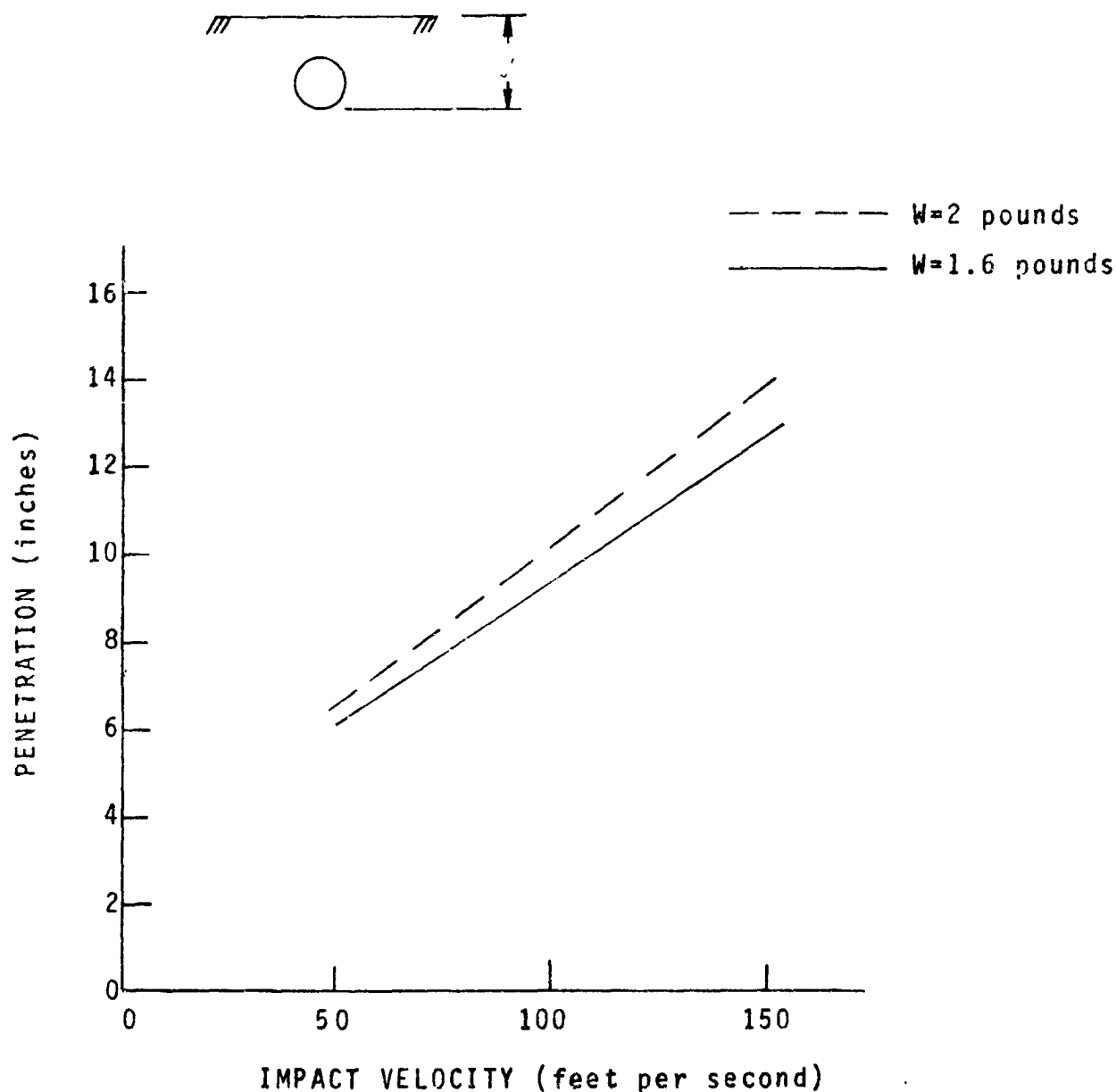


Fig. A2.6 - Depth of penetration into loose sand.